

**UCSF**

**UC San Francisco Electronic Theses and Dissertations**

**Title**

Structure, Polymerization, and Dynamics of a the First Bacteriophage Tubulin

**Permalink**

<https://escholarship.org/uc/item/0zq833cs>

**Author**

Kraemer, James Aaron

**Publication Date**

2014

Peer reviewed|Thesis/dissertation

Structure, Polymerization, and Dynamics of a the First Bacteriophage  
Tubulin: PhuZ

by

James A. Kraemer

DISSERTATION

Submitted in partial satisfaction of the requirements for the degree of

DOCTOR OF PHILOSOPHY

in

Biophysics

in the

GRADUATE DIVISION

of the

UNIVERSITY OF CALIFORNIA, SAN FRANCISCO

Copyright 2014

by

James A. Kraemer

## Acknowledgements

I must start by thanking a large group of people who helped me accomplish all of this work. No science is conducted in a vacuum (well, maybe some is), and I could never have achieved what I have without the help and support of many, many people. First and foremost, I have to thank all of the members of the Agard lab, both current and former, for all of their support. I could not have done it without you all! You are some of the smartest, most talented, craziest people I have ever had the pleasure of knowing. Thank you for accepting my crazy as part of the lab too!

There is a long list of people whom I must thank for their mentorship and friendship. Thank you to Dr. Christopher Waddling for teaching me how to do crystallography when I was a young student with no idea what I was doing. I am indebted to Dr. Elizabeth Montabana for convincing me to rotate in the lab, mentoring the shit out of me, and putting up with me for all those years. She really taught me to trust my gut and be a better scientist. Dr. Michelle Moritz has always been available as a fountain of tubulin knowledge and helpful advice, as well as being the rock of the centrosome subgroup. Thanks to Dr. Laura Lavery for unspeakable amounts of technical knowledge as well as an uncanny memory for movie and music quotations. A big thanks to Andrew Lyon for being a great drinking buddy and idea generator. Климент Верба супер-спай – никогда не останавливай шпионить. Daniel Elnatan, your creativity and constant excitement of science inspire me. Dr. Justin Kollman taught me much about science, but also about where to drink the best drinks, from Manhattans to margaritas (just do not eat the food at Tommy's). Thank you Elena Zehr for your hard work and insight on the PhuZ project and we dove into the brave new world of phage tubulin together. I must also thank Mariano Tabios for being the best lab manager, and always making sure things run smoothly.

I must give a big shoutout to the UCSF bacterial cytoskeleton community (all from Dyche Mullin's lab), past and present: Dr. Jessica Polka, Dr. Ethan Garner, Natalie Petek, and Dr. Chris Rivera. All of them provided me with countless amounts of advice and hours of great scientific discussions. I cannot wait for more in Boston with Jessica and Ethan.

I have to thank Joe Pogliano and the members of his laboratory for being amazing collaborators. Joe was like a second mentor for through my thesis and is a great scientist and person. Never in a million years would I have predicted becoming such good friends with my collaborator, Marcy. We basically experienced all of the travails of graduate school together (though separated by the distance of San Francisco and San Diego). I am forever grateful for her spirit, intelligence, and friendship. I am excited to be in the same town now as we both will be postdocs in Boston!

Of course, I must thank Dr. David Agard for so much. He has been a tremendous mentor though graduate school, and I know he will continue to be a mentor to me as I continue my scientific career. David has always pushed me to succeed and to follow what questions I thought were most interesting. He always asks the hard questions and definitely trained me to be, I hope, a great scientist. Thank you for everything, David.

On a personal note, I must thank all of my friends and family for supporting me through this journey. All of my friends from college and outside the lab here in San Francisco (too many to name) have helped to keep me sane through out these past six years. I can always rely on you to be there for me and to make me have a great time. Thank you to my parents for always supporting me in whatever I want to do. See you sometime soon. Thanks to my sister, Sarah, and my soon-to-be brother-in-law, Dave, for lots of fun and support; I love you. Although he didn't make it see me finish my PhD, I have to thank my grandfather, Herb "Poppa" Ratet. He and I

were very close, and although quite a character, he was always an inspiration to me. He inspired me to be the person I am today, to have a strong Jewish identity, and to follow my dreams. I will be forever grateful that I was living here near him for the last few years of his life and all of the time we were able to spend together.

Two chapters of this dissertation were published previously and reprinted here with permission. Chapter 2 is a reprint of material as it appears in *Cell*. 2012 Jun 22; 149(7): 1488-99. Chapter 3 is a reprint of material as it appears in *Structure*. 2014 Apr 8; 22(4): 539-48.

## Abstract

Tubulins are a superfamily of polymerizing GTPases, which are conserved from bacteria to man. Though they share a common fold and mode of longitudinal interaction (with the nucleotide at the interface), they have extremely diverse primary sequences and form diverse structures ranging from single protofilaments to rings to tubes. Tubulins rely on the energy from GTP to generate filament dynamics, which allows them to perform a diverse set of functions. Microtubules are dynamically unstable, switching from rapidly growing to shrinking states in order to search and capture chromosomes during mitosis. FtsZ filaments treadmill *in vitro* and organize the machinery for bacterial septation, though their *in vivo* dynamics are still not well understood. TubZ filaments treadmill to segregate large, low copy number plasmids in *Bacillus*. Although GTP is critical for polymerization and dynamics of tubulin superfamily members, the molecular requirement for GTP in polymerization and its role in dynamics are still not well understood.

The subject of this manuscript is the newly identified tubulin superfamily member PhuZ. PhuZ is encoded on the genomes of large *Pseudomonas* phage. This manuscript describes the early characterization of this tubulin, from its role in the phage lytic cycle to its structure and dynamics. A specific focus is on the structure and polymerization dynamics of PhuZ filaments. Understanding of how PhuZ polymerizes and uses GTP shed light on how tubulins use GTP in general, as well as unique characteristics of PhuZ filaments. We have determined that PhuZ forms dynamically unstable three-stranded filaments that are critical for centering replicated phage in the host cell. These filaments use a unique C-terminal tail to polymerize and their minus ends are stabilized at the cell poles to orient growth towards the center to properly center phage. PhuZ is the first known prokaryotic tubulin to form a bipolar spindle and be dynamically

unstable. The discovery of these properties has opened up a new frontier for the cell biology of viruses and provides new understanding of the evolution and GTP regulation of tubulin filaments.



## Table of Contents

<i>Title Page</i> .....	<i>i</i>
<i>Acknowledgements</i> .....	<i>iii</i>
<i>Abstract</i> .....	<i>vi</i>
<i>Table of Contents</i> .....	<i>viii</i>
<i>List of Tables</i> .....	<i>xi</i>
<i>List of Figures</i> .....	<i>xi</i>
<b>CHAPTER 1: INTRODUCTION</b> .....	<b>1</b>
ACTINS .....	3
INTERMEDIATE FILAMENTS.....	4
TUBULINS .....	5
REFERENCES .....	11
<b>CHAPTER 2: A PHAGE TUBULIN ASSEMBLES DYNAMIC FILAMENTS BY A NOVEL MECHANISM     TO CENTER VIRAL DNA WITHIN THE HOST CELL</b> .....	<b>18</b>
ABSTRACT.....	19
INTRODUCTION.....	20
RESULTS.....	22
DISCUSSION .....	34
ACKNOWLEDGEMENTS .....	38
MATERIALS AND METHODS .....	39
FIGURES .....	42
REFERENCES .....	53

SUPPLEMENTAL FIGURES .....	58
SUPPLEMENTAL TABLES .....	65
SUPPLEMENTAL METHODS .....	67
SUPPLEMENTAL REFERENCES .....	70

### **CHAPTER 3: THE STRUCTURE AND ASSEMBLY MECHANISM OF A NOVEL THREE-STRANDED**

<b>TUBULIN FILAMENT THAT CENTERS PHAGE DNA .....</b>	<b>72</b>
ABSTRACT.....	73
INTRODUCTION.....	74
RESULTS.....	76
DISCUSSION .....	86
ACKNOWLEDGEMENTS .....	90
MATERIALS AND METHODS .....	90
TABLE .....	95
FIGURES .....	96
REFERENCES .....	105
SUPPLEMENTAL FIGURES .....	109
SUPPLEMENTAL TABLE .....	116
SUPPLEMENTAL METHODS .....	118
SUPPLEMENTAL REFERENCES .....	119

### **CHAPTER 4: A BACTERIOPHAGE TUBULIN HARNESSSES DYNAMIC INSTABILITY TO CENTER**

<b>DNA IN INFECTED CELLS .....</b>	<b>120</b>
ABSTRACT.....	121
INTRODUCTION.....	122

RESULTS.....	125
DISCUSSION .....	131
MATERIALS AND METHODS .....	133
ACKNOWLEDGEMENTS .....	139
FIGURES .....	140
REFERENCES .....	154
<b>CHAPTER 5: PRELIMINARY STUDIES OF HIGH-RESOLUTION GTP-BINDING AND HYDROLYSIS</b>	
.....	<b>157</b>
INTRODUCTION.....	158
RESULTS AND DISCUSSION .....	158
MATERIALS AND METHODS .....	167
FIGURES .....	170
REFERENCES .....	191
<b>CHAPTER 6: FUTURE DIRECTIONS .....</b>	<b>193</b>
INTRODUCTION.....	194
MOLECULAR ORIGINS OF POLYMERIZATION.....	194
MECHANISM OF PHAGE CENTERING .....	199
BIOLOGY OF VIRUSES .....	202
REFERENCES .....	204
<b>APPENDIX .....</b>	<b>205</b>

## LIST OF TABLES:

### CHAPTER 2:

TABLE S1: TABLE OF X-RAY DATA AND STRUCTURE REFINEMENT STATISTICS .....	65
TABLE S2: TABLE OF TLS GROUPS AS DETERMINED BY THE TLS SERVER.....	66

### CHAPTER 3:

TABLE 1: STRAINS AND PLASMIDS USED .....	95
TABLE S1: CRITICAL CONCENTRATIONS OF PHU <sub>Z</sub> <sub>201</sub> WILD TYPE AND MUTANT CONSTRUCTS.....	116

## LIST OF FIGURES:

### CHAPTER 2:

FIGURE 1: PHYLOGENETIC RELATIONSHIP AND CONSERVED SEQUENCES OF PHU <sub>Z</sub> AND OTHER DISTANTLY RELATED TUBULINS .....	42
FIGURE 2: PHU <sub>Z</sub> POLYMER ASSEMBLY IN <i>P. CHLORORAPHIS</i> .....	44
FIGURE 3: <i>IN VITRO</i> POLYMERIZATION OF PHU <sub>Z</sub> .....	45
FIGURE 4: STRUCTURE AND NUCLEOTIDE BINDING OF PHU <sub>Z</sub> .....	46
FIGURE 5: CRYSTAL LATTICE CONTAINS FILAMENT-LIKE CONTACTS WITH THE C-TERMINAL TAIL PROVIDING MOST OF THE CONTACT SURFACE.....	47
FIGURE 6: A SINGLE CELL ASSAY FOR PHAGE INFECTION REVEALS THAT PHU <sub>Z</sub> ASSEMBLES FILAMENTS <i>IN VIVO</i> DURING INFECTION OF THE HOST CELL WITH 201 $\phi$ 2-1 .....	49
FIGURE 7: AFTER 201 $\phi$ 2-1 INFECTS A CELL, THE HOST CHROMOSOME IS DEGRADED AND SHORT PHU <sub>Z</sub> FILAMENTS APPEAR THAT EVENTUALLY EXTEND FROM THE POLES OF THE CELL TO THE PHAGE NUCLEOID IN THE CENTER .....	52
FIGURE S4: RELATED TO FIGURE 5.....	58

FIGURE S2: RELATED TO FIGURE 3.....	59
FIGURE S3: RELATED TO FIGURE 4.....	60
FIGURE S1: RELATED TO FIGURE 2.....	61
FIGURE S5: RELATED TO FIGURE 6.....	62

**CHAPTER 3:**

FIGURE 1: PHUZ <sub>201</sub> ASSEMBLES THREE-STRANDED FILAMENTS AND FORMS A HEXAMERIC NUCLEUS.....	96
FIGURE 2: CRYO-EM MAP AND PSEUDO-ATOMIC MODEL OF PHUZ <sub>201</sub> FILAMENT.....	97
FIGURE 3: PHUZ <sub>201</sub> SUBUNIT IS UNIQUELY ORIENTED WITHIN THE FILAMENT AND MAKES LATERAL CONTACTS VIA A SET OF CONSERVED RESIDUES .....	98
FIGURE 4: MUTATIONS TO RESIDUES PREDICTED TO MEDIATE LATERAL CONTACTS DISRUPT PHUZ <sub>201</sub> ASSEMBLY <i>IN VITRO</i> .....	99
FIGURE 5: PHUZ <sub>201</sub> ASSEMBLES VIA THE SAME SET OF LATERAL SURFACES <i>IN VIVO</i> AS <i>IN VITRO</i> .....	101
FIGURE 6: COMPARISON OF THE LONGITUDINAL PACKING BETWEEN PHUZ <sub>201</sub> -GDP, PHUZ <sub>KZ</sub> -GDP-LIKE AND THE THREE-STRANDED FILAMENT .....	102
FIGURE 7: MODEL FOR PHUZ ASSEMBLY .....	104
FIGURE S1: RELATED TO FIGURE 2.....	109
FIGURE S2: RELATED TO FIGURE 3.....	111
FIGURE S3: RELATED TO FIGURE 4.....	113
FIGURE S4: PHUZ FAMILY TUBULINS ASSEMBLE THREE-STRANDED FILAMENTS .....	114

**CHAPTER 4:**

FIGURE 1: TIRF MICROSCOPY REVEALS POLARITY AND DYNAMIC INSTABILITY IN PHUZ FILAMENTS ....	140
FIGURE 2: NUCLEOTIDE HYDROLYSIS DESTABILIZES PHUZ FILAMENTS.....	141

FIGURE 3: PHUZ FORMS A BIPOLAR SPINDLE COMPOSED OF DYNAMICALLY UNSTABLE FILAMENTS <i>IN VIVO</i>	143
FIGURE 4: FLUORESCENCE <i>IN SITU</i> HYBRIDIZATION (FISH) DURING PHAGE INFECTION.....	145
FIGURE 5: OBSERVATION OF PHAGE NUCLEOID MIGRATION BY TIME-LAPSE MICROSCOPY.....	147
FIGURE 6: INFECTION NUCLEOID CENTERING IS INDEPENDENT OF DNA REPLICATION .....	149
FIGURE 7: MODEL OF PHUZ BIPOLAR SPINDLE FORMATION DURING LYTIC GROWTH.....	151

## CHAPTER 5:

FIGURE 1: INITIAL CRYSTAL HITS OF WILD-TYPE PHUZ IN THE PRESENCE OF GMPCPP.....	170
FIGURE 2: WILD-TYPE PHUZ CYRSTALLIZED IN GMPCPP ONLY CONTAINS GDP.....	171
FIGURE 3: INITIAL CYRSTAL HIT OF $\Delta$ TAIL-PHUZ IN GDP .....	172
FIGURE 4: CRYSTAL STRUCTURE OF $\Delta$ TAIL-PHUZ TO 1.46 Å.....	173
FIGURE 5: THE CRYSTAL PACKING OF THE $\Delta$ TAIL-PHUZ CYRSTALS CONTAINS NO PROTOFILAMENT-LIKE CONTACTS.....	174
FIGURE 6: OVERLAY OF $\Delta$ TAIL-PHUZ WITH WILD-TYPE PHUZ .....	175
FIGURE 7: $\Delta$ TAIL-PHUZ CRYSTAL SOAKS HAVE GTP, BUT NO CONFORMATIONAL CHANGE .....	176
FIGURE 8: COMPARISON OF GTP COORDINATION BETWEEN PHUZ AND $\Gamma$ -TUBULIN .....	177
FIGURE 9: GALLERY OF CRYSTAL HITS FROM $\Delta$ TAIL-PHUZ GROWN IN GMPCPP OFF OF SEEDS .....	178
FIGURE 10: CRYSTAL HITS OF WILD-TYPE PHUZ CRYSTALS GROWN IN THE PRESENCE OF GMPCPP AND SEEDS.....	179
FIGURE 11: $\Delta$ TAILBINDING- AND $\Delta$ TAIL-PHUZ DO NOT COPOLYMERIZE AND MAY INTERACT .....	180
FIGURE 12: INITIAL HITS OF $\Delta$ TAILBINDING- AND $\Delta$ TAIL-PHUZ IN THE PRESENCE OF GMPCPP.....	181
FIGURE 13: CRYSTAL C FROM FIGURE 12 DIFFRACTED, BUT THE STRUCTURE COULD NOT BE SOLVED..	182
FIGURE 14: RIGHT-ANGLE LIGHT SCATTERING OF D303A/D305A-PHUZ AND D303A/D305A/D190A-PHUZ.....	183

FIGURE 15: CRYSTALS OF D303A/D305A-PHUZ IN THE PRESENCE OF GMPCPP .....	184
FIGURE 16: D303A/D305A-PHUZ CRYSTALLIZED AS A TUBE.....	185
FIGURE 17: D303A/D305A-PHUZ IS A DIMER IN THE ASYMMETRIC UNIT .....	186
FIGURE 18: NUCLEOTIDE BINDING OF PHUZ MEASURED BY ITC.....	187
FIGURE 19: GTP HYDROLYSIS BY PHUZ.....	188
FIGURE 20: PHUZ PHOSPHATE RELEASE.....	189
FIGURE 21: GTP TURNOVER MEASURED BY ENZYME-COUPLED ASSAY.....	190

## **Chapter One**

### **Introduction**



A cell, whether it is a bacterium, yeast, plant cell, animal cell, or anywhere in between must solve the fundamental problem of self-organization. All processes from DNA replication to protein translation to metabolism must occur at both an appropriate time and place. One way that cells have evolved to solve this problem is through the use of the polymer forming proteins that form up the cytoskeleton and the multitude of proteins that regulate these polymers in space and time.

The importance the eukaryotic cytoskeleton plays in the spatiotemporal organization of the eukaryotic cell has been appreciated for centuries (Frixione, 2000). Three main families of eukaryotic cytoskeletal filaments have been identified and well studied: microtubules, actin filaments, and intermediate filaments. All of these filaments form large fibers that are easily visible in a light microscope, which allowed for their identification and study long ago. These filaments are key for providing the eukaryotic cell with rigidity, tracks for cargo transport, machinery for segregating the DNA during cell division, and energy for motility.

Unlike their eukaryotic counterparts, with their large cytoskeletal structures such as the microtubule spindle, bacteria were long assumed to be simply “bags of enzymes,” lacking key properties allowing for spatial organization, including the cytoskeleton. It was not until about twenty years ago that the prokaryotic origin of the cytoskeleton finally became clear (Lowe and Amos, 1998; van den Ent et al., 2001). Since then, scores of homologs of tubulin, actin, and intermediate filaments have been identified in bacteria (Cabeen and Jacobs-Wagner, 2010; Derman et al., 2009; Michie and Lowe, 2006; Thanbichler and Shapiro, 2008). In recent years, it has even become apparent how bacteriophage can utilize cytoskeletal proteins to their advantage (Munoz-Espin et al., 2009).

A critical property of cytoskeletal polymers is their ability to dynamically assemble and disassemble. Tubulins and actins do this by harnessing the energy from nucleotide hydrolysis. This allows the filaments to grow and shrink, from one end or both, and to rearrange themselves in space in order to perform their functions.

I will now give a brief overview of the properties of members of each of these three main cytoskeletal families, with added emphasis on the tubulins, the main topic of this thesis:

## **Actins**

### Eukaryotic Actin

Eukaryotic actin filaments, sometimes called microfilaments, are the smallest of the eukaryotic cytoskeletal filaments at 5-9 nm in diameter. Actin monomers, G-actin, self-associate into polar, two-stranded, helical filaments (F-actin) in the presence of ATP. *In vivo* actin filaments are found in bundles in stress fibers, in a branched network in the lamellapodium, and the actomyosin cytokinetic ring. A multitude of actin-related and actin-binding proteins tightly control actin filament polymerization and depolymerization within the cell. Since the regulation of the actin cytoskeleton by a myriad of proteins is so essential for proper cellular function, actin is one of the most highly conserved proteins in eukaryotes, possessing 87% identity between yeast and human actin.

*In vitro* actin filaments polymerize very slowly. They also exhibit filament treadmilling, wherein one end of the filament grows faster (the plus, pointed end) than the other (the barbed, minus end) while the length of the filament is maintained. F-actin also does not necessarily require the energy from ATP to polymerize, with only an ~3 fold difference in critical concentration between ATP-actin and ADP-actin (Pollard, 1986). Actin undergoes a nucleotide-

dependent conformational change, in which the clamshell shape of actin closes (Chen et al., 2013), allowing ATP-actin to more readily incorporate into filaments.

### Prokaryotic Actins

MreB was the first actin-like protein (Alp) to be identified in bacteria (van den Ent et al., 2001). MreB is required conferring the shape of rod shaped bacteria (Wachi et al., 1987). Although originally proposed to form a spiral structure within the cell (Jones et al., 2001), it is now clear does not form continuous filaments (Dominguez-Escobar et al., 2011; Garner et al., 2011; van Teeffelen et al., 2011). The state of these filaments, how they are directly playing a role in cell shape, and the role of ATP are all still unanswered questions. Since the identification of MreB as an Alp, over 40 prokaryotic actins have been identified (Derman et al., 2009). Many of these proteins are involved in plasmid stabilization (e.g. ParM, AlfA, Alp7A), but have roles as diverse as aligning magnetic sensing “organelles.”

A striking difference between Alps and eukaryotic actin is their extreme diversity in polymer dynamics. In contrast to actin, most known Alps can rapidly assemble spontaneously (Garner et al., 2004; Polka et al., 2009). Few binding proteins are required for their spatiotemporal organization as well. Like eukaryotic actin, all known Alps also form two-stranded filaments (Orlova et al., 2007; Ozyamak et al., 2013; Polka et al., 2009).

## **Intermediate Filaments**

### Eukaryotic Intermediate Filaments

Intermediate filaments get their name from being of intermediate size between actin filaments and microtubules. Unlike actins and tubulins (discussed below), intermediate filaments

do not rely on the energy from nucleotide hydrolysis to assemble as disassemble. Intermediate filaments are formed by coiled-coil interactions between the individual proteins and form non-polar, overlapping tetramers. As such, intermediate filaments are strong, bendable filaments, which provide a large amount of structure to the nucleus (via the nuclear lamins), cell junctions, and the cytoplasm.

### Prokaryotic Intermediate Filaments

Intermediate filaments were the last class of cytoskeletal proteins identified to have a prokaryotic homolog with the discovery of crescentin. Crescentin is found on the genome of the curved-shaped rod bacterium *Caulobacter crescentus*, and was found to be involved in determining the curved shape of the cell (Ausmees et al., 2003). Crescentin localized to the inner cell curvature in *C. crescentus*, and it appears to mechanically cause curvature through interactions with the membrane and cell wall (Cabeen et al., 2009; Kim and Sun, 2009). Similarly to its eukaryotic counterparts, Crescentin appears to directly apply mechanical force without the energy of nucleotide hydrolysis. Intermediate filaments have now been described in bacteria other than *C. crescentus* (Bagchi et al., 2008), but their function is less well understood.

## **Tubulins**

### Eukaryotic tubulins

In eukaryotes, the microtubule cytoskeleton is made up of hollow polymers of  $\alpha/\beta$ -tubulin heterodimers.  $\alpha/\beta$ -tubulin exist as an obligate heterodimer, which associate laterally and longitudinally to form 13 protofilament microtubules *in vivo*. In cells, microtubules are critical tracks for shipping cargo and segregating sister chromatids during mitosis. In order to localize

microtubules correctly, the cell employs microtubule-organizing centers (MTOCs) consisting of  $\gamma$ -tubulin complexes. MTOCs ensure that microtubules grow from specific, correct locations. There are other monomeric tubulins, such as  $\delta$ - and  $\epsilon$ -tubulin, whose roles are less well understood than  $\alpha$ -,  $\beta$ -, or  $\gamma$ -tubulin. Like actin, tubulins are highly conserved proteins, with sequence identity of  $\alpha/\beta$ -tubulin being >75% (Fygenon et al., 2004).

All tubulins share a conserved tubulin fold, with an N-terminal nucleotide-binding domain bridged by a long central helix, H7, to a globular activation domain containing the catalytic T7 loop (Nogales et al., 1998). The activation domain is followed by a pair of C-terminal helices, H11 and H12, which form the exterior surface of the microtubule. A key defining sequence of tubulins is the tubulin consensus sequence, or G-box, GGGTG(S/T)G. This sequence is key in coordinating the phosphate groups of the nucleotide. Beyond this consensus sequence and the catalytic T7 loop, few other residues are conserved. (Nogales et al., 1998)

$\alpha/\beta$ -tubulin heterodimers oligomerize into microtubules in a GTP-dependent manner. Only the nucleotide from  $\beta$ -tubulin is exchangeable, and it resides at the longitudinal interface in the protofilament. It is here, that the catalytic T7 loop comes into contact with the nucleotide (Nogales et al., 1995). This enables tubulins to directly couple polymerization and nucleotide hydrolysis. This leads to the existence of a GTP cap, wherein the newest layers of the microtubule consist of GTP-bound subunits and the body of the microtubule lattice contains GDP bound subunits (Mitchison and Kirschner, 1984). The GTP cap allows microtubules to possess the property of dynamic instability – the stochastic switching between rapid growth and disassembly (Mitchison and Kirschner, 1984). How microtubules use the energy from GTP hydrolysis for dynamic instability has been a hotly contested issue.

Although tubulin's requirement of GTP for polymerization has been known for a long time, the detailed role of GTP and its hydrolysis in tubulin polymerization and metastability has remained contested. Tubulin has been found to exist in two distinct conformations structurally: curved (Aldaz et al., 2005; Ayaz et al., 2012; Ravelli et al., 2004) and straight (Lowe et al., 2001), with a third, intermediate conformation now been shown (Peng et al., 2014). It has long been debated whether or not GTP binding directly modulates these conformations. Not long before I joined the lab, Dr. Luke Rice had showed that the microtubule lattice itself is likely acting as an allosteric regulator of tubulin conformation, not GTP (Rice et al., 2008). GTP binding allows  $\alpha/\beta$ -tubulin to more easily access the straight conformation and overcome the energy barrier to entering the filament. Once in the microtubule, the GDP dimers in the straight conformation build up strain, which allows the energy from GTP to be stored in the lattice. Subsequently, this allows for catastrophic depolymerization upon loss of a stabilizing GTP cap.

Even though the lattice model had been presented just before I started graduate school, there were still many unanswered questions. Is this a universal property of tubulins? What about the  $\gamma$ -phosphate allows for microtubule polymerization? Is it simply providing more binding energy at the longitudinal interface? Much of the Agard lab is still fascinated by these questions, especially the questions concerning how and where the cell makes new microtubules. The study of a diverse set of tubulins can help shed light on some of these questions about the tubulin family.

### FtsZ

The first identified tubulin homolog in prokaryotes was FtsZ, which is ubiquitous in bacteria. Due to having extremely low sequence homology (~15%), it was not until structures of

both  $\alpha/\beta$ -tubulin and FtsZ were solved that FtsZ was confirmed to be members of the same protein superfamily (Lowe and Amos, 1998; Nogales et al., 1998). FtsZ forms the center of the bacterial divisome, forming a dynamic ring structure at mid-cell required for proper septation, recruiting many proteins (de Boer, 2010; Lowe and Amos, 2009; Lutkenhaus, 2007). The *in vivo* structure of the Z-ring is still hotly debated, but GTP hydrolysis by FtsZ is necessary for proper function (Holden et al., 2014; Li et al., 2007; Meier and Goley, 2014). There is also still a large amount of debate surrounding if and how much force FtsZ filaments generate.

*In vitro*, FtsZ filaments can form a wide variety of structures from single filaments, to spirals, to sheets. These filaments do not appear to undergo dynamic instability, and they may well treadmill with the help of FtsZ binding partners (Loose and Mitchison, 2014). Unlike other tubulins, FtsZ is believed to polymerize as single protofilaments, which are straight in their GTP form and curved in their GDP form (Lu et al., 2000). Just as with  $\alpha/\beta$ -tubulin, the answers to questions surrounding the role of nucleotide-state and GTP in FtsZ filament polymerization remain murky. Structures of FtsZ in various nucleotide-states from a variety of species showed that FtsZ monomers did not appear to undergo a nucleotide-dependent conformational change (Oliva et al., 2007). More recently, there have been implications that the FtsZ monomer might, indeed, undergo a nucleotide-dependent conformational change, though this result needs to be further tested (Matsui et al., 2014). Recent work has also demonstrated that FtsZ filaments might undergo a hinge opening after hydrolyzing GTP, leading to the curving of filaments (Li et al., 2013). Although this may be the case, FtsZ filaments all have been shown to polymerize using the same longitudinal interactions as in  $\alpha/\beta$ -tubulin. More work will need to be carried out to determine if FtsZ filaments apply a force during septation, and how the energy from GTP is being used in filament polymerization and dynamics.

## TubZ

TubZ was the first plasmid-encoded tubulin identified and is critical for maintaining the stability of large, low-copy number plasmids (Larsen et al., 2007). Unlike microtubules, TubZ does not display dynamic instability, instead treadmilling (Larsen et al., 2007). Although first described as solely forming two-stranded helical filaments similar to actins (Aylett et al., 2010; Chen and Erickson, 2008), it has recently become clear that TubZ filaments undergo a dramatic rearrangement from unstable two-stranded to stable four-stranded filaments upon the hydrolysis of GTP to GDP (Montabana and Agard, 2014). Although there is a dramatic nucleotide-dependent filament change, the change in the TubZ monomer conformation is minimal between the GTP- and GDP-filament states. It was also demonstrated that the C-terminus of TubZ is critical for filament nucleation (Montabana and Agard, 2014). Recently, TubZs have been identified on the genomes of bacteriophage that have a plasmid-like lysogenic state (Oliva et al., 2012). There are many interesting directions the study of TubZ can go to further understand the control of filament dynamics, which will have insight for not only TubZ, but the tubulin superfamily as well.

## BtubA/BtubB

BtubA/BtubB is a curious pair of tubulin homologs encoded on the genome of *Prostheco bacter dejongeei*. They are more closely related to  $\alpha/\beta$ -tubulin than any other prokaryotic tubulin (~35% sequence identity) (Jenkins et al., 2002). Not only are they more closely related to  $\alpha/\beta$ -tubulin in sequence, but they have a structure more similar and require each other to polymerize as well (Schlieper et al., 2005; Sontag et al., 2005). Although their



function is still unknown, BtubA/BtubB appear to form five-stranded tubes (Pilhofer et al., 2011) and may be a simpler model system for gaining molecular insights into the polymerization and evolution of  $\alpha/\beta$ -tubulin.

## PhuZ

At the time I joined the Agard lab, the lab of Dr. Joe Pogliano (UCSD) identified a new tubulin superfamily member, PhuZ, for phage tubulin/FtsZ, encoded on the genomes of very large *Pseudomonas* phage. Encoded on the genomes of  $\Phi$ KZ family phage, PhuZ presented a unique problem to undertake. We were interested in expanding our understanding of tubulin family members, and PhuZ presented both a new tubulin as well as a new biological system – it was the first identified tubulin encoded by a bacteriophage.

This thesis seeks to address 4 main questions: 1) What is the role of PhuZ in the phage “life” cycle, 2) What are the structural determinants of PhuZ polymerization and what do the filaments look like, 3) What are the dynamics of PhuZ filaments, and 4) How are these dynamics controlled by GTP on a molecular level. Chapter 2 outlines the discovery of PhuZ, the preliminary characterization of PhuZ filaments, the monomer structure PhuZ detailing a unique C-terminal tail required for polymerization, and the role of PhuZ in centering phage DNA. Chapter 3 discusses the high-resolution cryo-EM structure of the three-stranded PhuZ filament, revealing more roles for the C-terminal tail and a possible mechanism for filament metastability. Chapter 4 covers the identification of PhuZ dynamic instability, filament polarity, and the formation of a bipolar spindle. Chapter 5 covers preliminary experiments towards gaining a high-resolution understanding of the role of GTP and PhuZ GTPase activity in filament polymerization and dynamics. Chapter 6 briefly discusses potential future directions.

## References

- Aldaz, H., Rice, L.M., Stearns, T., and Agard, D.A. (2005). Insights into microtubule nucleation from the crystal structure of human gamma-tubulin. *Nature* *435*, 523-527.
- Ausmees, N., Kuhn, J.R., and Jacobs-Wagner, C. (2003). The bacterial cytoskeleton: an intermediate filament-like function in cell shape. *Cell* *115*, 705-713.
- Ayaz, P., Ye, X., Huddleston, P., Brautigam, C.A., and Rice, L.M. (2012). A TOG:alphabeta-tubulin complex structure reveals conformation-based mechanisms for a microtubule polymerase. *Science* *337*, 857-860.
- Aylett, C.H., Wang, Q., Michie, K.A., Amos, L.A., and Lowe, J. (2010). Filament structure of bacterial tubulin homologue TubZ. *Proceedings of the National Academy of Sciences of the United States of America* *107*, 19766-19771.
- Bagchi, S., Tomenius, H., Belova, L.M., and Ausmees, N. (2008). Intermediate filament-like proteins in bacteria and a cytoskeletal function in *Streptomyces*. *Molecular microbiology* *70*, 1037-1050.
- Cabeen, M.T., Charbon, G., Vollmer, W., Born, P., Ausmees, N., Weibel, D.B., and Jacobs-Wagner, C. (2009). Bacterial cell curvature through mechanical control of cell growth. *The EMBO journal* *28*, 1208-1219.
- Cabeen, M.T., and Jacobs-Wagner, C. (2010). The bacterial cytoskeleton. *Annual review of genetics* *44*, 365-392.
- Chen, X., Ni, F., Tian, X., Kondrashkina, E., Wang, Q., and Ma, J. (2013). Structural basis of actin filament nucleation by tandem W domains. *Cell reports* *3*, 1910-1920.

Chen, Y., and Erickson, H.P. (2008). In vitro assembly studies of FtsZ/tubulin-like proteins (TubZ) from Bacillus plasmids: evidence for a capping mechanism. *The Journal of biological chemistry* 283, 8102-8109.

de Boer, P.A. (2010). Advances in understanding E. coli cell fission. *Current opinion in microbiology* 13, 730-737.

Derman, A.I., Becker, E.C., Truong, B.D., Fujioka, A., Tucey, T.M., Erb, M.L., Patterson, P.C., and Pogliano, J. (2009). Phylogenetic analysis identifies many uncharacterized actin-like proteins (Alps) in bacteria: regulated polymerization, dynamic instability and treadmilling in Alp7A. *Molecular microbiology* 73, 534-552.

Dominguez-Escobar, J., Chastanet, A., Crevenna, A.H., Fromion, V., Wedlich-Soldner, R., and Carballido-Lopez, R. (2011). Processive movement of MreB-associated cell wall biosynthetic complexes in bacteria. *Science* 333, 225-228.

Frixione, E. (2000). Recurring views on the structure and function of the cytoskeleton: a 300-year epic. *Cell motility and the cytoskeleton* 46, 73-94.

Fygenon, D.K., Needleman, D.J., and Sneppen, K. (2004). Variability-based sequence alignment identifies residues responsible for functional differences in alpha and beta tubulin. *Protein science : a publication of the Protein Society* 13, 25-31.

Garner, E.C., Bernard, R., Wang, W., Zhuang, X., Rudner, D.Z., and Mitchison, T. (2011). Coupled, circumferential motions of the cell wall synthesis machinery and MreB filaments in B. subtilis. *Science* 333, 222-225.

Garner, E.C., Campbell, C.S., and Mullins, R.D. (2004). Dynamic instability in a DNA-segregating prokaryotic actin homolog. *Science* 306, 1021-1025.

Holden, S.J., Pengo, T., Meibom, K.L., Fernandez Fernandez, C., Collier, J., and Manley, S. (2014). High throughput 3D super-resolution microscopy reveals *Caulobacter crescentus* in vivo Z-ring organization. *Proceedings of the National Academy of Sciences of the United States of America* *111*, 4566-4571.

Jenkins, C., Samudrala, R., Anderson, I., Hedlund, B.P., Petroni, G., Michailova, N., Pinel, N., Overbeek, R., Rosati, G., and Staley, J.T. (2002). Genes for the cytoskeletal protein tubulin in the bacterial genus *Prostheco bacter*. *Proceedings of the National Academy of Sciences of the United States of America* *99*, 17049-17054.

Jones, L.J., Carballido-Lopez, R., and Errington, J. (2001). Control of cell shape in bacteria: helical, actin-like filaments in *Bacillus subtilis*. *Cell* *104*, 913-922.

Kim, J.S., and Sun, S.X. (2009). Morphology of *Caulobacter crescentus* and the Mechanical Role of Crescentin. *Biophysical journal* *96*, L47-49.

Larsen, R.A., Cusumano, C., Fujioka, A., Lim-Fong, G., Patterson, P., and Pogliano, J. (2007). Treadmilling of a prokaryotic tubulin-like protein, TubZ, required for plasmid stability in *Bacillus thuringiensis*. *Genes & development* *21*, 1340-1352.

Li, Y., Hsin, J., Zhao, L., Cheng, Y., Shang, W., Huang, K.C., Wang, H.W., and Ye, S. (2013). FtsZ protofilaments use a hinge-opening mechanism for constrictive force generation. *Science* *341*, 392-395.

Li, Z., Trimble, M.J., Brun, Y.V., and Jensen, G.J. (2007). The structure of FtsZ filaments in vivo suggests a force-generating role in cell division. *The EMBO journal* *26*, 4694-4708.

Loose, M., and Mitchison, T.J. (2014). The bacterial cell division proteins FtsA and FtsZ self-organize into dynamic cytoskeletal patterns. *Nature cell biology* *16*, 38-46.

Lowe, J., and Amos, L.A. (1998). Crystal structure of the bacterial cell-division protein FtsZ. *Nature* *391*, 203-206.

Lowe, J., and Amos, L.A. (2009). Evolution of cytomotive filaments: the cytoskeleton from prokaryotes to eukaryotes. *The international journal of biochemistry & cell biology* *41*, 323-329.

Lowe, J., Li, H., Downing, K.H., and Nogales, E. (2001). Refined structure of alpha beta-tubulin at 3.5 Å resolution. *Journal of molecular biology* *313*, 1045-1057.

Lu, C., Reedy, M., and Erickson, H.P. (2000). Straight and curved conformations of FtsZ are regulated by GTP hydrolysis. *Journal of bacteriology* *182*, 164-170.

Lutkenhaus, J. (2007). Assembly dynamics of the bacterial MinCDE system and spatial regulation of the Z ring. *Annual review of biochemistry* *76*, 539-562.

Matsui, T., Han, X., Yu, J., Yao, M., and Tanaka, I. (2014). Structural change in FtsZ Induced by intermolecular interactions between bound GTP and the T7 loop. *The Journal of biological chemistry* *289*, 3501-3509.

Meier, E.L., and Goley, E.D. (2014). Form and function of the bacterial cytokinetic ring. *Current opinion in cell biology* *26*, 19-27.

Michie, K.A., and Lowe, J. (2006). Dynamic filaments of the bacterial cytoskeleton. *Annual review of biochemistry* *75*, 467-492.

Mitchison, T., and Kirschner, M. (1984). Dynamic instability of microtubule growth. *Nature* *312*, 237-242.

Montabana, E.A., and Agard, D.A. (2014). Bacterial tubulin TubZ-Bt transitions between a two-stranded intermediate and a four-stranded filament upon GTP hydrolysis. *Proceedings of the National Academy of Sciences of the United States of America* *111*, 3407-3412.

Munoz-Espin, D., Daniel, R., Kawai, Y., Carballido-Lopez, R., Castilla-Llorente, V., Errington, J., Meijer, W.J., and Salas, M. (2009). The actin-like MreB cytoskeleton organizes viral DNA replication in bacteria. *Proceedings of the National Academy of Sciences of the United States of America*.

Nogales, E., Downing, K.H., Amos, L.A., and Lowe, J. (1998). Tubulin and FtsZ form a distinct family of GTPases. *Nature structural biology* *5*, 451-458.

Nogales, E., Wolf, S.G., Khan, I.A., Luduena, R.F., and Downing, K.H. (1995). Structure of tubulin at 6.5 Å and location of the taxol-binding site. *Nature* *375*, 424-427.

Oliva, M.A., Martin-Galiano, A.J., Sakaguchi, Y., and Andreu, J.M. (2012). Tubulin homolog TubZ in a phage-encoded partition system. *Proceedings of the National Academy of Sciences of the United States of America* *109*, 7711-7716.

Oliva, M.A., Trambaiolo, D., and Lowe, J. (2007). Structural insights into the conformational variability of FtsZ. *Journal of molecular biology* *373*, 1229-1242.

Orlova, A., Garner, E.C., Galkin, V.E., Heuser, J., Mullins, R.D., and Egelman, E.H. (2007). The structure of bacterial ParM filaments. *Nature structural & molecular biology* *14*, 921-926.

Ozyamak, E., Kollman, J., Agard, D.A., and Komeili, A. (2013). The bacterial actin MamK: in vitro assembly behavior and filament architecture. *The Journal of biological chemistry* *288*, 4265-4277.

Peng, L.X., Hsu, M.T., Bonomi, M., Agard, D.A., and Jacobson, M.P. (2014). The free energy profile of tubulin straight-bent conformational changes, with implications for microtubule assembly and drug discovery. *PLoS computational biology* *10*, e1003464.

Pilhofer, M., Ladinsky, M.S., McDowall, A.W., Petroni, G., and Jensen, G.J. (2011). Microtubules in bacteria: Ancient tubulins build a five-protofilament homolog of the eukaryotic cytoskeleton. *PLoS biology* 9, e1001213.

Polka, J.K., Kollman, J.M., Agard, D.A., and Mullins, R.D. (2009). The structure and assembly dynamics of plasmid actin AlfA imply a novel mechanism of DNA segregation. *Journal of bacteriology* 191, 6219-6230.

Pollard, T.D. (1986). Rate constants for the reactions of ATP- and ADP-actin with the ends of actin filaments. *The Journal of cell biology* 103, 2747-2754.

Ravelli, R.B., Gigant, B., Curmi, P.A., Jourdain, I., Lachkar, S., Sobel, A., and Knossow, M. (2004). Insight into tubulin regulation from a complex with colchicine and a stathmin-like domain. *Nature* 428, 198-202.

Rice, L.M., Montabana, E.A., and Agard, D.A. (2008). The lattice as allosteric effector: structural studies of alphabeta- and gamma-tubulin clarify the role of GTP in microtubule assembly. *Proceedings of the National Academy of Sciences of the United States of America* 105, 5378-5383.

Schlieper, D., Oliva, M.A., Andreu, J.M., and Lowe, J. (2005). Structure of bacterial tubulin BtubA/B: evidence for horizontal gene transfer. *Proceedings of the National Academy of Sciences of the United States of America* 102, 9170-9175.

Sontag, C.A., Staley, J.T., and Erickson, H.P. (2005). In vitro assembly and GTP hydrolysis by bacterial tubulins BtubA and BtubB. *The Journal of cell biology* 169, 233-238.

Thanbichler, M., and Shapiro, L. (2008). Getting organized--how bacterial cells move proteins and DNA. *Nature reviews Microbiology* 6, 28-40.

van den Ent, F., Amos, L.A., and Lowe, J. (2001). Prokaryotic origin of the actin cytoskeleton. *Nature* *413*, 39-44.

van Teeffelen, S., Wang, S., Furchtgott, L., Huang, K.C., Wingreen, N.S., Shaevitz, J.W., and Gitai, Z. (2011). The bacterial actin MreB rotates, and rotation depends on cell-wall assembly. *Proceedings of the National Academy of Sciences of the United States of America* *108*, 15822-15827.

Wachi, M., Doi, M., Tamaki, S., Park, W., Nakajima-Iijima, S., and Matsubishi, M. (1987). Mutant isolation and molecular cloning of mre genes, which determine cell shape, sensitivity to mecillinam, and amount of penicillin-binding proteins in *Escherichia coli*. *Journal of bacteriology* *169*, 4935-4940.



## Chapter Two

### **A phage tubulin assembles dynamic filaments by a novel mechanism to center viral DNA within the host cell**

James A Kraemer<sup>1,\*</sup>, Marcella L Erb<sup>2,\*</sup>, Christopher A Waddling<sup>1</sup>, Elizabeth A Montabana<sup>1</sup>,  
Elena A Zehr<sup>1</sup>, Hannah Wang<sup>2</sup>, Katrina Nguyen<sup>2</sup>, Duy Stephen L Pham<sup>1,3</sup>, David A Agard<sup>1</sup>, and  
Joe Pogliano<sup>2</sup>

<sup>1</sup>Department of Biochemistry and Biophysics and the Howard Hughes Medical Institute,  
University of California, San Francisco, CA 94158

<sup>2</sup>Division of Biological Sciences, University of California, San Diego, CA 92093

<sup>3</sup>Current address: Department of Chemistry and Biochemistry, University of California, Los  
Angeles, CA 90095

\*These authors contributed equally

This work was previously published in *Cell* and is reprinted here with permission.

## Abstract

Tubulins are essential for the reproduction of many eukaryotic viruses, but historically bacteriophage were assumed not to require a cytoskeleton. Here we identify a tubulin-like protein, PhuZ, from bacteriophage 201 $\phi$ 2-1 and show that it forms filaments *in vivo* and *in vitro*. The PhuZ structure has a conserved tubulin fold, with a novel, extended C-terminus that we demonstrate to be critical for polymerization *in vitro* and *in vivo*. Longitudinal packing in the crystal lattice mimics packing observed by EM of *in vitro* formed filaments, indicating how interactions between the C-terminus and the following monomer drive polymerization. Finally, we show that PhuZ assembles a spindle-like array required for positioning phage DNA within the bacterial cell. Correct positioning to the cell center and optimal phage reproduction only occur when the PhuZ filament is dynamic. This is the first example of a prokaryotic tubulin array that functions analogously to the microtubule-based spindles of eukaryotes.

## Introduction

Long thought to be a defining eukaryotic feature, the cytoskeleton is now known to have evolved first in prokaryotes (Cabeen and Jacobs-Wagner, 2010; Michie and Lowe, 2006; Thanbichler and Shapiro, 2008). Prokaryotic actin and tubulin homologs possess low protein sequence identity to their eukaryotic counterparts; however, the degree of structural homology is quite high. The cell shape determining protein MreB, for example, is structurally similar to actin even though it only shares limited sequence identity within residues that line the nucleotide-binding pocket (Thanbichler and Shapiro, 2008; van den Ent et al., 2001). Since the discovery of MreB, >35 families of actin homologues have been identified that perform a diverse set of functions from forming scaffolds to actively segregating DNA (Derman et al., 2009; Thanbichler and Shapiro, 2008). Despite having similar monomeric structures, many of these actins have evolved unique biochemical properties and form filaments with distinct structural features (Becker et al., 2006; Derman et al., 2009; Polka et al., 2009; Popp et al., 2010; Rivera et al., 2011).

While it is now clear that a key feature of the bacterial actin cytoskeleton is its remarkable diversity of sequence and function, relatively few families of tubulin-like proteins have been characterized in prokaryotes, raising the question of whether bacterial tubulins are similarly biochemically and structurally diverse. The most widely conserved bacterial tubulin is FtsZ, which is found in nearly all bacteria and many archaea. FtsZ assembles an essential component of the cytokinetic ring required for septation (de Boer, 2010; Lowe and Amos, 2009; Lutkenhaus, 2007; Margolin, 2009). Besides FtsZ, two other families of bacterial tubulin-like proteins (BtubA/BtubB and TubZ) have been characterized. BtubA/BtubB of *Prostheco bacter dejongeii* are closely related to  $\alpha/\beta$ -tubulin, but their functions are currently unknown (Schlieper

et al., 2005; Sontag et al., 2005). TubZ actively segregates large, low copy number plasmids of many *Bacillus* species by interaction with the TubR DNA binding protein and the *tubC* locus (Anand et al., 2008; Larsen et al., 2007; Ni et al., 2010). Structures of TubZ and FtsZ reveal a striking conservation of the tubulin fold even though the degree of primary sequence homology to eukaryotic tubulin is extremely low (<14%) (Aylett et al., 2010; Lowe and Amos, 1998; Ni et al., 2010; Nogales et al., 1998a). Inter-subunit longitudinal contacts within filaments have been mostly conserved throughout the tubulin families, whereas other contacts appear to be more divergent (Aylett et al., 2010; Lowe and Amos, 2009).

Here we report a novel family of divergent tubulins, named “PhuZ” for Phage Tubulin/FtsZ, encoded within phage genomes. We characterize one member of this family (GP59) from *Pseudomonas chlororaphis* phage 201 $\phi$ 2-1 (Thomas et al., 2008). Isolated from soil samples in 2001, 201 $\phi$ 2-1 is one of the largest phage genomes in Genbank at 316 kb. We determined the structure of PhuZ to 1.67 Å resolution and characterized PhuZ polymerization *in vivo* and *in vitro*. We show that PhuZ assembles dynamic polymers required for positioning phage DNA at the cell center, and that accurate positioning is important for phage reproduction.

## Results

### Identification of phage encoded family of tubulins, PhuZ

We surveyed the genomic database and found a number of tubulin-like protein sequences encoded within several different phage genomes. A phylogenetic tree demonstrates that these phage-encoded tubulins are extraordinarily diverse and are only distantly related to the cell division protein FtsZ and the plasmid segregation protein TubZ (Figure 1A,B). All of the phage genomes encoding these tubulins are very large, ranging from 186 to 316 kb and they infect both Gram negative and Gram positive bacteria. Although many of these phage have been characterized previously, no evidence for a tubulin-based cytoskeletal polymer has been reported.

### PhuZ forms dynamic filaments *in vivo* and *in vitro*

To study one of these novel tubulin-like proteins and determine if it had the ability to polymerize *in vivo*, we generated a GFP fusion to the *phuZ* gene (*gp59*) from phage 201φ2-1 and expressed it from the arabinose promoter (Qiu et al., 2008) on a plasmid in *Pseudomonas chlororaphis*. When expressed at 30°C at low levels (0.15% or 0.25% arabinose), fluorescence from GFP-PhuZ was uniform throughout the cell (Figure 2A). As the arabinose concentration increased, a threshold concentration (0.4%) was reached where the majority of cells (82%) spontaneously assembled filaments (Figure 2A,E). Quantitation of GFP-PhuZ expression using in-gel fluorescence demonstrated that the fusion protein was full length and that expression increased linearly with arabinose concentration (Figure S1). When expressed just above the threshold inducer concentration for assembly (0.4%), cells contained multiple filaments (Figure

2A) that moved rapidly throughout the cell (Movie S1). At higher expression levels (1%), GFP-PhuZ filaments extended the entire length of the cell (Figure 2A).

To gain insight into the nature of PhuZ filaments observed *in vivo*, PhuZ was expressed recombinantly, purified (Figure S2A) and its *in vitro* polymer growth kinetics examined by right-angle light scattering. As with other tubulins, PhuZ polymerizes in a GTP-dependent manner, with no polymerization observed in the presence of GDP (Figure 3A). It also displays a lag phase characteristic of a nucleation-extension mechanism of polymer growth. As expected, the length of the lag phase and maximum signal at the plateau are proportional to the concentration of PhuZ, from which we determine the critical concentration to be  $2.8 \pm 0.1 \mu\text{M}$  (Figure S2B).

To assess the morphology of PhuZ filaments, PhuZ was polymerized *in vitro* in the presence of the non-hydrolyzable GTP analog GMPCPP and examined by negative-stain EM. Figure 3C shows a representative micrograph of individual PhuZ filaments together with high magnification views (also Figure S2). The morphology of PhuZ filaments is distinct from microtubules formed by tubulin and single-stranded filaments formed by FtsZ, but is reminiscent of the two-stranded, helical filaments formed by TubZ (Aylett et al., 2010; Chen and Erickson, 2008). Although crossover events are observed in the PhuZ filaments, they appear at irregular intervals, and their architecture is not immediately evident. Further EM analysis will be required to determine the detailed structure of the filaments.

### **Structure of the PhuZ-GDP monomer**

To better understand the similarities and differences between PhuZ and other tubulins, crystals of wild-type and Se-Met PhuZ were grown in the presence of GDP and the structure of Se-Met PhuZ was solved by MAD phasing (Table S1) and subsequently refined using the  $1.67 \text{ \AA}$

resolution, wild-type PhuZ-GDP data (Figure 4A). The initial  $2F_o-F_c$  electron density maps at 1.67Å showed strong density for GDP in the nucleotide-binding pocket (Figure 4B). As in other tubulins, the structure of PhuZ consists of two domains: an N-terminal domain containing the nucleotide binding pocket (Figure 4B) and C-terminal domain, bridged by a long, central helix, H7. Notably, a short loop replaces the normally highly conserved tubulin inter-domain helix, H6. The structure of PhuZ represents the first tubulin homologue in which all of the C-terminal residues have been observed, revealing that they form an extended C-terminal tail (residues 295-315) appended to a long helix, H11. Overlays of the PhuZ backbone structure with those of  $\alpha$ -tubulin (Nogales et al., 1998b), *Aquifex aeolicus* FtsZ (Oliva et al., 2007), and TubZ (Aylett et al., 2010) result in calculated RMSD values of 2.9, 2.6, and 2.9 Å, respectively (Figure S3). The PhuZ structure is too divergent from  $\alpha\beta$ -tubulin to unambiguously determine if this represents a straight or curved conformation.

Although the tertiary structure of PhuZ is highly consistent with the structure of other tubulin family members, there are several notable differences. As in tubulins, PhuZ lacks the N-terminal extension present in both FtsZ and TubZ. Surprisingly, H6, which makes key longitudinal contacts in forming tubulin and FtsZ protofilaments (Downing and Nogales, 1998) is missing in PhuZ. The absence of H6 leaves an acidic surface patch in its place (Figure S3D). The PhuZ C-terminal domain is smaller in size than in other tubulin family members due to smaller loops and helices, especially H10. Like TubZ, PhuZ contains a long helix, H11, after the conserved C-terminal domain (Aylett et al., 2010; Ni et al., 2010).

**The nucleotide-binding pocket is conserved and contains key catalytic residues required for polymer dynamics**

Within the highly conserved nucleotide-binding pocket (Figure 4A,B), backbone nitrogen atoms in loops L1 and L4 coordinate the phosphates. While the GQxG motif in L1 is conserved across eukaryotic tubulins and TubZ, in PhuZ, L1 contains the sequence 11-GGTG-14, replacing the conserved Gln with a Gly, as in FtsZ (Figure 1B). As a consequence, the L1 loop has a tighter turn leading into H1. How this affects nucleotide binding is unclear. The GGGTGT/SG tubulin consensus sequence, or G-box, in L4 is also slightly varied to 91-GGGSGSV-97 in PhuZ (Figure 1B), although the presence of the Val side chain does not appear to affect the conserved structural elements (Figure S3). As expected, the nucleotide base pi-stacks with Y161 and hydrogen-bonds with N16, N155, and N165 (Figure 4B). Residues S89, E122, N126, and Y161, plus two water molecules, all provide hydrogen-bonding interactions with the sugar. These interactions are consistent with the highly conserved nucleotide binding-mode of other tubulins.

The catalytic loop, T7, which normally inserts itself into the nucleotide-binding pocket of the preceding longitudinal monomer to aid in GTP hydrolysis, is modified from the GxxNx DxxD/E tubulin/FtsZ consensus sequence to NxxRx DxxD, although the key catalytic DxxD residues are conserved. To confirm the functional assignment of these aspartates, they were separately mutated to alanines. Similar mutations in TubZ and FtsZ compromise GTP hydrolysis but not GTP binding and as a result, the mutant proteins form long static polymers (Larsen et al., 2007; Lu et al., 2001). GFP-PhuZD187A (Figure S4A) and D190A (Figure 2B-E) mutants were expressed from the arabinose promoter in *P. chlororaphis*. Both of the mutant proteins behaved similarly and were dramatically different from wild type. When expressed at low arabinose concentrations at 30°C (0.15%), both of the mutant proteins assembled short polymers in approximately 80% of the cells, suggesting that they had a lower threshold concentration for assembly (Figure 2B, E, S3). There was also no detectable accumulation of



diffuse fluorescence in the background of the cells and a significant percentage of cells (10% for D187A and 18% D190A) assembled filaments even when no arabinose was present, suggesting that even the smallest amount of expressed protein assembled polymers (Figure 2E, S3). When expressed at higher levels (0.4% arabinose), both mutants formed long filaments that often chained the cells together (Figure 2C). In contrast to wild type filaments, the mutant filaments appeared relatively immobile in time-lapse experiments (Movie S2). We used FRAP to quantitate turnover dynamics within these mutant filaments. Unlike wild-type filaments (Figure S4B), no recovery or movement of the bleached zone over time (Figure 2D; Movie S3) was observed in the mutants, even after extended periods, indicating that the filaments are completely static. These results are consistent with an essential role for these two residues for PhuZ GTP hydrolysis and polymerization dynamics.

### **PhuZ forms a filament in the crystal with longitudinal spacing consistent EM observations**

Figure 5A shows PhuZ surrounded by its four symmetry-related molecules in the crystal, revealing two parallel protofilaments, related by  $2_1$  crystallographic symmetry. We propose that the intermolecular contacts, especially the longitudinal contacts, observed in the crystal are informative for those made within a PhuZ filament. Like all other tubulin-like proteins, the nucleotide resides at the longitudinal monomer-monomer interface. However, the longitudinal spacing of 47 Å between monomers observed in the crystal lattice is 3-7 Å longer than that of  $\alpha/\beta$ -tubulin (Nogales et al., 1998b), FtsZ (Oliva et al., 2004; Oliva et al., 2007), or TubZ (Aylett et al., 2010), resulting in the smallest longitudinal interface seen among tubulins. In PhuZ, terminal side chain atoms of only ten residues in the longitudinal interface lose solvent accessible surface area due to crystal packing, burying only 188 Å<sup>2</sup>/monomer as compared with typical

values of 1666 and 1034 Å<sup>2</sup> for α/β-tubulin and FtsZ respectively. While the gap between monomers is highly solvated, no single water directly contacts the two monomers, and no waters which bridge the two are resolved. This interaction mode is related to, but more extreme than the one observed for *A. aeolicus* FtsZ, which has a smaller interaction surface than other FtsZs at 655 Å<sup>2</sup> (Oliva et al., 2007). In both of these cases, interactions between the intermediate domain of one monomer and H10 of the other are missing. In PhuZ, the residues of the catalytic T7 loop do not appear to be positioned correctly for hydrolysis, with the catalytic Asp side chains being displaced by more than 3 Å from where expected if they were to be able to interact with the γ-phosphate. This is likely a consequence of the structure containing GDP, and there may well be changes in local conformation or monomer packing upon GTP binding.

Unlike eukaryotic tubulins, PhuZ does not make canonical lateral interactions. Instead, each PhuZ is rotated by 180° about an axis parallel to the filament and translated by 23.5 Å, resulting in interdigitated corner contacts defining a flat ribbon. Although roughly analogous to interactions in TubZ, the TubZ translation is significantly smaller and the rotation angle is ~190° (Aylett et al., 2010), resulting in a helical filament reminiscent of actin-like polymers. More precisely, the lateral corner contacts between PhuZ monomers are defined by interactions of H3 on one monomer with H4 and H5 on another (Figure 5A), with this interaction occurring twice so as to interact with two lateral PhuZ monomers, burying a total surface area of 476 Å<sup>2</sup> per monomer, stabilizing the connection between the two longitudinal protofilaments.

To assess the relevance of the putative filaments formed within the crystal lattice we compare more closely to the filaments seen by negative-stain EM (Figure 5C). Two-dimensional averages of 1000 defined segments were generated to produce a reliable view of monomer packing. Although the filament architecture is not yet clear, the average reveals a PhuZ filament

morphology similar to that observed in the crystals. Of particular importance, the longitudinal spacing derived from EM ( $\sim 45$  Å) is consistent with the 47 Å spacing in the crystal, supporting our hypothesis that the crystal lattice provides a suitable model for interactions stabilizing filament formation. This observed spacing is longer than observed for other tubulins, 40-42 Å, and would require a compaction of the lattice in order for the catalytic residues of the T7 loop to come into position for nucleotide hydrolysis. It is possible that the crystal lattice represents an expansion of the filament lattice that would occur after GTP is hydrolyzed to GDP.

### **The unique PhuZ C-terminal tail makes extensive interactions required for polymer formation**

By contrast with the minimal direct longitudinal interface, the 21 C-terminal residues make extensive contacts with the neighboring longitudinal monomer, with a total buried surface area of 1226 Å<sup>2</sup>/monomer. Many of these contacts are driven by either electrostatic or polar interactions (Figure 5B). The 13 most C-terminal residues of the protein contain six acidic residues (D303, D305, D306, D309, D311, E310) forming an acidic “knuckle” that is inserted into a basic patch of the longitudinal symmetry mate formed by helices H3, H4, and H5, containing R60, R68 and K135. Non-polar residues of the knuckle interact with L64, L104, and I140 on the symmetry mate providing further stabilization. While the most C-terminal residues make the most extensive contacts, significant interactions are also provided by the extended 8 residues that lie between Helix-11 and the knuckle, including significant interactions of R298 with E138, Q297 with Q207, and F295 with I227. These residues, especially the aspartic acids of the acid knuckle, are also conserved in the other PhuZ sequences (Figure 1C), suggesting that other phage tubulins may contain a similar C-terminal tail.

Given the extensive interactions contributed by the C-terminal tail, and the otherwise rather limited interactions that stabilize the longitudinal interface, the tail is likely quite important for polymer formation. To test this, we made two point mutants (R298A, D311A) to disrupt salt bridges as well as a truncation mutant,  $\Delta$ I302 that removed the last 13 residues (knuckle region) and examined the functional consequences *in vitro* by light scattering (Figure 3B). Even at a concentration of 20  $\mu$ M and in the presence of 1 mM GTP, PhuZ- $\Delta$ I302 was unable to form detectable polymer *in vitro*, whereas wild-type PhuZ polymerizes efficiently at concentrations above 5  $\mu$ M (Figure 3A,B). Similarly, both the R298A and D311A mutants, which disrupt salt bridge and H-bond formation with H5 and H11 and H3, respectively, also compromise *in vitro* filament formation, with no detectable polymerization at 20  $\mu$ M (Figure 3B).

These mutants were also tested for their ability to form polymers *in vivo* by expressing them in *P. chlororaphis*. GFP fusion proteins containing point mutations (D311A and R298A) in the tail were severely impaired for assembly and only formed polymers at the highest expression levels (1% or 2 % arabinose, Figure 5D,E & F). The C-terminal tail truncation ( $\Delta$ I302) completely abolished filament formation *in vivo* at all expression levels (Figure 5F). Using in-gel fluorescence we demonstrated that all of the C-terminal fusions were stably produced at the expected levels *in vivo* (Figure S1). These findings demonstrate the importance of the C-terminal 21 residues of PhuZ in polymerization.

**PhuZ assembles a dynamic spindle-like array during phage lytic growth.**

No specific role in the life cycle of a phage has ever been ascribed to a tubulin cytoskeletal protein. One anticipated function for PhuZ is as a DNA segregation system during lysogeny if 201 $\phi$ 2-1 replicates separately from the chromosome like a plasmid. While an attractive hypothesis, so far we have been unable to obtain lysogens of 201 $\phi$ 2-1 in *P. chlororaphis*. Therefore, we sought to determine if PhuZ was expressed and assembled polymers during lytic growth. First, we used RT-PCR to show that *phuZ* mRNA accumulates at two hours post infection (Figure S5A). Second, we devised a microscopic single cell assay to determine if PhuZ assembles polymers during an infection cycle. To accomplish this, *P. chlororaphis* cells were grown on an agarose pad at 30°C and GFP-PhuZ was expressed from the arabinose promoter below its critical threshold for assembly (0.15% arabinose at 30°C). We then infected cells with phage and performed time-lapse microscopy in which GFP-PhuZ assembly, phage production and phage-mediated cell lysis were simultaneously monitored. Since GFP-PhuZ does not spontaneously assemble polymers at this expression level, polymers would only be observed if additional PhuZ (or a regulator of PhuZ assembly) was expressed by the phage. By including DAPI and DNaseI in the pad, the release of phage upon cell lysis could be visualized. DNaseI degrades any remaining cellular DNA but not DNA packaged within viral capsids. At the terminal time point, after cells had lysed, we captured images of DAPI fluorescence, allowing the number of released phage particles to be counted. Cell lysis was detected using the membrane dye FM 4-64, which only faintly stains wild type *P. chlororaphis* but intensely stains cell debris.

In the first example (Figure 6A), GFP-PhuZ formed diffuse fluorescence at the beginning of the experiment (15 min after the addition of phage). Within 56 minutes, GFP-PhuZ assembled a polymer that extended from pole to pole (Figure 6A). This cell maintained at least one polymer

for the next 175 minutes, at which point the cell lysed. DAPI staining alongside DNaseI treatment confirmed that this cell had released phage particles, indicating that lysis was phage induced.

In the example shown in Figure 6B, GFP-PhuZ was expressed at a slightly higher level (0.25% arabinose) to allow for brighter images and more frequent time-points. At early time-points (18 min after phage addition) fluorescence was uniform, but over time, one (39 min) and then multiple (59 min) filaments formed (Figure 6B). Filaments were very dynamic (Figure 6B, Movie S4), undergoing cycles of assembly and disassembly, with at least one filament always assembled until the cell ultimately lysed.

To gain additional insight into the role of PhuZ polymers during lytic growth, we simultaneously visualized GFP-PhuZ and DNA in fixed cells that had been stained with DAPI. During lytic growth, cells became elongated and formed an unusual bulge at the cell midpoint (Figure 6C). DAPI staining revealed that the central bulge contained a high concentration of DNA, which we refer to as the "infection nucleoid", while the rest of the cell contained very little DNA (Figure 6C). In comparison, uninfected cells contained one or two vegetative nucleoids that filled the majority of the cytoplasm (Figure S5B). Quantitation showed that most cells contained just a single infection nucleoid (Figure 6K) that was located within 5% of the middle of the cell in 80% of cells and within 10% of the middle in 98% of cells (Figure 6I). PhuZ filaments frequently appeared to make contact with the edge of the infection nucleoid, forming an array on either side of this structure (Figure 6D). Multiple filaments of various lengths (ranging from 0.2 to 2 $\mu$ m) were observed in fixed cells (Figure 6D), as might be expected for a population of cells containing dynamic polymers trapped in various states of polymerization.

To determine if the centrally located DNA masses contained phage encapsidated DNA, we digested them with DNaseI. As shown in the examples in Figure 6E-G, upon DNaseI treatment, much of the centrally located DNA was degraded, leaving DNaseI resistant foci indicative of phage encapsidated DNA. PhuZ filaments were extended on each side of these DNA foci (Figure 6E). Optical sectioning revealed that these phage encapsidated DNA molecules occurred in a rosette-like structure at the edges of the digested nucleoid (Figure 6F and G; Movie S5), suggesting that phage DNA occurs in an organized structure at the cell mid point.

### **Dynamic filaments are required for phage positioning and maximal burst size**

Since the majority of phage infected cells contained PhuZ polymers that extended on each side of the centrally located infection nucleoid, we speculated that PhuZ participates in DNA organization or positioning. To test this idea, we examined DNA positioning in cells expressing either wild type GFP-PhuZ or a mutant version (GFP-PhuZD190A) that we demonstrated (Figure 2) assembles static polymers *in vivo*. In other tubulins, including TubZ (Larsen, et. al. 2007) and FtsZ (Lu, et.al. 2001), catalytic mutants defective in GTP hydrolysis co-assemble with the wild type and behave as dominant negatives. Positioning of the nucleoid during infection was severely affected by expression of GFP-PhuZD190A; only 39% of mutant cells positioned the infection nucleoid within 5% of the middle (compared to 80% for wild type; Figure 6I). In many cells, the PhuZD190A filaments appeared to make contact with the edge of an infection nucleoid that was mispositioned close to the cell pole (Figure 6H). Significant mispositioning occurred in the mutant cells regardless of their size (Figure 6J). In addition, while 94% of cells infected in the presence of wild type PhuZ had a single large nucleoid, more than a

third of infected cells expressing PhuZD190A contained either two or three nucleoids (Figure 6H, K), typically present at random positions, further indicating disruption of DNA localization. Taken together, these results suggest that PhuZ assembles a dynamic cytoskeletal element that functions to position phage at the cell midpoint during phage lytic growth.

To assess the importance of PhuZ to phage yield, we attempted population based phage growth curves, but phage infections rates were too low to make the results interpretable. We therefore performed single cell infection assays and found a significant decrease in burst size when cells expressed the PhuZD190A catalytic mutant, from an average of 16 phage per cell for wild type (n=25) to an average of 7 (n=25) for the mutant (p=0.0001). Proper phage centering by PhuZ thus contributes significantly to the efficiency of phage production. Such a 50% reduction in yield would be a significant evolutionary disadvantage.



## **Discussion**

### **Identification of a prokaryotic DNA positioning spindle**

Here we describe a phage encoded spindle-like array assembled from a distant relative of tubulin. No phage encoded actin or tubulin cytoskeletal element has been previously characterized and therefore the function of this protein was unclear. Since many phage replicate as plasmids during lysogenic growth, we initially suspected that the function and polymerization properties of PhuZ might be similar to those of the *Bacillus thuringiensis* plasmid segregation protein TubZ. Surprisingly, we found that PhuZ has both a completely novel structure and function that provide new paradigms for understanding the mechanism of tubulin polymerization and its cellular activity. We show that the C-terminal tail of PhuZ drives polymerization of a dynamic filament that positions phage DNA within the center of the cell, making it the first example of a prokaryotic cytoskeleton that performs a function analogous to the microtubule based spindle that positions chromosomes on the metaphase plate or tubulin cytoskeletal elements that position nuclei (Tran et al., 2001) in eukaryotes.

### **Unique features of the PhuZ monomer define polymer contacts**

Although the overall fold of PhuZ is tubulin-like, the structure of the monomer possesses key differences from tubulin/FtsZ/TubZ family members, leading to a unique filament organization. While the C-terminal extensions of other tubulins are known to be important interaction sites for accessory proteins that modulate polymer state, or otherwise affect function (e.g. microtubule-associated proteins (MAPs), FtsA, MinC, TubR), our results reveal that the PhuZ C-terminus has uniquely evolved a critical role in polymer formation, providing the vast majority of the buried surface area that stabilizes filament formation.

The other striking feature of PhuZ is the lack of helix H6. In other tubulins, the conserved H6 provides a surface for key longitudinal interactions between monomers. Lack of this helix in PhuZ leaves a large open surface on what we believe to be the outside of the polymer. In  $\alpha/\beta$ -tubulin, a concerted movement of helices 6 and 7 is key to the transition between the curved and straight conformations, which affects both the ease of incorporation into the growing microtubule lattice and the degree of metastability once GTP hydrolyzes. While it is unclear if motion of helix H7 is relevant to PhuZ function, it is intriguing to speculate that the acidic pocket created by the loss of helix H6 could serve as a binding surface for interacting proteins thereby coupling the binding to altered polymer dynamics.

The structure provides few clues as to how nucleotide controls PhuZ polymerization, though it suggests that it polymerizes through a novel mechanism for a tubulin family member. There is no indication that the C-terminal tail interactions, which dominate longitudinal association, are in any way modulated by nucleotide. The disordered L3 loop (residues 55-57) near where the  $\gamma$ -phosphate should bind may very well become ordered by GTP binding, but seems too distant from the next monomer to directly affect polymerization. It is quite possible that PhuZ undergoes a nucleotide-dependent conformational change, like that seen for TubZ. An interesting possibility for PhuZ is that the lattice might compact longitudinally with GTP, both enhancing “classical” longitudinal interactions and bringing the catalytic residues into proximity for hydrolysis. Thus, the potential of the C-terminal tail to provide a unique degree of flexibility in the longitudinal interface may be an important feature of the PhuZ polymer required for *in vivo* function and the control of its dynamics. Ultimately, it will be necessary to solve structures of PhuZ bound to other nucleotides, as well as in a non-polymer state, to gain mechanistic insight into the role of nucleotide binding and hydrolysis in polymer formation and dynamics.

### **Conservation of the PhuZ polymerization mechanism**

The C-terminal tail of PhuZ is conserved among a number of prokaryotic tubulins, including a set of *Clostridium* proteins (Figure 1C), which are otherwise highly divergent in sequence, suggesting that this mechanism of polymerization is not restricted to *Pseudomonas* phage. Among three *Pseudomonas* phage proteins and four *Clostridial* phage proteins, the acidic knuckle, the hydrophobic amino acids, and R298 are all conserved. Some of the amino acids that interact with the tail are also conserved, such as R60, which is conserved in all seven of these proteins. E138, which makes a salt bridge with R298, is also conserved among the *Pseudomonas* proteins, and although the *Clostridial* proteins lack E138, they contain a conserved aspartic acid residue nearby that could complete the salt bridge. Intriguingly, residues D303, D305 and D306 are highly conserved among these seven proteins, even though they all point out into the solvent in the structure, suggesting that they may be conserved for other protein-protein interactions. Curiously, GP16 of *Pseudomonas* phage EL is missing the conserved C-terminal tail amino acids (R298 and the IIDIDD motif), the corresponding salt bridge residues (R60 and E138), and contains multiple substitutions in the highly conserved G-box suggesting its mechanism of polymerization has diverged.

### **PhuZ controls positioning of phage DNA**

PhuZ represents the first identified tubulin cytoskeletal element encoded by a phage. PhuZ assembles a dynamic array that positions phage DNA at the center of the cell. How might a tubulin polymer position phage DNA? We recently demonstrated that dynamically unstable polymers can center DNA in a bacterial cell by constantly applying pushing forces that readjust

its position relative to the poles of the cell (Drew and Pogliano, 2011), much like *S. pombe* nuclei are positioned by pushing of interphase microtubule arrays (Tran et al., 2001). We therefore speculate that PhuZ forms dynamically unstable polymers capable of exerting pushing forces that position phage DNA at midcell (Figure 7). Consistent with this model, during phage infection GFP-PhuZ formed highly dynamic polymers that appeared to undergo many cycles of assembly and disassembly. Altering the polymerization dynamics of PhuZ filaments by expressing a catalytic mutant strongly disrupted DNA positioning, showing that dynamic assembly is important for its centering activity. Coupling of the pushing force to the DNA likely involves one or more adaptor proteins that interact with one end of the PhuZ polymer and also with either phage DNA or proteins involved in phage replication and/or capsid assembly.

What is the advantage of positioning phage 201 $\phi$ 2-1 DNA in the cell center? Many eukaryotic viruses replicate in a specific region of the cell, including in the cytosol, the nucleoplasm, or in tight association with specific intracellular membrane compartments (Leopold and Pfister, 2006; Radtke et al., 2006). Concentrated zones of viral replication (often referred to as factories) likely increase the efficiency of viral replication and assembly. Gamma Herpes virus, for example, forms replication factories surrounded by newly assembled viral particles (Iwasaki and Omura, 2010). We show here that encapsidated 201 $\phi$ 2-1 DNA occurs at midcell in a rosette-like structure surrounding a larger DNA mass, suggestive of the formation of a viral factory. Expression of the catalytic mutant decreased phage yield by 50%, indicating dynamic PhuZ filaments improve the overall efficiency of phage production. We speculate that localization of phage DNA at midcell might facilitate replication, phage assembly, or phage release, although we currently cannot distinguish between these possibilities. For example, keeping phage DNA concentrated in the center may facilitate efficient packaging into capsids

and be especially important for very large genomes where movement by diffusion would be severely limited. Consistent with this idea, all of the tubulin-encoding phage that we have so far identified are very large, with genomes ranging in size from 185 (Sakaguchi et al., 2005) to 316 kb (Thomas et al., 2008). While midcell localization of phage DNA might also be related to the formation of the central bulge, we note that in mutants in which phage DNA is mis-positioned near the cell pole, a bulge still forms in the cell center (Fig 6H), demonstrating that the DNA itself is not responsible for the bulge. Instead, phage DNA may be positioned near the center to take advantage of other important events that might be associated with the bulge, such as capsid production or cell lysis. These results suggest that, as for eukaryotic viruses, large bacterial viruses also benefit from localization to discrete regions of the cell.

### **Cytoskeletal proteins are widespread among bacterial viruses**

We have identified at least 7 different phage that encode a tubulin-like gene, suggesting that the function of PhuZ may be conserved among very large phage. Previous work has shown that MreB is important for DNA replication of several phage in *E.coli* and *B. subtilis* (Munoz-Espin et al., 2009). We recently described Alp6A, an actin-like protein encoded by *Bacillus thuringiensis* phage 0305φ8-36 that forms polymers of unknown function (Derman et al., 2009). These results suggest that some phage have evolved to use a host cytoskeletal protein (MreB) while other, larger phage may have evolved their own specialized cytoskeletal element (PhuZ and Alp6A). Understanding divergent tubulins like PhuZ may provide broader insight into the functions and mechanisms underlying the bacterial tubulin cytoskeleton.

### **Acknowledgements**

We thank Justin Farlow for help with early experiments, Dr. Justin Kollman for EM advice, and Jessica Polka for many helpful discussions. We also thank Dr. Julie Thomas and Dr. Steven Hardies of UT Health Sciences San Antonio for the 201 $\phi$ 2-1 phage and Dr. Hongwei D Yu of Marshall University for the pHERD30T vector. This work was funded by HHMI and NIH grant GM310627 (DAA, JAK, CAW, EAM, EAZ, SP) and by NIH grants GM084334 and GM073898 (JP). JAK is supported by a Genentech predoctoral fellowship.

## **Materials and Methods**

### **Protein Expression and Purification**

The PhuZ gene was cloned into the pET28a expression vector with a 6-His tag on the N-terminus and expressed in BL21(DE3) cells under an IPTG inducible T7 promoter. PhuZ was purified by Ni-affinity chromatography followed by gel filtration (Superdex 200). For additional details, please see supplemental materials.

### **Crystallization, Structure Determination, and Electron Microscopy**

Crystals were grown by the hanging-drop, vapor diffusion method in 2  $\mu$ L drops containing 1  $\mu$ L of concentrated protein (2 mg/mL) and 1  $\mu$ L of precipitant solution (15% PEG 6000, 0.1M HEPES pH 7.5, 0.5M Ammonium Acetate, 0.05M MgCl<sub>2</sub>). Protein structure was determined as described in the supplemental materials. Electron micrographs were obtained with a Tecnai T12 microscope at a voltage of 120 kV at a magnification of X52,000. Images were recorded with a

Gatan 4k x 4k charge-coupled device camera, for additional details please see supplement.

## **Light Scattering**

Right angle light scattering was conducted by mixing PhuZ with a polymerization buffer containing GTP using a stop-flow system designed in-house. An excitation wavelength of 530 nm was used. The critical concentration was determined by plotting the maximum intensity versus PhuZ concentration. The x-intercept of this plot was used as the critical concentration.

## **Strains, media and growth conditions**

*Pseudomonas chlororaphis* strain 200-B was grown on Hard Agar plates and liquid (Serwer et al., 2004). Plasmids were introduced into *P. chlororaphis* by electroporation (Howard et al., 2007). Lysates of 201 $\phi$ 2-1 were made by adding 50  $\mu$ l of a high-titer lysate ( $10^9$  pfu/ml) to exponentially growing *P. chlororaphis* shaking at 30°C and incubating for 6 hours. Lysates were clarified by centrifugation at 16,000 rpm and stored at 4°C with chloroform.

## **Microscopy**

*P. chlororaphis* cells were grown on 1.2% agarose pads containing 1/4x Luria Broth, 15  $\mu$ g/ml Gentamycin sulfate, 1  $\mu$ g/ml FM-464 (Pogliano et al., 1999), and either 0, 0.15, 0.25, 0.40, 0.50, 0.75, 1.0, or 2.0% arabinose. The slides were then incubated for 3 hours at either RT or 30°C. The cells were imaged with a DeltaVision Spectris Deconvolution microscope (Applied Precision, Issaquah). For Fluorescence Recovery After Photobleaching (FRAP) experiments, please see supplemental materials.

### **Single cell phage replication assays**

*P. chlororaphis* cells were inoculated on a 1.2% agarose pad containing 1/4x Luria Broth, 15 µg/ml gentamycin sulfate, 1 µg/ml FM4-64 (Pogliano et al., 1999), 1 µg/ml DAPI, and either 0.15% or 0.25% arabinose and incubated at 30°C for 2-4 hours without a coverslip in a humidified box. At time zero, 3 µl of high titer lysate and 3 µl of 1mg/ml DNaseI (New England Biolab) was added on top of the cells, and then images taken every 5-10 min for 180 min. To image DAPI and GFP-PhuZ polymers during infection, cells were fixed as described in supplemental materials.

### **Plasmid constructions and In-gel fluorescence assays**

Plasmids were constructed as described in the supplemental materials. PhuZ-GFP protein expression was examined using in-gel fluorescence as described in the supplemental materials.



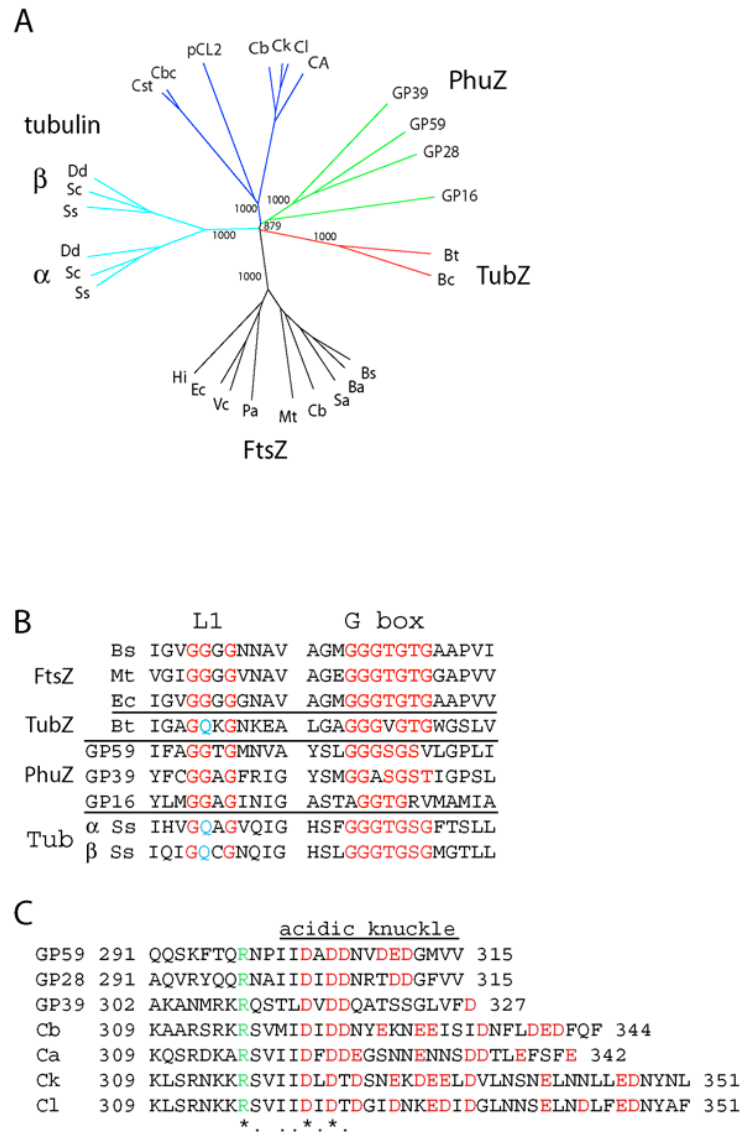


**Figure 1.** Phylogenetic relationship and conserved sequences of PhuZ and other distantly related tubulins.

A. Phylogenetic tree showing the relationship of divergent tubulins encoded by *Pseudomonas* phage (PhuZ), *Clostridial* sequences from chromosomes (Cb,Ck,Cl,CA), plasmid (pCL2), and phage (Cst, Cbc), TubZ (pBtoxis/*B.thuringiensis* and pH308197/*B. cereus*) and representative bacterial FtsZ sequences. PhuZ sequences (green): GP59 (*P.chlororaphis* phage 201 $\phi$ 2-1); GP39 (*P.aeruginosa* phage  $\phi$ KZ), and GP16 (*P.aeruginosa* phage EL). FtsZ sequences: Bs, *B.subtilis*; Ba, *B.anthraxis*; Sa, *S.aureus*; Cb, *C.botulinum*; Mt, *M.tuberculosis*, Ec, *E.coli*; Vc, *V.cholerae*, Pa, *P.aeruginosa*; Hi, *H.influenzae*. *Clostridial* sequences (blue): CA, CAC3459 *Clostridium acetobutylicum* ATCC824; Cb, CBY3413 *C.butyricum* 5521; Ck, CKL0570 *C. kluuyveri* DSM555; Cl, Cloce14294 *C.cellulovorans* 743B; pCL2, pCLG2A0045 *C.botulinum str.1873*; Cst, Cst189 *C.botulinum* phage C-st, Cbc, CBCA1765 *C.botulinum C str. Eklund*; eukaryotic  $\alpha/\beta$  tubulin sequences (cyan): Dd, *Dictyostelium discoideum*, Sc, *Saccharomyces cerevisiae*, Ss, *Sus scrofa*. Sequences were aligned using Tcoffee and the tree was generated using ClustalW. Bootstrap values are given for selected branches.

B. Alignment of L1 and G box motifs for PhuZ, TubZ,  $\alpha/\beta$  tubulin and representative bacterial FtsZ sequences. Conserved residues are in red. PhuZ GP59 (phage 201 $\phi$ 2-1) GP39 (phage  $\phi$ KZ), and GP16 (phage EL), TubZ from pBtoxis, FtsZ sequences (Bs, *B.subtilis*; Mt, *M.tuberculosis*; Ec, *E.coli*).  $\alpha/\beta$ -tubulin of Ss, *Sus scrofa*

C. Alignment of the last 13 amino acids of PhuZ (GP59) that make up the acidic knuckle with PhuZ related proteins encoded by phage  $\phi$ KZ (GP39) and EL (GP16). Conserved acidic residues are in red.

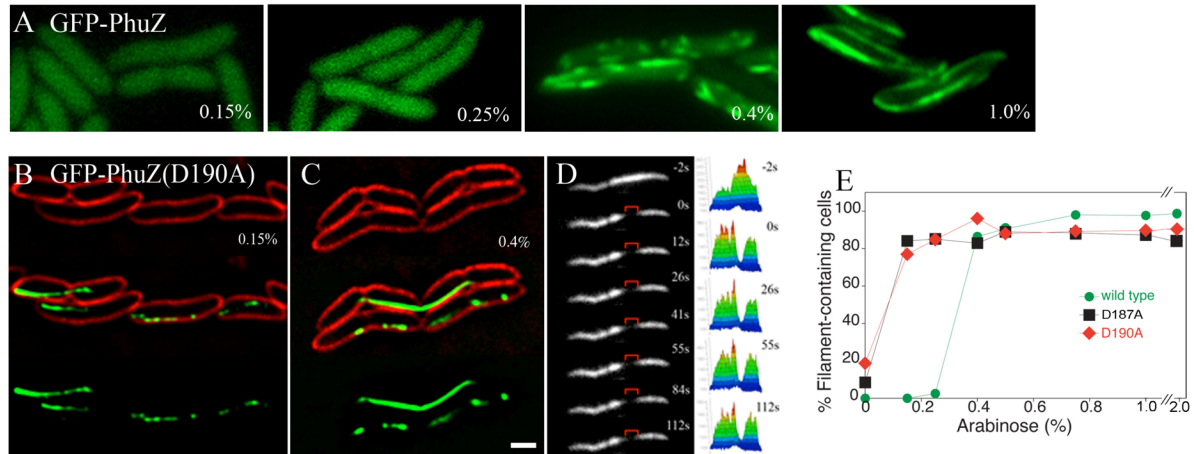


**Figure 2.** PhuZ polymer assembly in *P. chlororaphis*.

A. Fluorescent micrographs of *P. chlororaphis* cells expressing wild type GFP-PhuZ grown at 30°C and induced with the indicated amount (%) of arabinose. Scale bar equals 1 micron.

B and C. The catalytic point mutant GFP-PhuZD190A forms filaments that become trapped in septa. Membranes are stained red with FM4-64.

D. Photobleaching of GFP-PhuZD190A. The bleached zone generated at t0 seconds (red bracket) does not move or recover after 112s, indicating that the filaments are static.

E. Graphs showing the percentage of cells containing filaments when fusion proteins are expressed at increasing levels. Cells were grown at 30°C for wild type and catalytic point mutants.

See also Figure S4, Movies S1, S2, S3.

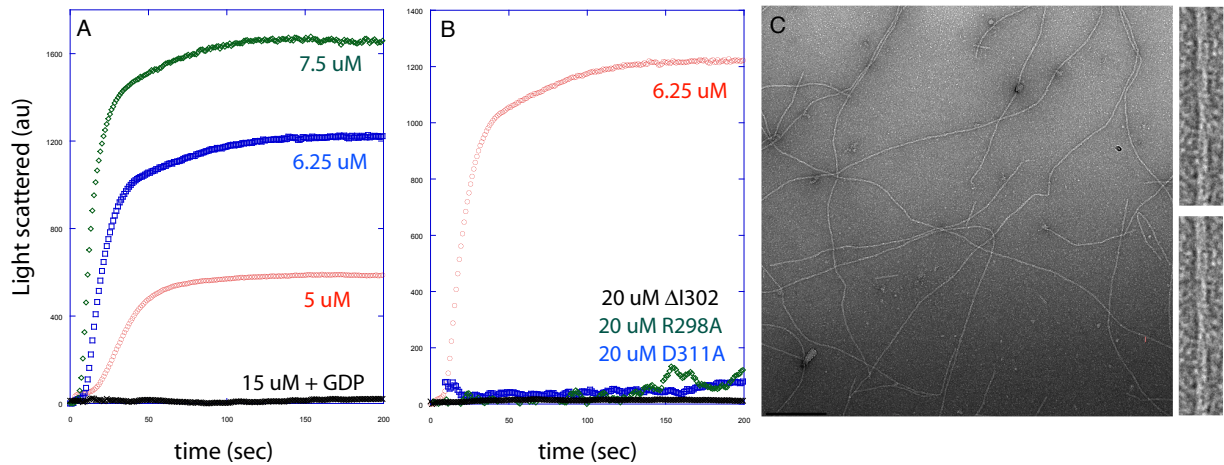


**Figure 3.** *In vitro* polymerization of PhuZ

A. Right angle light scattering traces of PhuZ polymerization at 5 (red), 6.25 (blue), 7.5 (green)  $\mu\text{M}$  upon addition of 1 mM GTP. Black trace is of 15  $\mu\text{M}$  PhuZ with 1 mM GDP.

B. Right angle light scattering traces of PhuZ mutants at 20  $\mu\text{M}$  ( $\Delta\text{I302}$ , black; R298A, green; D311A; blue) show no detectable polymer formation. 6.25  $\mu\text{M}$  wild-type trace shown for comparison.

C. Negative stain EM of 7  $\mu\text{M}$  PhuZ polymerized in the presence of 1 mM GMPCPP at 36000x. Two boxed segments of filaments collected at 52000x are shown at right to show detailed filament.

See also Figure S2.

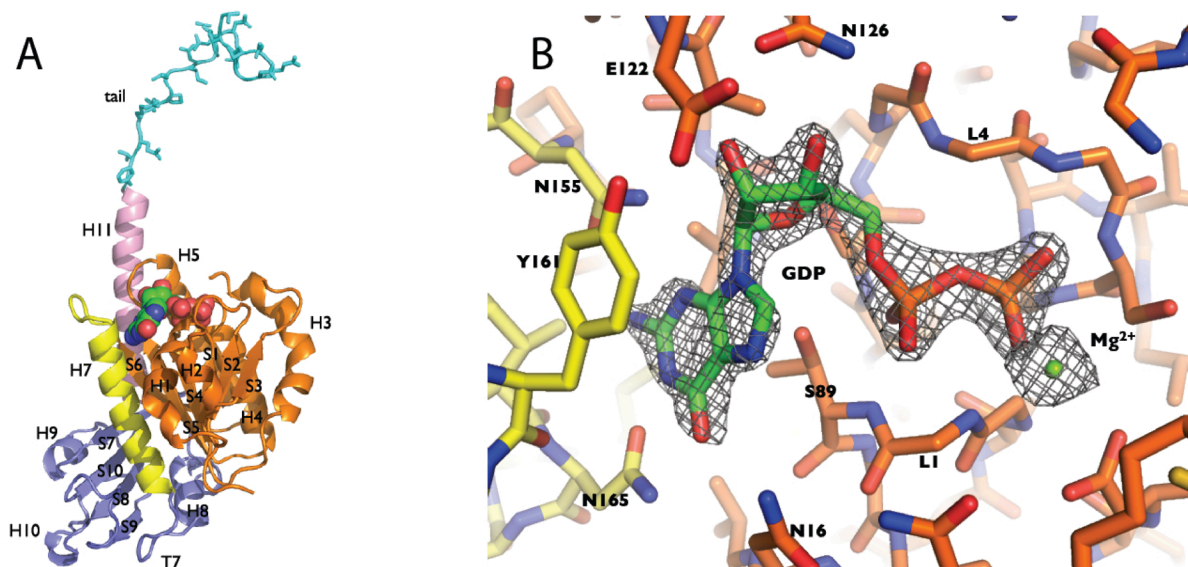


**Figure 4.** Structure and nucleotide binding of PhuZ

A. Cartoon representation of the PhuZ structure with the N-terminal domain shown in orange, the interdomain in yellow, the C-terminal domain in slate, helix H11 in pink, and the C-terminal tail in cyan. The bound GDP is shown as spheres.

B. Top-down view of the nucleotide-binding pocket.  $2F_o - F_c$  prior to addition of Mg-GDP to model shown as mesh at  $2\sigma$

See also Figure S3, Tables S1, S2.

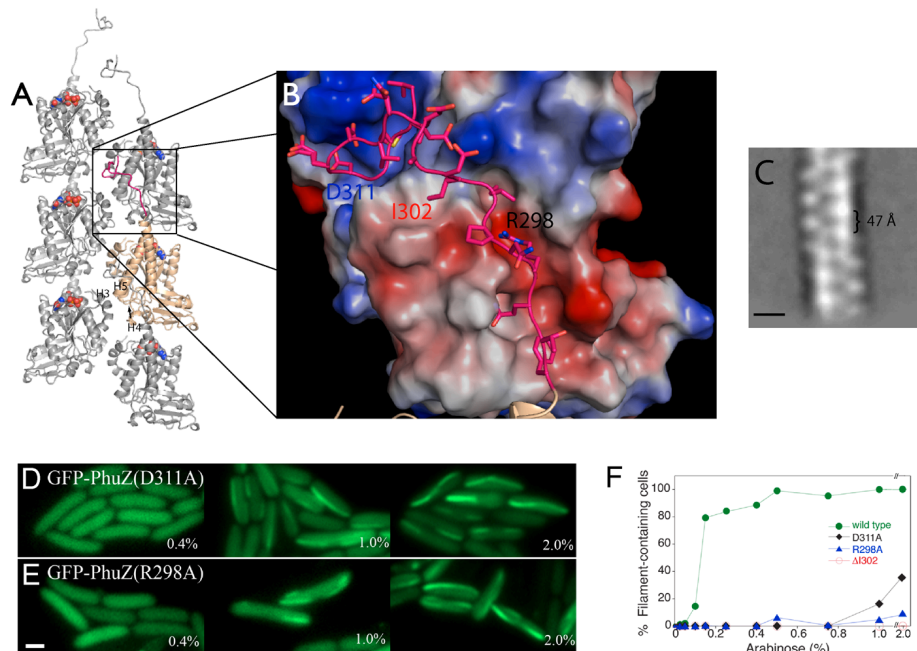


**Figure 5.** Crystal lattice contains filament-like contacts with the C-terminal tail providing most of the contact surface

A. Cartoon representation of PhuZ (wheat with hot pink tail) with five symmetry mates (grey), nucleotide shown as spheres, reveals two-stranded filament within the crystal lattice and extensive contacts by the C-terminal tail.

B. Electrostatic surface of PhuZ shown interacting with the C-terminal tail. The tail buries 1226 Å<sup>2</sup> of surface area per monomer. Residues R298, I302, and D311 are highlighted.

C. Average of 500 segments of PhuZ polymers observed by negative-stain EM. Spacing between longitudinal monomers is ~47 Å.

D-E. Fluorescent micrographs of *P.chlororaphis* cells expressing the C-terminal tail mutants D311A (D) and R298A (E) grown at room temperature and induced with the indicated amount

(%) of arabinose. Both fail to assemble polymers except at the highest expression levels (1% and 2%). Scale bar equals 1 micron.

F. Graph showing the percentage of cells containing filaments when fusion proteins are expressed at increasing levels at 25°C.

See also Figure S1.

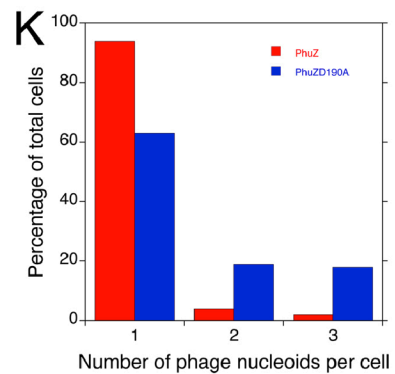
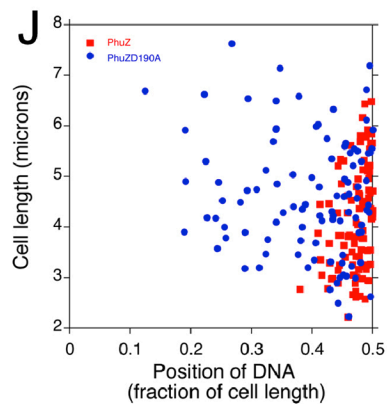
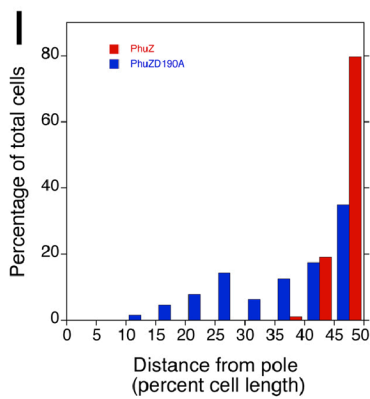
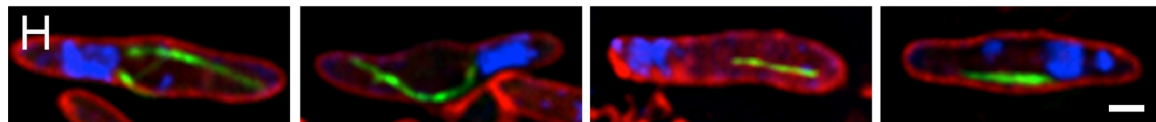
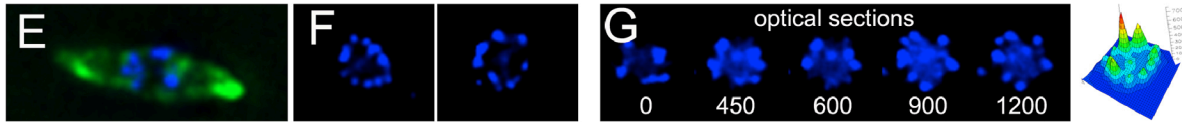
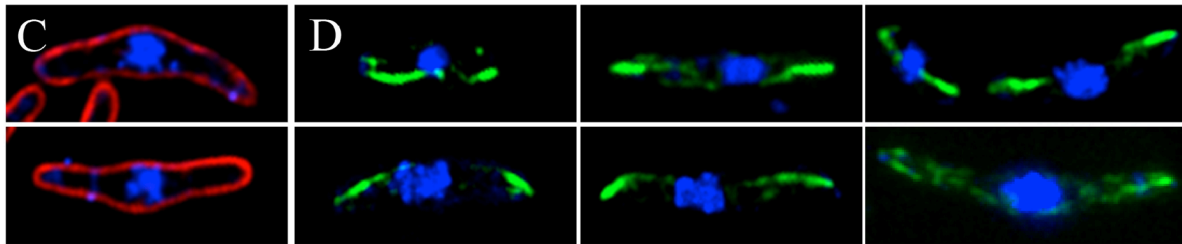
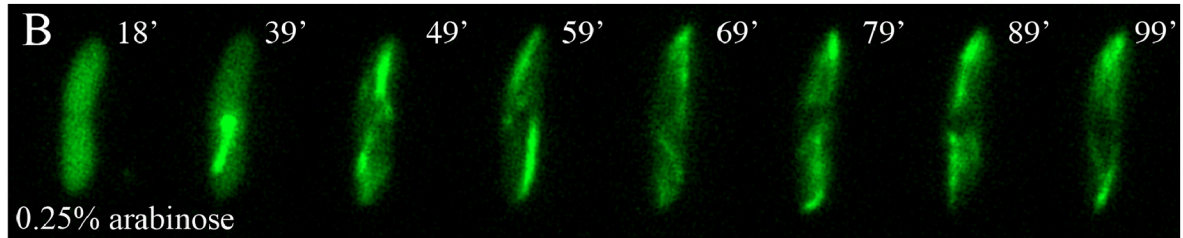
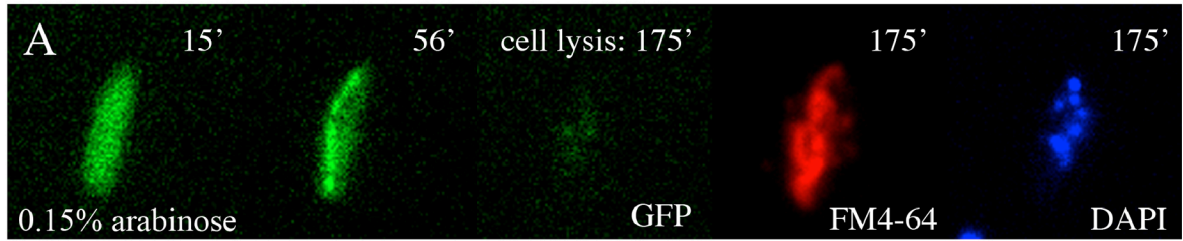




**Figure 6.** A single cell assay for phage infection reveals that PhuZ assembles filaments *in vivo* during infection of the host cell with 201 $\phi$ 2-1.

A. In cells grown with 0.15% arabinose (below critical threshold inducer concentration), filaments first appeared 56 minutes after phage addition and the cell lysed after 175 minutes, as revealed by FM4-64 staining. Staining with DAPI/DNAseI indicates phage release.

B. In cells grown with 0.25% arabinose, filaments first appeared 39 minutes after phage addition and polymers underwent cycles of assembly and disassembly until the cell lysed after 140 minutes. Scale bar equals 1 micron.

C. Two examples of infected cells stained with FM4-64 (red) and DAPI (blue) at 90 minutes post infection showing a large mass of DNA in the center of the cell.

D. Six examples of infected cells showing filaments of GFP-PhuZ on either side of a centrally located DAPI stained nucleoid.

E-G. Cells were fixed and treated with DNAse I to degrade all DNA except that encapsidated by phage. E. An example of GFP-PhuZ filaments surrounding DAPI foci at midcell.

F. Two examples of rosette structures formed during infection and visualized after DNAseI digestion.

G. A series of optical sections through a DNAseI digested nucleoid showing phage encapsidated DNA occurs in a circular pattern. Numbers indicate distance in nanometers from the first optical section. On the far right, a 3-D fluorescence intensity graph of DAPI fluorescence corresponding to the 900nm optical section showing the rosette pattern of foci localization.

H. Four panels showing DAPI stained cells expressing the GTPase mutant GFP-PhuZD190A after 90 minutes of phage infection. The phage nucleoid is frequently positioned at the pole of the cell. Some cells (far left) contain two or three nucleoids.

I. Histogram showing the percentage of cells with the phage nucleoid located near the center (50% cell length) of the cell for wild type GFP-PhuZ (red) or mutant GFP-PhuZD190A (blue).

J. Graph showing the position of the phage nucleoid as a fraction of cell length versus cell length for wild type GFP-PhuZ (red) or mutant GFP-PhuZD190A (blue).

K. Histogram showing the percentage of infected cells expressing either wild type GFP-PhuZ (red) or mutant GFP-PhuZD190A (blue) containing one, two or three phage nucleoids.

See also Figure S5, Movies S4, S5, S6.

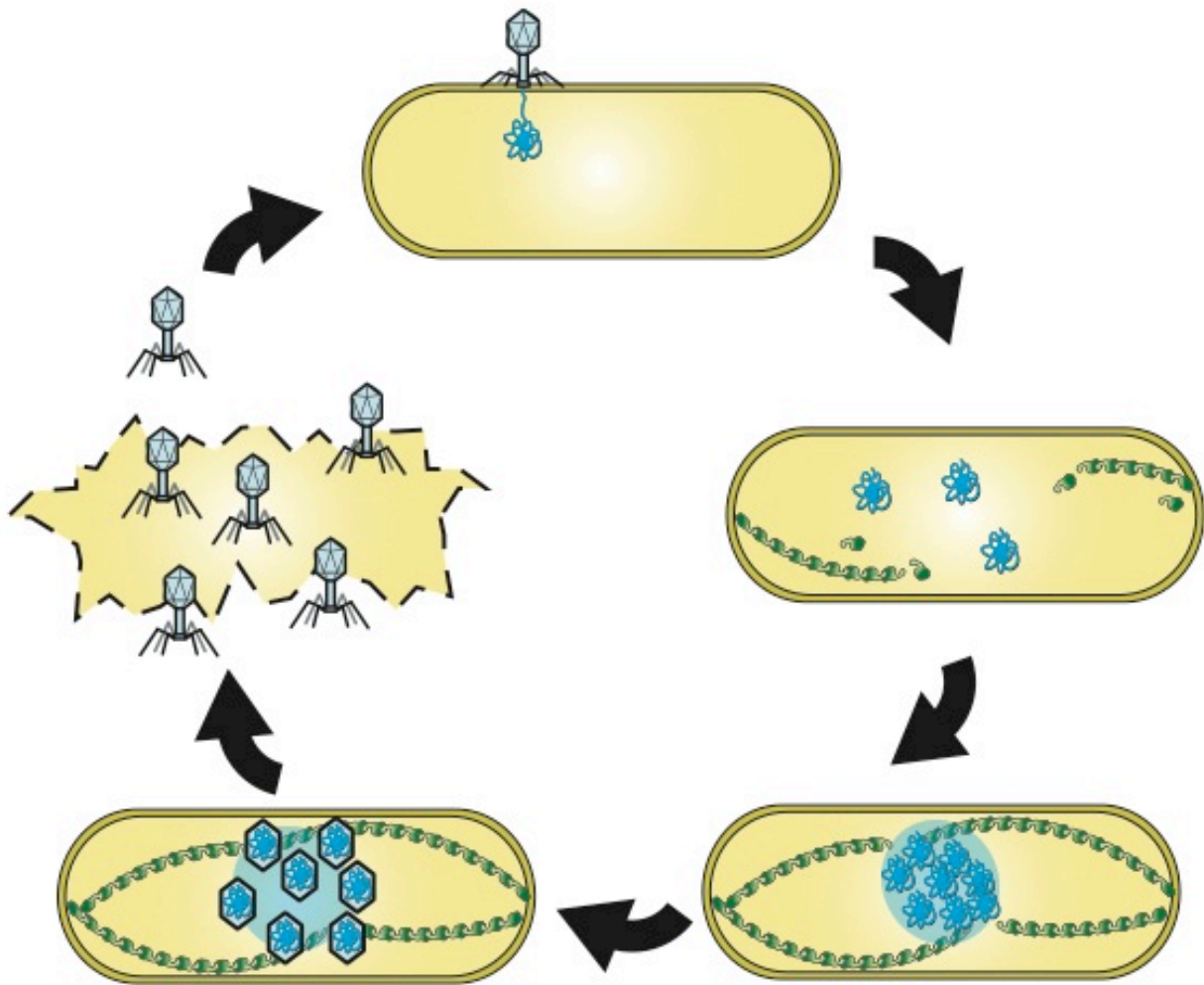


**Figure 7.** After 201φ2-1 infects a cell, the host chromosome is degraded and short PhuZ filaments appear that eventually extend from the poles of the cell to the phage nucleoid in the center. The PhuZ spindle positions the phage DNA in the center of the cell to allow 201φ2-1 genomes to be efficiently replicated and/or packaged into the capsids. After the completion of phage assembly, the cell lyses, expelling mature phage into the environment.

## References

- Anand, S.P., Akhtar, P., Tinsley, E., Watkins, S.C., and Khan, S.A. (2008). GTP-dependent polymerization of the tubulin-like RepX replication protein encoded by the pXO1 plasmid of *Bacillus anthracis*. *Molecular microbiology* 67, 881-890.
- Aylett, C.H., Wang, Q., Michie, K.A., Amos, L.A., and Lowe, J. (2010). Filament structure of bacterial tubulin homologue TubZ. *Proc Natl Acad Sci U S A* 107, 19766-19771.
- Becker, E., Herrera, N.C., Gunderson, F.Q., Derman, A.I., Dance, A.L., Sims, J., Larsen, R.A., and Pogliano, J. (2006). DNA segregation by the bacterial actin AlfA during *Bacillus subtilis* growth and development. *EMBO J* 25, 5919-5931.
- Cabeen, M.T., and Jacobs-Wagner, C. (2010). The bacterial cytoskeleton. *Annu Rev Genet* 44, 365-392.
- Chen, Y., and Erickson, H.P. (2008). In vitro assembly studies of FtsZ/tubulin-like proteins (TubZ) from *Bacillus* plasmids: evidence for a capping mechanism. *J Biol Chem* 283, 8102-8109.
- de Boer, P.A. (2010). Advances in understanding *E. coli* cell fission. *Curr Opin Microbiol* 13, 730-737.
- Derman, A.I., Becker, E.C., Truong, B.D., Fujioka, A., Tucey, T.M., Erb, M.L., Patterson, P.C., and Pogliano, J. (2009). Phylogenetic analysis identifies many uncharacterized actin-like proteins (Alps) in bacteria: regulated polymerization, dynamic instability and treadmilling in Alp7A. *Mol Microbiol* 73, 534-552.
- Downing, K.H., and Nogales, E. (1998). Tubulin and microtubule structure. *Current opinion in cell biology* 10, 16-22.

- Drew, K.R., and Pogliano, J. (2011). Dynamic instability-driven centering/segregating mechanism in bacteria. *Proc Natl Acad Sci U S A* *108*, 11075-11080.
- Howard, G.T., Mackie, R.I., Cann, I.K., Ohene-Adjei, S., Aboudehen, K.S., Duos, B.G., and Childers, G.W. (2007). Effect of insertional mutations in the pueA and pueB genes encoding two polyurethanases in *Pseudomonas chlororaphis* contained within a gene cluster. *Journal of applied microbiology* *103*, 2074-2083.
- Iwasaki, K., and Omura, T. (2010). Electron tomography of the supramolecular structure of virus-infected cells. *Curr Opin Struct Biol* *20*, 632-639.
- Larsen, R.A., Cusumano, C., Fujioka, A., Lim-Fong, G., Patterson, P., and Pogliano, J. (2007). Treadmilling of a prokaryotic tubulin-like protein, TubZ, required for plasmid stability in *Bacillus thuringiensis*. *Genes Dev* *21*, 1340-1352.
- Leopold, P.L., and Pfister, K.K. (2006). Viral strategies for intracellular trafficking: motors and microtubules. *Traffic* *7*, 516-523.
- Lowe, J., and Amos, L.A. (1998). Crystal structure of the bacterial cell-division protein FtsZ. *Nature* *391*, 203-206.
- Lowe, J., and Amos, L.A. (2009). Evolution of cytomotive filaments: the cytoskeleton from prokaryotes to eukaryotes. *Int J Biochem Cell Biol* *41*, 323-329.
- Lu, C., Stricker, J., and Erickson, H.P. (2001). Site-specific mutations of FtsZ--effects on GTPase and in vitro assembly. *BMC Microbiol* *1*, 7.
- Lutkenhaus, J. (2007). Assembly dynamics of the bacterial MinCDE system and spatial regulation of the Z ring. *Annu Rev Biochem* *76*, 539-562.
- Margolin, W. (2009). Sculpting the bacterial cell. *Curr Biol* *19*, R812-822.

Michie, K.A., and Lowe, J. (2006). Dynamic filaments of the bacterial cytoskeleton. *Annu Rev Biochem* 75, 467-492.

Munoz-Espin, D., Daniel, R., Kawai, Y., Carballido-Lopez, R., Castilla-Llorente, V., Errington, J., Meijer, W.J., and Salas, M. (2009). The actin-like MreB cytoskeleton organizes viral DNA replication in bacteria. *Proc Natl Acad Sci U S A*.

Ni, L., Xu, W., Kumaraswami, M., and Schumacher, M.A. (2010). Plasmid protein TubR uses a distinct mode of HTH-DNA binding and recruits the prokaryotic tubulin homolog TubZ to effect DNA partition. *Proc Natl Acad Sci U S A* 107, 11763-11768.

Nogales, E., Downing, K.H., Amos, L.A., and Lowe, J. (1998a). Tubulin and FtsZ form a distinct family of GTPases. *Nat Struct Biol* 5, 451-458.

Nogales, E., Wolf, S.G., and Downing, K.H. (1998b). Structure of the alpha beta tubulin dimer by electron crystallography. *Nature* 391, 199-203.

Oliva, M.A., Cordell, S.C., and Lowe, J. (2004). Structural insights into FtsZ protofilament formation. *Nat Struct Mol Biol* 11, 1243-1250.

Oliva, M.A., Trambaiolo, D., and Lowe, J. (2007). Structural insights into the conformational variability of FtsZ. *J Mol Biol* 373, 1229-1242.

Pogliano, J., Osborne, N., Sharp, M.D., Abanes-De Mello, A., Perez, A., Sun, Y.L., and Pogliano, K. (1999). A vital stain for studying membrane dynamics in bacteria: a novel mechanism controlling septation during *Bacillus subtilis* sporulation. *Mol Microbiol* 31, 1149-1159.

Polka, J.K., Kollman, J.M., Agard, D.A., and Mullins, R.D. (2009). The structure and assembly dynamics of plasmid actin AlfA imply a novel mechanism of DNA segregation. *J Bacteriol* 191, 6219-6230.

Popp, D., Xu, W., Narita, A., Brzoska, A.J., Skurray, R.A., Firth, N., Ghoshdastider, U., Maeda, Y., Robinson, R.C., and Schumacher, M.A. (2010). Structure and filament dynamics of the pSK41 actin-like ParM protein: implications for plasmid DNA segregation. *J Biol Chem* 285, 10130-10140.

Qiu, D., Damron, F.H., Mima, T., Schweizer, H.P., and Yu, H.D. (2008). PBAD-based shuttle vectors for functional analysis of toxic and highly regulated genes in *Pseudomonas* and *Burkholderia* spp. and other bacteria. *Appl Environ Microbiol* 74, 7422-7426.

Radtke, K., Dohner, K., and Sodeik, B. (2006). Viral interactions with the cytoskeleton: a hitchhiker's guide to the cell. *Cell Microbiol* 8, 387-400.

Rivera, C.R., Kollman, J.M., Polka, J.K., Agard, D.A., and Mullins, R.D. (2011). Architecture and assembly of a divergent member of the ParM family of bacterial actin like proteins. *J Biol Chem*.

Sakaguchi, Y., Hayashi, T., Kurokawa, K., Nakayama, K., Oshima, K., Fujinaga, Y., Ohnishi, M., Ohtsubo, E., Hattori, M., and Oguma, K. (2005). The genome sequence of *Clostridium botulinum* type C neurotoxin-converting phage and the molecular mechanisms of unstable lysogeny. *Proc Natl Acad Sci U S A* 102, 17472-17477.

Schlieper, D., Oliva, M.A., Andreu, J.M., and Lowe, J. (2005). Structure of bacterial tubulin BtubA/B: evidence for horizontal gene transfer. *Proc Natl Acad Sci U S A* 102, 9170-9175.

Serwer, P., Hayes, S.J., Zaman, S., Lieman, K., Rolando, M., and Hardies, S.C. (2004). Improved isolation of undersampled bacteriophages: finding of distant terminase genes. *Virology* 329, 412-424.

Sontag, C.A., Staley, J.T., and Erickson, H.P. (2005). In vitro assembly and GTPase hydrolysis by bacterial tubulins BtubA and BtubB. *J Cell Biol* 169, 233-238.

Thanbichler, M., and Shapiro, L. (2008). Getting organized--how bacterial cells move proteins and DNA. *Nat Rev Microbiol* 6, 28-40.

Thomas, J.A., Rolando, M.R., Carroll, C.A., Shen, P.S., Belnap, D.M., Weintraub, S.T., Serwer, P., and Hardies, S.C. (2008). Characterization of Pseudomonas chlororaphis myovirus 201varphi2-1 via genomic sequencing, mass spectrometry, and electron microscopy. *Virology* 376, 330-338.

Tran, P.T., Marsh, L., Doye, V., Inoue, S., and Chang, F. (2001). A mechanism for nuclear positioning in fission yeast based on microtubule pushing. *J Cell Biol* 153, 397-411.

van den Ent, F., Amos, L., and Lowe, J. (2001). Prokaryotic origin of the actin cytoskeleton. *Nature* 413, 39-44.



## Supplemental Data

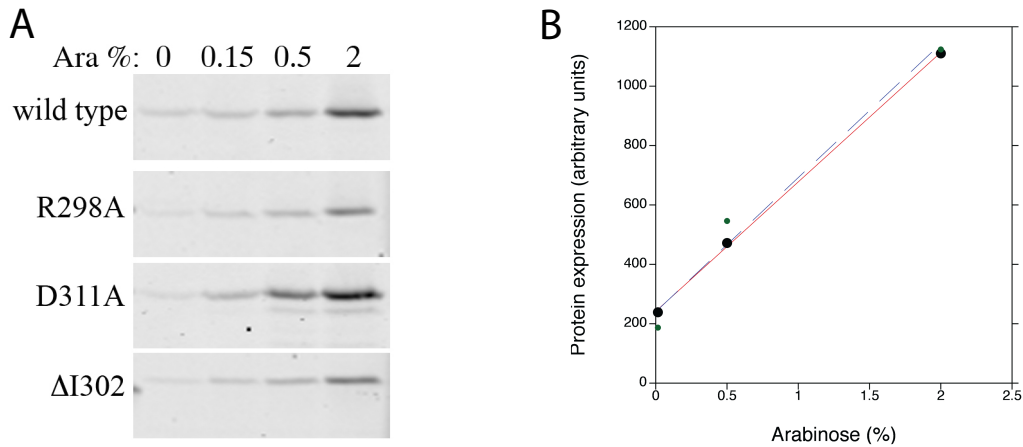


**Figure S4 related to Figure 5:** a) Wild type and mutant GFP-PhuZ proteins are expressed at increasing levels with increasing arabinose concentrations and are proteolytically stable.

*P.chlororaphis* cells containing plasmids expressing the fusion proteins from the arabinose promoter were grown with increasing amounts of arabinose, ranging from 0 to 2% and the fusion proteins visualized by in-gel fluorescence.

b) Graph showing linear relationship between percent arabinose and the amount of GFP-PhuZ protein produced at 0.15%, 0.5%, and 2% arabinose respectively. Green dots with blue dashed line represents GFP-PhuZ and black dots with red solid line represents a GFP control driven off of the same arabinose promoter.

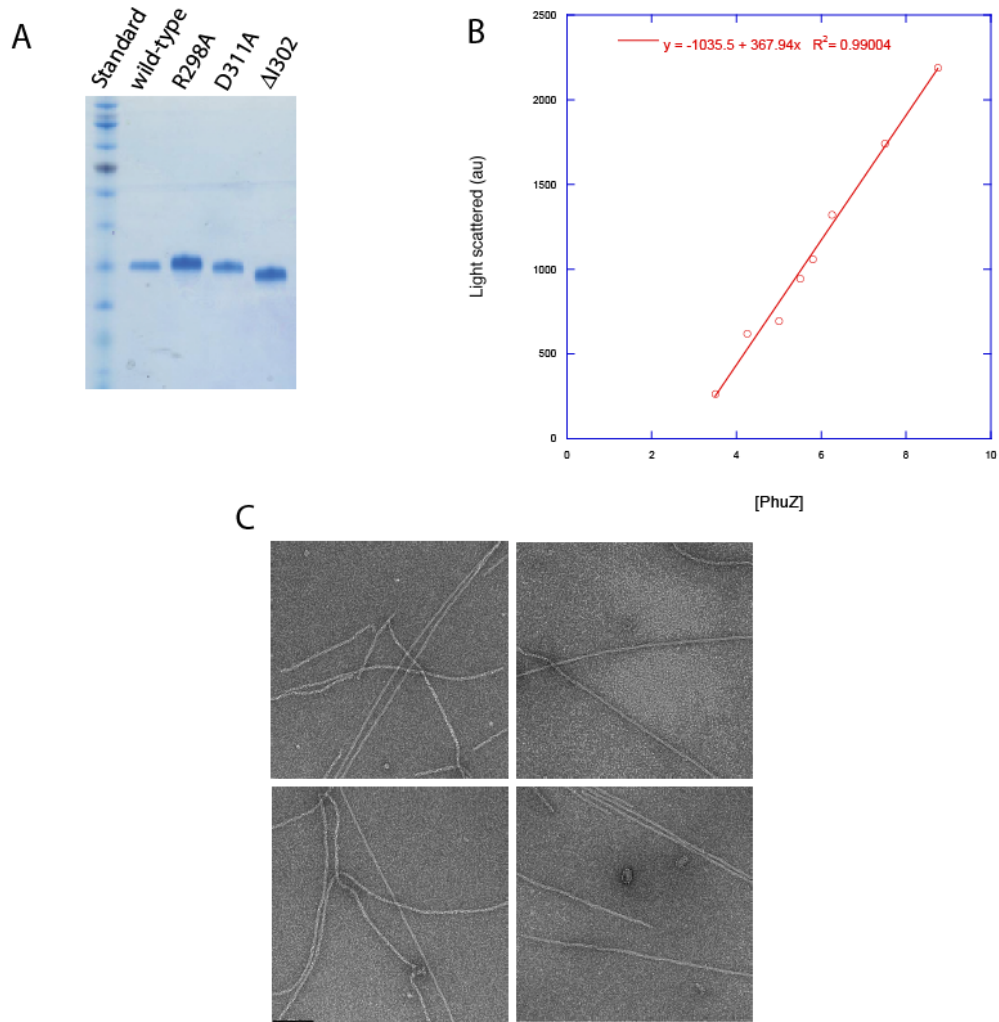


**Figure S2, related to Figure 3: Purity and *in vitro* studies of PhuZ.**

a) Gel displaying purity of PhuZ constructs used.

b) Plot of maximal light scattered versus initial PhuZ concentration. As light scattering is proportional to total polymer, the x-intercept of the trend line represents the critical concentration, calculated as  $2.8 \pm 0.1 \mu\text{M}$ .

c) Gallery of high magnification (52000X) EM images of PhuZ filaments. Scale bar represents 100 nm.

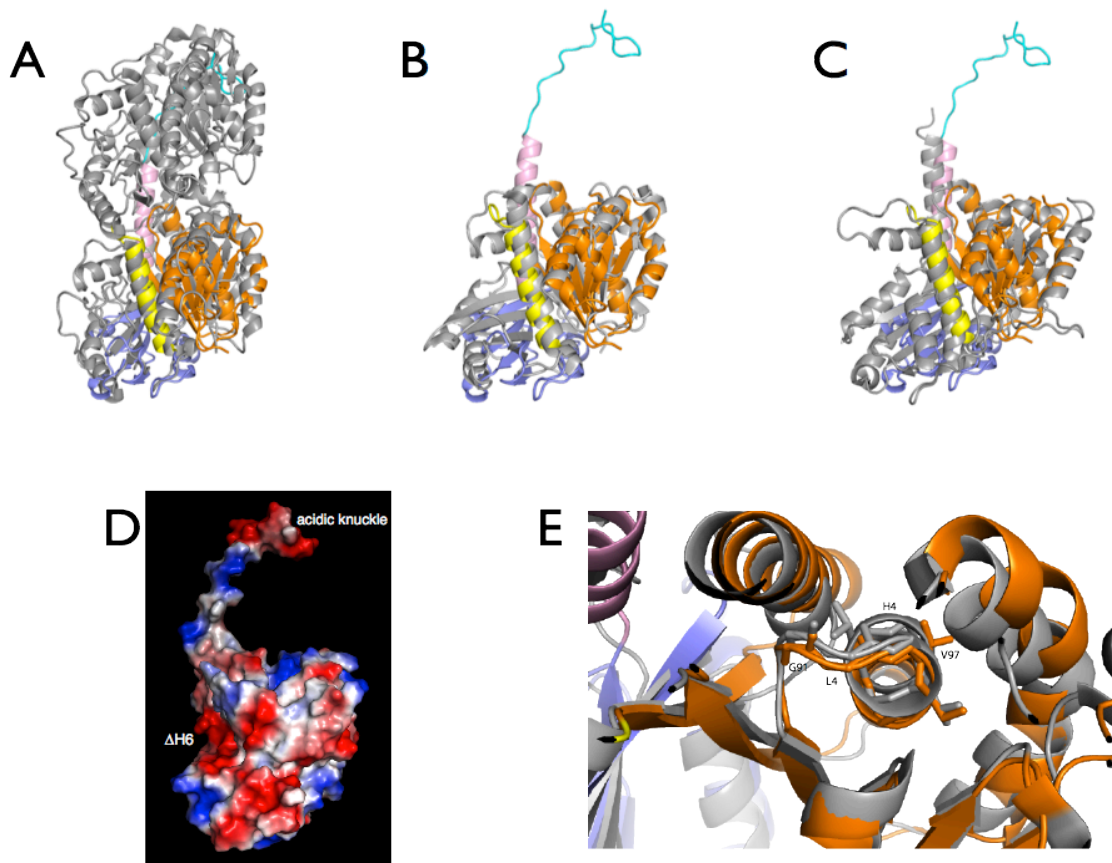


**Figure S3, related to Figure 4:** Overlays of the PhuZ backbone structure with those of a)  $\alpha$ -tubulin, b) *Aquifex aeolicus* FtsZ, and c) TubZ result in calculated RMSD values of 2.9, 2.6, and 2.9 Å, respectively.

d) Electrostatic surface of PhuZ. The acidic knuckle and acidic patch left by lack of helix H6 are highlighted.

e) Top-down view of L4 (G box). Overlay of PhuZ with *A. aeolicus* FtsZ shown. G box residues shown as sticks, showing the replacement of the final Gly with a Val residue does not affect the structure.

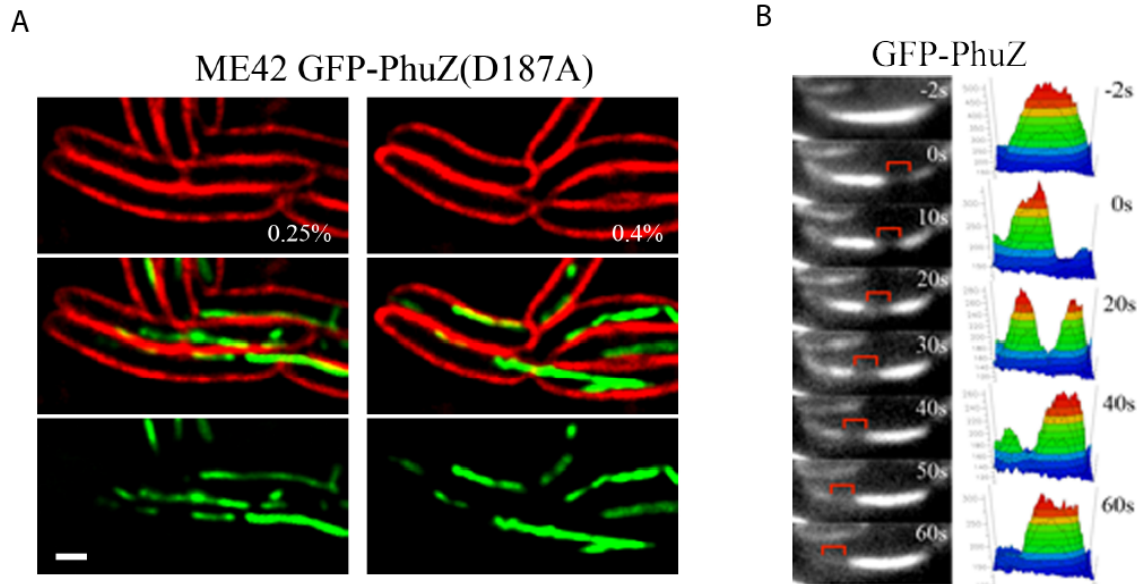


**Figure S1, related to Figure 2:** a) Fluorescent micrographs of *P. chlororaphis* cells (ME42) expressing GFP-PhuZD187A grown at 30°C and induced with the indicated amount (%) of arabinose. The catalytic point mutant GFP-PhuZ (D187A) forms static filaments that become trapped in septa. Membranes are stained red with FM4-64. Scale bar equals 1 micron.

b) Time-lapse fluorescent micrographs and corresponding pixel intensity plots of GFP-PhuZ filaments after photobleaching for wild type filaments. The bleached zones generated at  $t_0$  seconds (red bracket) migrate through the cells over time (seconds) indicating that filaments are treadmilling in place. This is distinct from the catalytic mutants which are completely static in both time-lapse and photobleaching studies. These FRAP results are directly comparable to the experiments with the catalytic mutants. Since there is no FRAP data for filament dynamics during infection with phage, it is not known if wild type filaments will move this way in the presence of phage.

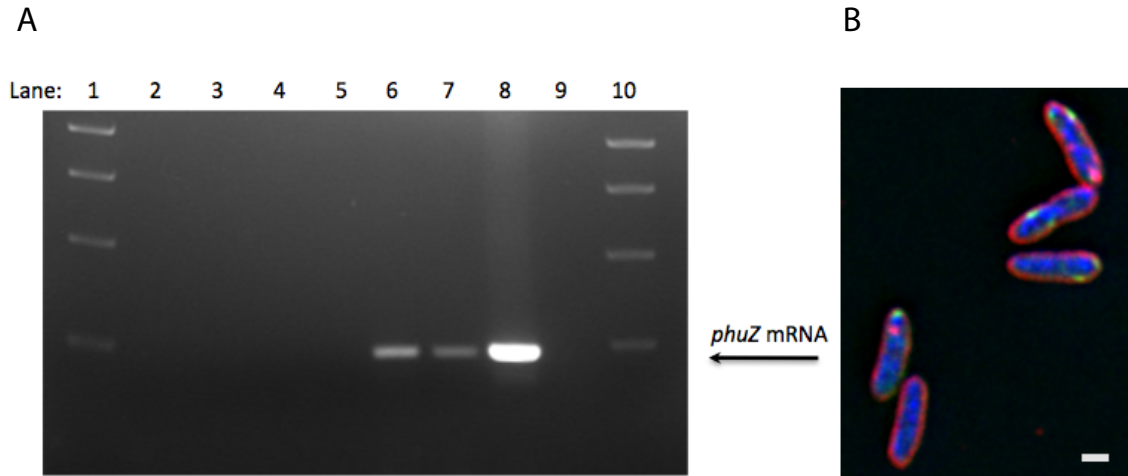


**Figure S5, related to Figure 6:** a) A culture of *P. chlororaphis* was infected with phage 201 $\phi$ 2-1 and the presence of *phuz* mRNA was assayed using reverse-transcriptase PCR. PCR products were electrophoresed on a 0.7% agarose gel. Lanes 1 and 10 are New England Biolab 1 KB DNA ladder. Lane 2: pre-infection sample (taken before the addition of bacteriophage); Lane 3: time 0 (immediately after addition of phage); Lane 4: 30 min post-infection; Lane 5: 1 hour post-infection; Lane 6: 2 hours post-infection; Lane 7: 6 hours post-infection; Lane 8: positive control (bacteriophage lysate); Lane 9: blank. The expression of *PhuZ* mRNA was detected at both 2 hours (lane 6) and 6 hours (lane 7) post infection.

b) Fluorescent micrographs of *P. chlororaphis* cells that were induced at 0.25% arabinose, but not phage infected, that have been grown and fixed using the same protocol as those in Figure 6. Membranes are stained red with FM4-64 and DNA is stained blue with DAPI. Cells are rod shaped with large de-condensed chromosomes. Scale bar equals 1 micron.

### **Supplemental Movie Legends:**

**Movie S1, related to Figure 2:** Fluorescence micrograph of *P. chlororaphis* cells, grown on a 1.2% agarose pad, expressing GFP-PhuZ from the arabinose promoter, induced with 0.4% arabinose. Note the multiple short dynamic filaments per cell. Total time lapsed is 1 min 33.32 sec. Scale bar equals 5 microns.

**Movie S2, related to Figure 2:** Time-lapse fluorescence micrograph of *P. chlororaphis* cells, grown on a 1.2% agarose pad, expressing GFP-PhuZD190A from the arabinose promoter, induced with 1.0% arabinose. In contrast to wild type filaments, these filaments appear static and often chain cells together. Total time elapsed is 33.263 sec. Scale bar equals 5 microns.

**Movie S3, related to Figure 2:** Fluorescence recovery after photobleaching (FRAP) of a GFP-PhuZD190A filament in *P. chlororaphis* expressed at 1.0% arabinose. Bleach spot appears at the right hand side of the filament and exhibits no recovery over the total time lapsed (1 min). Scale bar equals 5 microns.

**Movie S4, related to Figure 6:** Time-lapse fluorescence micrograph of a *P. chlororaphis* cell infected with 201 $\phi$ 2-1, grown on a 1.2% agarose pad, expressing GFP-PhuZ from the arabinose promoter, induced with 0.25% arabinose. Red: FM4-64 membrane stain, Green: GFP-PhuZ. Total time lapsed: 1 hour, 12 min, 41.453 sec. Scale bar equals 5 microns.

**Movie S5, related to Figure 6:** 3D rotation about the x-axis of a late stage (120 min post-phage addition) infection nucleoid in *P. chlororaphis*. Cells were fixed using 16% paraformaldehyde as

described, washed, and then subsequently treated with DNaseI for 1 hr at 37°C. Sample was then stained with DAPI. Unprotected DNA has been digested away and capsid-protected DNA remains intact, appearing as bright foci arrayed about the edge of the nucleoid. Scale bar equals 1.7 microns.

**Table S1, related to Figure 4:** Table of X-ray data and structure refinement statistics.

<i>Data Statistics</i>	
Space group	P2 <sub>1</sub> 2 <sub>1</sub> 2 <sub>1</sub>
Unit cell dimensions (Å)	a=47.065, b=75.935, c=92.798
I/σ(I)	9.7
Completeness (%)	96.0 (84.5)
R <sub>sym</sub> (%)	10.7
n <sub>refl</sub>	71727
<i>Structure Refinement</i>	
Resolution range (Å)	46.40 - 1.67
R (%)	18.59
R <sub>free</sub> (%)	21.63
Protein residues	311 (of 315)
Water	277
GDP	1
Mg <sup>2+</sup>	1
Average isotropic B-factors	
Protein atoms (Å <sup>2</sup> )	33.80
Side-chain atoms (Å <sup>2</sup> )	36.58
Solvent atoms (Å <sup>2</sup> )	38.93
GDP (Å <sup>2</sup> )	25.33



**Table S2, related to Figure 4:** Table of TLS groups as determined by the TLS server.

TLS group number:	Residue numbers:
1	2-28
2	29-51
3	52-80
4	81-156
5	157-171
6	172-228
7	229-255
8	256-270
9	271-294
10	295-315

## Supplemental methods

### In Gel Fluorescence

Exponentially growing cells (*E. coli* JP313 (Economou et al., 1995) or *P. chlororaphis* 200-B (Thomas et al., 2007)) were induced with the indicated amount of arabinose for 1 hour (*E. coli*) and 1.5 hr (*P. chlororaphis*) and then washed in 1x PBS. Cell pellets were resuspended in 25µl of PBS/In Gel Fluorescence Sample Buffer (Drew et al., 2008). Samples were passed through a 21.5 gage syringe until homogenized and then electrophoresed on a 10% SDS-PAGE gel. Gels were then washed with distilled water and imaged on a GE Typhoon.

### Syto 16 single burst experiments

*P. chlororaphis* cells were inoculated on a 1.2% agarose pad containing 1/4x Luria Broth, 25 µg/ml gentamycin sulfate, 1 µg/ml FM4-64 (Pogliano et al., 1999), 0.25% arabinose, and 1 µM of Syto 16 green fluorescent nucleic acid stain (Molecular Probes). Pads were incubated at 30°C for 2 hours without a coverslip in a humidified box. At time zero, 5 µl of high titer lysate and 3 µl of 1mg/ml DNaseI (New England Biolab) was added on top of the cells, and then images taken at 55, 75, 95 and 115 minutes post infection.

### Plasmid constructions

Strain construction: The *phuZ* gene was amplified via standard PCR directly from high titer ( $10^{10}$  pfu/ml) liquid lysate of 201φ2-1 using the following primers: Phuz209NewF = CTATGGGATCCCCTGTTAAAGTCTGTCTGATC; Phuz209NewRS = CTCACCTGCAGTCAAACCTACCATGCCGTCTTC . This product was digested with BamHI and PstI (New England Biolabs) and ligated into the pDSW209 vector (Qiu et al., 2008) that had

been digested the same way. This yielded an N-terminal fusion of green fluorescent protein with PhuZ with an 8 amino acid linker designated as pME4. Once this fusion was confirmed to make filaments in *E. coli*, the GFP-PhuZ piece was amplified out of pME4 (primers: GFPcontrol30TF = CTATGTCTAGA**atgagtaaaggagaagaactt**TTC; GFPPhuZ30TR = CTTCACcctgcaggTCAAACTACCATGCCGTCTTC). This piece was digested with XbaI and SbfI (New England Biolabs) then ligated into the pHERD30T vector (reference), which had also been digested with SbfI and XbaI. This yielded pME28, which is GFP-PhuZ under the control of the arabinose promoter.

GFP-PhuZ D187A (pME10) and D190A (pME11) were generated from pME4 using a two primer site directed mutagenesis PCR protocol (citation). These two mutations were introduced exactly the same way as the wild type GFP-PhuZ gene into pHERD30T to generate pME29 and pME30 respectively. The c-terminal tail mutations (D311A and R298A) and truncation ( $\Delta$ I302) were generated via the same two primer SDM PCR protocol directly on pME28, generating pME36, pME34, and pME39 respectively. Strains of *Pseudomonas chlororaphis* 200B-1 were ME41 (pME4 GFP-PhuZ), ME42 (pME10 GFP-PhuZD187A), ME43 (pME11 GFP-PhuZD190A), ME54 (pME36 GFP-PhuZD311A), ME55 (pME34 GFP-PhuZR298A), ME60 (pME39 GFP-PhuZ $\Delta$ I302).

### **Protein Expression and Purification**

1 mM IPTG was added once cells reached an OD600 of ~0.5 and protein was allowed to express for 4 hours before the cells were pelleted. Buffers contained 250 mM KCl, 50 mM HEPES pH 8, 1 mM MgCl<sub>2</sub>, 15 mM thioglycerol, and 10% glycerol. EDTA-free protease inhibitor tablets were included during lysis. 125 mM imidazole pH 8 was added to elute the

protein from the Ni-NTA resin. The 6-His tag was cleaved overnight at 4 °C by thrombin protease. Glycerol was omitted from the buffer during gel filtration for protein used for crystallography.

### **Crystallization and Structure Determination**

Hanging drops were equilibrated over 1mL of precipitant solution for 24-hours. Crystals were then harvested and used in microseeding fresh drops. A microseed suspension was prepared, using the Hampton Seed Bead Kit™, from one small crystal in 50 µl of precipitant solution. Multiple crystals grew in drops seeded with 1 µl of a 1:4,000 or 1:16,000 (v/v) dilution of the microseed suspension. Rod-like crystals with a cone-shaped void extending from either end toward the center of each crystal grew to their maximum size following incubation for about one week at room temperature.

Data from the SeMet-PhuZ-GDP crystal were collected using the multiple anomalous dispersion (MAD) technique at two wavelengths, 0.979640Å and 0.972425Å, at Beamline 8.3.1 at the Advanced Light Source (ALS, Lawrence Berkeley National Laboratory). Data were processed using HKL2000, CNS v1.2 (Brunger et al., 1998), eight of the nine possible selenium sites were located in the anomalous Fourier maps, resulting in clear maps suitable for accurate placement of the majority of the protein and nucleotide (Table 1). Iterative cycles of refinement and model building were performed using Phenix and Coot. Data from the PhuZ-GDP crystal were collected at ALS Beamline 8.3.1 at a wavelength of 1.115889Å. Data were processed using Elves, and the SeMet-PhuZ structure was used as a molecular replacement model. Iterative cycles of refinement and model building were performed using Phenix and Coot. 10 TLS groups (Table S1) were determined using the TLS server, and applied to the last stage of refinement.

The refined native model at 1.67Å includes protein residues 2-54, 58-315, a GDP-Mg<sup>2+</sup>, 277 water molecules, and one chloride ion and has R<sub>work</sub>/R<sub>free</sub> of 18.61/23.16% (Fig 4A, Table S1). The final structure was assessed using MolProbity (Chen et al., 2010). Data processing and refinement statistics are summarized in Table S1. PDB codes are 3R4V and 3RB8 for native and SeMet PhuZ respectively.

### **Electron Microscopy**

1 mM GMPCPP was added to 7.5 μM PhuZ in a buffer of 250 mM KCl, 50 mM HEPES pH 8, 5 mM MgCl<sub>2</sub>, 5% glycerol, and 15 mM thioglycerol, and polymers were allowed to grow for 1-2 minutes. 5 μl of the reaction mixture was applied to glow-discharged 400-mesh carbon-coated copper grids (PELCO) and negatively stained with 0.75% uranyl formate.

### **Fluorescence Recovery After Photobleaching**

Filaments were photobleached using a laser (QLM module, API) for 0.05 sec at 100% power and then followed with time lapse imaging recorded every 5 seconds.

### **Supplemental References**

Brunger, A.T., Adams, P.D., Clore, G.M., DeLano, W.L., Gros, P., Grosse-Kunstleve, R.W., Jiang, J.S., Kuszewski, J., Nilges, M., Pannu, N.S., *et al.* (1998). Crystallography & NMR system: A new software suite for macromolecular structure determination. *Acta Crystallogr D Biol Crystallogr* 54, 905-921.

Chen, V.B., Arendall, W.B., 3rd, Headd, J.J., Keedy, D.A., Immormino, R.M., Kapral, G.J., Murray, L.W., Richardson, J.S., and Richardson, D.C. (2010). MolProbity: all-atom structure validation for macromolecular crystallography. *Acta Crystallogr D Biol Crystallogr* 66, 12-21.

Drew, D., Newstead, S., Sonoda, Y., Kim, H., von Heijne, G., and Iwata, S. (2008). GFP-based optimization scheme for the overexpression and purification of eukaryotic membrane proteins in *Saccharomyces cerevisiae*. *Nature protocols* 3, 784-798.

Economou, A., Pogliano, J.A., Beckwith, J., Oliver, D.B., and Wickner, W. (1995). SecA membrane cycling at SecYEG is driven by distinct ATP binding and hydrolysis events and is regulated by SecD and SecF. *Cell* 83, 1171-1181.

Qiu, D., Damron, F.H., Mima, T., Schweizer, H.P., and Yu, H.D. (2008). PBAD-based shuttle vectors for functional analysis of toxic and highly regulated genes in *Pseudomonas* and *Burkholderia* spp. and other bacteria. *Appl Environ Microbiol* 74, 7422-7426.

Thomas, J.A., Hardies, S.C., Rolando, M., Hayes, S.J., Lieman, K., Carroll, C.A., Weintraub, S.T., and Serwer, P. (2007). Complete genomic sequence and mass spectrometric analysis of highly diverse, atypical *Bacillus thuringiensis* phage 0305phi8-36. *Virology* 368, 405-421.

## Chapter Three

### The structure and assembly mechanism of a novel three-stranded tubulin filament that centers phage DNA

Elena A. Zehr<sup>1,\*</sup>, James A. Kraemer<sup>1,\*</sup>, Marcella L. Erb<sup>2</sup>, Joanna K.C. Coker<sup>2</sup>, Elizabeth A. Montabana<sup>1</sup>, Joe Pogliano<sup>2</sup>, and David A. Agard<sup>1</sup>

<sup>1</sup>Department of Biochemistry and Biophysics and the Howard Hughes Medical Institute,  
University of California, San Francisco, CA 94158

<sup>2</sup>Division of Biological Sciences, University of California, San Diego, CA 92093

\*These authors contributed equally

This work was previously published in *Structure* and is reprinted here with permission.

## Abstract

Tubulins are a universally conserved protein superfamily that carry out diverse biological roles by assembling filaments with very different architectures. The underlying basis of this structural diversity is poorly understood. Here, we determine a 7.1 Å cryo-EM reconstruction of the bacteriophage-encoded PhuZ filament and provide molecular-level insight into its cooperative assembly mechanism. The PhuZ family of tubulins is required to actively center the phage within infected host cells, facilitating efficient phage replication. Our reconstruction and derived model reveal the first example of a three-stranded tubulin filament. We show that the elongated C-terminal tail simultaneously stabilizes both longitudinal and lateral interactions, which in turn define filament architecture. Identified interaction surfaces are conserved within the PhuZ family, and their mutagenesis compromises polymerization *in vitro* and *in vivo*. Combining kinetic modeling of PhuZ filament assembly and structural data we suggest a common filament structure and assembly mechanism for the PhuZ family of tubulins.



## Introduction

Tubulins play diverse and critical roles in eukaryotic and prokaryotic cell biology. In eukaryotes,  $\alpha/\beta$ -tubulin heterodimers typically assemble into 13-protofilament microtubules required for chromosome segregation and cellular trafficking. By contrast, monomers of FtsZ facilitate septation in bacteria and archaea via protofilaments, and perhaps sheet-like structures (Lu et al., 2000; Li et al., 2007; Aylett et al., 2011), and the plasmid segregation protein TubZ from *Bacillus thuringiensis* forms 2- and 4-stranded filaments (Aylett et al., 2010) (Montabana & Agard, unpublished data). This remarkable diversity in polymer architecture is mirrored by a significant divergence in protein sequence, which leads to variations in the length of loops and the presence or absence of N/C-terminal extensions (Nogales et al., 1998a; Ni et al., 2010). However, the underlying physical basis for these differences in filament structure is only poorly understood.

Despite significant divergence in primary amino acid sequences, the core fold of the tubulin/FtsZ superfamily of proteins is highly conserved. The structure consists of the nucleotide-binding N-terminal domain and the activation domain, which facilitates GTP hydrolysis via interaction of catalytic residues on the T7 loop, and H8 with the nucleotide-binding domain of the previous subunit in the filament. The two globular domains are separated by a long central helix, H7. Limited regions of strong sequence conservation are found in the loops required for GTP binding and hydrolysis, such as the G-box, the T7 loop and H8 (Nogales et al., 1998a). The divergent C-terminal tails of many tubulins are directly involved in binding associated factors and regulatory proteins (Aylett et al., 2011). Beyond these core structural elements, all tubulin homologues have a remarkably similar longitudinal (head-to-tail) mode of assembly (Nogales et al., 1998b; Lowe and Amos, 1999) that is dependent on GTP binding

(Weisenberg, 1972; Bramhill and Thompson, 1994). Moreover, assembly juxtaposes the catalytic T7 loop of one subunit with the GTP exposed in the interface of the one below, whereupon stimulating its hydrolysis.

Recently a new set of tubulin-like proteins, encoded by bacteriophages, has been described (Oliva et al., 2012; Kraemer et al., 2012; Aylett et al., 2013). One of these proteins, PhuZ, from bacteriophage 201 $\phi$ 2-1 (hereafter referred to as PhuZ<sub>201</sub>) was shown to form a highly-dynamic, spindle-like cytoskeleton within infected *Pseudomonas chlororaphis* cells that functions to both cluster and center 201 $\phi$ 2-1 phage particles at the cell midpoint. Interfering with PhuZ<sub>201</sub> dynamics perturbs centering and compromises phage production (Kraemer et al., 2012). PhuZ<sub>201</sub> belongs to the PhuZ family of tubulin homologues (Kraemer et al., 2012), encoded by the genomes of very large bacteriophages from the “ $\phi$ KZ-like viruses” genus and the phage EL (Krylov et al., 2007; Lavigne et al., 2009). Virion particles of these giant *Pseudomonas* phages (211-317 kb in size) can have heads as large as 145 nm in diameter and 200 nm tails (Fokine et al., 2007). For such large viruses, diffusion within the host cell is likely quite restricted, perhaps explaining the reliance on a tubulin cytoskeletal element.

The atomic structure of PhuZ<sub>201</sub> bound to GDP showed that while PhuZ<sub>201</sub> has a conserved tubulin/FtsZ-like fold, it possesses several unique features, including an unusually long helix H11, and an extended C-terminus. PhuZ<sub>201</sub> also lacks H6, which contributes to longitudinal interactions in other tubulin homologues (Kraemer et al., 2012; Nogales et al., 1999), raising questions as to how PhuZ<sub>201</sub> forms filaments. Though the crystal lattice appeared to contain protofilaments, adjacent longitudinal subunits were separated far more than usual, forming a “relaxed” longitudinal interface, and the vast majority of intra-protofilament interactions were derived from the interactions between the C-terminal tail and the adjacent

longitudinal subunit. Highly conserved acidic residues on the C-terminal tail of one subunit (the “acidic knuckle”) make electrostatic contacts with a basic patch, formed by H3, H4 and H5, of its longitudinal neighbor. The importance of these C-terminal tail interactions for filament assembly was confirmed both *in vitro* and *in vivo* by mutagenesis (Kraemer et al., 2012). Together, these structural and functional results suggested a unique mechanism of filament assembly. Recently, atomic structures of a closely related PhuZ protein, PhuZ<sub>KZ</sub> ( $\phi$ KZ TubZ), encoded by the bacteriophage  $\phi$ KZ, were solved revealing a high degree of structural similarity to PhuZ<sub>201</sub>, equivalent extensive longitudinal interactions mediated by the C-terminal tail, but with a more canonical tubulin/FtsZ “tense” longitudinal interface (Aylett et al., 2013).

In this work, we use cryo-EM to define the first high resolution three-dimensional (3D) architecture of a three-stranded tubulin filament, and use a combination of solution polymerization measurements, kinetic modeling, and mutational analyses to confirm the relevance of this architecture *in vitro* and *in vivo*, and to understand the PhuZ<sub>201</sub> assembly mechanism. Based on a derived pseudo-atomic model and site-directed mutagenesis, conserved charged residues within the C-terminus are identified that are essential for stabilizing three-stranded lateral interactions and filament assembly. These data allow us to propose a model for the structural origins of polymer metastability. Finally, by virtue of the high conservation of the residues that form filament contacts in PhuZ<sub>201</sub>, we propose that the mechanism of PhuZ<sub>201</sub> filament assembly and its architecture are also conserved among the members of the PhuZ family.

## **Results**

### **PhuZ<sub>201</sub> assembles three-stranded filaments**

To gain molecular insight into the mechanism of phage centering by PhuZ<sub>201</sub>, we sought to determine the three-dimensional filament structure by electron microscopy (EM). While the filaments might have seemed to be two-stranded at first, the unusual pattern of regular intensities along the filament axis seen in reference-free two-dimensional (2D) class averages of negatively stained PhuZ<sub>201</sub> filaments is more consistent with a three-stranded architecture (Fig. 1A). These observations suggested a filament geometry distinct from that seen in the crystal (Kraemer et al., 2012). Fourier transforms of reference-free 2D averages of 500 segments of PhuZ<sub>201</sub> polymerized in either 1mM GTP or the slowly-hydrolysable GTP analogue, GMPCPP, looked indistinguishable, suggesting a similar filament architecture in the GDP or GTP state (Fig. 1B). As a result, and to avoid potential structural heterogeneity resulting from variability in GTP hydrolysis, the reconstruction was performed on frozen-hydrated PhuZ<sub>201</sub> filaments assembled in the presence of 1mM GMPCPP.

To look for complementary evidence of this unusual three-stranded organization and to gain insight into the assembly mechanism, PhuZ<sub>201</sub> growth kinetics were measured by right-angle light scattering at various concentrations in saturating (1 mM) GTP (Fig. 1C). Polymerization experiments were carried out in BRB80 buffer pH 7.2 to limit the formation of bundles, and the resultant critical concentration of  $2.5 \pm 0.1 \mu\text{M}$  was slightly lower than that previously reported for polymerization at pH 6.8 (Kraemer et al., 2012). No single step model for progression to the nucleus, defined as the minimum number of monomers assembled where polymerization is more favorable than depolymerization, fit the experimental data. Instead, a multi-step formalism derived from that developed by Flyvbjerg and colleagues (Flyvbjerg et al., 1996), where multiple subunits can come together in multiple steps, was applied with modeling in Berkeley Madonna, a differential equation-based modeling software. The data were best

described by a model wherein filaments form in two major kinetic steps: first bringing six monomers together, followed by further addition of a dimer. A nucleus size of six is consistent with a three-stranded filament, where forming two full layers would satisfy all inter-monomer contacts required for growth.

Cryo-EM in conjunction with a single particle helical analysis method (Frank et al., 1996; Egelman, 2000, 2007) was used to determine the 3D structure of the PhuZ<sub>201</sub>-GMPCPP filament (Experimental Procedures). To better assess the resolution of the final map and to minimize overfitting, we used the “gold standard” procedure in which two separate reconstructions are independently developed from non-overlapping halves of the data and then compared at each cycle to optimize estimation of the current resolution, and filtering for the next round of parameter refinement (Scheres and Chen, 2012). The final PhuZ<sub>201</sub> 3D map had a conservative resolution of 7.1 Å, based on the 0.5 Fourier Shell Correlation cutoff (Fig. S1A), and had refined to the helical symmetry parameters of -116.4° rotation and 14.4 Å axial rise per subunit. The determined helical parameters were robust, as convergence to the same solution was achieved from different starting values of both helical parameters (Fig. S1B, and data not shown). While the filament is a left-handed one-start helix, the azimuthal rotation of less than -120° per subunit results in an overall right-handed supertwist (Fig. 2A). The hand of the supertwist was confirmed by tomography (data not shown). Moreover, computational experiments using different helical symmetries were done to demonstrate that all three strands were parallel (data not shown). The three-stranded architecture of the polymer is distinct from that of other cytomotive filaments characterized to date (Fig. 2B).

### **PhuZ<sub>201</sub> subunits are uniquely oriented within the filament**

To interpret the cryo-EM map on a molecular level a pseudo-atomic model of the PhuZ<sub>201</sub> filament was built using the known atomic structure (Kraemer et al., 2012) (Fig. 2C). At the obtained resolution, although individual  $\beta$ -strands were not resolvable, all  $\alpha$ -helices, many loops and the C-terminal tail (the most C-terminal 21 residues) could readily be fit, allowing unambiguous docking of the PhuZ<sub>201</sub> atomic model into the map. Fitting of the two globular domains and H7 separately into the map density resulted in a better fit to the map; the overall displacement was less than 1 Å suggestive of slight conformational changes within the tubulin core. However, such simplistic fitting resulted in a worse fit for a number of loops, and we felt the resolution was insufficient to justify the significant rebuilding required. Consequently, we focus here on the compromise fit, treating the entire core as a single rigid body. By contrast, the C-terminus (H11 and the C-terminal tail) required significant adjustments to fit into its corresponding cryo-EM density (Fig. S1). Particularly, the acidic knuckle (the last 13 residues of the 21 residues of the C-terminal tail) (Kraemer et al., 2012) needed to be moved together with the upper subunit, which resulted in  $\sim 6$  Å displacement and  $10.8^\circ$  rotation of the knuckle towards the outer surface of the filament (Fig. S1C). This preserved all of the acidic knuckle interactions observed in the crystal structure (Kraemer et al., 2012). An important consequence of this movement was to prevent clashes between the knuckle with H5 of the upper subunit and H9 of a subunit in the neighboring strand. To adapt to the movement, the rest of the tail structure needed to be repositioned towards the neighboring strand. Since the required motion was complex, a flexible fitting procedure was used (Supplemental Experimental Procedures), shifting residues F295-I302 of the tail by on average 3.5 Å towards the adjacent strand to bring them into their map density (Fig. S1D). Additionally, H11 was tilted by  $6^\circ$  towards the lumen to reposition it more upright within the three-stranded filament (Fig. S1E). The overall correlation coefficient

between the model and the map improved from a starting value of 0.610 to 0.640 following fitting.

The model of the PhuZ<sub>201</sub> filament (Fig. 2C, Movie S1) revealed that the subunit orientation along the filament axis is unique with the subunit rotated by  $\sim 180^\circ$  about the long axis of the filament when compared with  $\alpha/\beta$ -tubulin's orientation within microtubules and TubZ subunit's orientation within the four-stranded filament (Nogales et al., 1999), (Montabana & Agard, unpublished data). Particularly, the PhuZ<sub>201</sub> N-terminus faces the exterior of the filament and most of the C-terminus (H11 and the C-terminal tail) faces the interior (Fig. 3A, B). The N-terminal domain defines the outer surface of the filament, whereas the lumen is dominated by the activation domain, H11 and the C-terminal tail. The acidic knuckle is largely sequestered from solvent along the axis of the filament (except for E310), but, of course, would be fully solvent-exposed at the plus end of the filament. The crescent-shaped subunits are oriented such that the curved helices H1, H2 and H3 construct the outer surface of the filament (Fig. 3A), and the straight long helices H5, H7, and H11 (Fig. 3B), surrounding the large acidic pocket left in place of the missing H6, outline the lumen. The filament is not a hollow tube, as its lumen is filled by the map densities connecting the protofilaments and the densities corresponding to the C-termini (Fig. 2B, Movie S1). The unique monomer orientation arises as a consequence of distinctive lateral interactions for a tubulin/FtsZ-like filament.

Based on the fit model, the C-terminus of each PhuZ<sub>201</sub> subunit contacts three other subunits: a laterally adjacent dimer as well as the adjacent longitudinal subunit (Fig. 3C). To aid in describing the unique interactions that a subunit makes within the three-stranded filament, we label subunits contacted by a subunit (#0) as follows: #1 is a longitudinally adjacent subunit within the same protofilament, #2 is a laterally adjacent subunit at the plus end and #3 is a

laterally adjacent subunit at the minus end of the neighboring protofilament (Fig. 3C). As described previously, the nine, primarily charged, most distal C-terminal residues of the acidic knuckle of the subunit #0 contact subunit #1 (Kraemer et al., 2012), while at least three other contacts are formed between other residues in the C-terminal tail and residues in the subunits #2 and #3. These interactions are electrostatic/polar in nature and contribute 680 Å<sup>2</sup>/subunit of buried surface area. In detail, D303 and D305 of the acidic knuckle of the subunit #0 were found to be in close proximity to K238 of H10 and R217 of H9 of the subunit #2 (Fig. 3D). Additionally, N299 of the subunit #0 seems to form a polar interface with Q157, found in the S6-H7 loop of the subunit #3, while R290 of H11 (#0) contacts E225 in the H9-S8 loop of the subunit #3 (Fig. 3D, E). The abovementioned fitting adjustments to the C-terminus were essential to make these inter-strand contacts, thereby providing insights into structural rearrangements that accompany filament formation.

### **Mutations to conserved residues in the predicted lateral interface disrupt PhuZ<sub>201</sub> filament formation**

To test the validity of the predicted lateral interaction surfaces, point mutations to some of the residues were generated and mutants were tested for the ability to polymerize by right-angle light scattering, high-speed pelleting assay and negative stain EM. Based on proximity in the model, alanine mutations were made to putative salt-bridge forming residues D303, D305 within the conserved IIDXDD motif and the also well-conserved R217 (Fig. S2). Importantly, D303 and D305 were solvent-exposed in the PhuZ<sub>201</sub> crystal structure and consequently did not appear to be relevant for the formation of longitudinal interactions (Kraemer et al., 2012). The



D303A mutation had a mild effect on PhuZ<sub>201</sub> assembly, with a critical concentration of  $3.7 \pm 0.2$   $\mu\text{M}$  and a slightly longer lag phase than that observed for the wild type (Table S1, Fig. 4A). The D305A mutation was more severe, with the mutant assembling at a critical concentration of  $4.1 \pm 0.4$   $\mu\text{M}$  (Table S1). The D305A assembly curve had a long lag phase and decayed soon after it reached its peak, which suggested assembly of less stable filaments (Fig. 4A). Combining these mutations had an additive effect, with the D303A/D305A double mutant polymerizing with a critical concentration of  $9.4 \pm 0.3$   $\mu\text{M}$  (Table S1), a lag phase longer than either of the single mutants, and a rising and falling polymerization curve similar to the one measured for D305A, likely indicative of polymer instability (Fig. 4A). In order to examine unstable structures the double mutant formed, it was assembled in excess GMPCPP and imaged via negative stain EM. The mutant still formed three-stranded filaments, although very rarely (Fig. S3A). By contrast, the R217A mutation resulted in no detectable polymerization measured by right-angle light scattering, even at concentrations as high as 30  $\mu\text{M}$  (Fig. 4A). In the presence of GMPCPP, PhuZ<sub>201</sub>-R217A formed only amorphous structures (Fig. S3B).

These observations supported the relevance of R217 and D305, which are predicted by the model to form a salt bridge stabilizing the lateral interface (Fig. 3D). To test this prediction, individual charge reversal mutations, R217D and D305R, along with the charge-swap double mutant, R217D/D305R, were generated, and their functional consequences examined. Similar to the R217A mutant, PhuZ<sub>201</sub>-R217D was unable to form any detectable polymer at concentrations up to 30  $\mu\text{M}$  (Fig. 4A, B), but formed amorphous structures in GMPCPP (Fig. 4C). The D305R mutant was also severely polymerization-compromised (Fig. 4A, B), with a critical concentration of  $8.0 \pm 0.2$   $\mu\text{M}$  (Table S1). The mutant no longer appeared to assemble into three-stranded filaments, but formed rare, short and twisted structures with a variable number of strands (Fig.

4D). PhuZ<sub>201</sub>-D305R polymerized with almost no lag phase and was unstable in GTP, suggesting that the structures it formed lacked key stabilizing interactions (Fig. 4A). By contrast, combining the R217D and D305R mutations recovered polymerization (Fig. 4A, B), albeit with a significantly higher critical concentration ( $5.9 \pm 0.3 \mu\text{M}$ ) (Table S1). Importantly, the double mutant also restored formation of three-stranded filaments (Fig. 4E). These observations support the existence of a salt bridge between R217 and D305, and confirm its importance for polymer assembly.

To test whether PhuZ<sub>201</sub> uses the same surfaces for its assembly *in vivo*, we examined the ability of these mutant proteins to make filaments in *P. chlororaphis* cells. Fusion constructs of the wild type and the mutant versions of PhuZ<sub>201</sub> fused to green fluorescent protein were generated, and conditionally expressed from a plasmid. Both the D303A and D305A mutations impaired filament formation *in vivo* (Fig. 5A, B), with the D305A single mutant and the D303A/D305A double mutant having the most severe affects. Additionally, the R217A, R217D or D305R mutants completely eliminated filament formation in cells (Fig. 5C, D). In accordance with the *in vitro* observations, the double mutant R217D/D305R resulted in a partial restoration of the ability to assemble filaments in about 15% of cells when expressed at high levels (grown in the presence of 2% arabinose) (Fig. 5C, D). Those filaments that formed were dynamic and appeared to be similar to the wild type filaments. The *in vivo* observations are completely consistent with the *in vitro* assembly behavior of the mutants, suggesting that PhuZ<sub>201</sub> assembles into filaments with at least three strands. These findings demonstrate the importance of the conserved residues for the establishment and stability of lateral interactions, and suggest a conserved mechanism for the filament formation within the PhuZ family of tubulin homologues.

## Comparison of the filament structure to crystal structures reveals origins of twist and movement of the C-terminal tail

As demonstrated nicely by a morph (Movie S2) between the crystallographic protofilaments (3r4v and 3ZBQ) (Kraemer et al., 2012; Aylett et al., 2013) and the structure of the three-stranded filament, the PhuZ<sub>201</sub> dimer undergoes a striking rearrangement upon incorporation into the filament lattice. PhuZ<sub>201</sub> subunits form a canonical tense tubulin/FtsZ longitudinal interface in the presence of the  $\gamma$ -phosphate (Movie S2). Within the PhuZ<sub>201</sub>-GMPCPP filament a subunit buries 840 Å<sup>2</sup> surface area at the tense interface as opposed to 188 Å<sup>2</sup>/subunit at the relaxed interface observed within the PhuZ<sub>201</sub>-GDP crystal (Kraemer et al., 2012) (Fig. 6A). To compare subunit packing within the filament to the post GTP-hydrolysis arrangement depicted within the PhuZ<sub>KZ</sub>-GDP (3ZBQ) protofilament (having no twist and 43.5 Å pitch) (Aylett et al., 2013), we modeled the straight protofilament by separately superimposing two PhuZ<sub>201</sub> monomers over a PhuZ<sub>KZ</sub> longitudinal dimer using the N-terminal domains (residues 2-160 in PhuZ<sub>201</sub> and 4-174 in PhuZ<sub>KZ</sub>), but excluding the activation domains and the C-termini, for alignment. The post-hydrolysis longitudinal interface in the PhuZ<sub>KZ</sub>-like dimer model buries 930 Å<sup>2</sup>/subunit. While the  $\sim 11^\circ$  twist between longitudinally adjacent subunits and the slightly smaller pitch of the PhuZ<sub>201</sub>-GMPCPP filament (43.2 Å) results in a small decrease in the longitudinal buried surface area compared to the PhuZ<sub>KZ</sub>-like subunit packing, the overall effect is to tighten contacts around the GTP-binding pocket. Within a GMPCPP dimer the contact surface between H10 and H7 is weakened, but tighter contacts are established between the T7 and the S2-S3 loops, and the catalytic N-terminus of H8 with the T3 loop of the subunits #1 and #0 respectively (Fig. 6B). Measured distances from the catalytic Asp on the T7 loop to the  $\beta$ -phosphate are the same in the PhuZ<sub>201</sub>-GMPCPP dimer and the PhuZ<sub>KZ</sub>-

like state: 6.7 Å and 6.8 Å respectively, but much shorter than in PhuZ<sub>201</sub>-GDP (10.5 Å) (Fig. 6B).

The other significant consequence of filament formation is that both the twist and the structural rearrangement of the C-terminus contribute to the establishment of the lateral interface (Movie S2). The twist between longitudinal subunits brings the finger-like IIDXDD motif of the subunit #0 and the shape-complementary basic cavity, defined by R217 and K238, of the laterally adjacent subunit #2, ~5 Å closer towards each other. Moreover, the C-terminus of the subunit #0 pulls away from the side of the longitudinal subunit #1 in order to form lateral interactions with the subunits #2 and #3 (Fig. 6A and Movie S2). While the majority of the contacts made by residues of the acidic knuckle remain intact, the remaining residues of the C-terminal tail and H11 (K294-D306) separate in order to establish lateral interactions (Fig. 6A). This movement shifts the C<sup>α</sup> of N299 of the subunit #0 ~2 Å closer towards the C<sup>α</sup> of Q157 of the subunit #3 placing the two alpha carbons ~5 Å apart. The C-terminal helix, H11, of the subunit #0 is also tilted towards the central axis of the filament to form a putative salt bridge between R290 and E225 of the subunit #3. The net result of these C-terminal tail movements is a significant loss of the intra-subunit buried surface area: 780 Å<sup>2</sup>/subunit in the filament vs. 1,226 Å<sup>2</sup>/subunit in the crystal (Kraemer et al., 2012) (Fig. 6A). This energetically unfavorable loss of intra-protofilament interactions is compensated by the establishment of new lateral interactions, resulting in an overall larger surface area buried per subunit in the three-stranded filament versus the crystallographic protofilament.

## Discussion

While the core tertiary structure is well conserved in the tubulin/FtsZ superfamily, a high degree of sequence variation, including insertions and deletions in loops and termini, leads to divergent filament morphologies. Since only the structures of microtubules and TubZ have been determined to even moderate resolution (Sui and Downing, 2010), (Montabana & Agard, unpublished data), we are just beginning to understand how these sequence variations define polymer architecture. Here, we describe the unique three-stranded filament structure of a phage-encoded tubulin homologue, PhuZ<sub>201</sub>, at 7.1 Å resolution by cryo-EM. Docking the crystal structure of PhuZ<sub>201</sub>-GDP (Kraemer et al., 2012) into the map reveals the critical role that the C-terminal tail plays in filament assembly. As previously noted, the acidic residues in the tail of one subunit (#0) bind to a well-defined basic pocket in the longitudinal subunit (#1) to stabilize protofilament interactions (Kraemer et al., 2012). Remarkably, the other solvent exposed acidic residues, within the conserved IIDXDD motif, are shown here to mediate lateral interactions with both #2 and #3 subunits in adjacent protofilaments. To mediate lateral contacts, the C-terminal tail undergoes a significant conformational rearrangement upon assembly, trading off intra-protofilament interactions for inter-protofilament interactions, with only the acidic knuckle retaining its original longitudinal contacts. While tubulin C-termini have been described to be involved in binding interactions with non-tubulin partners, this use of a C-terminus in defining filament architecture, leading to cooperative assembly represents a new polymerization mechanism.

Importantly, residues forming both the lateral and longitudinal contacts observed here for PhuZ<sub>201</sub> are conserved in the related phage tubulins PhuZ<sub>PA3</sub> and PhuZ<sub>KZ</sub> (Fig. S2 and Fig. S4A,

B). While D303, D305 and R217 are found in all three homologues, lysine (K238) is conservatively substituted for arginine in PhuZ<sub>PA3</sub> and PhuZ<sub>KZ</sub>. Moreover, the putative polar interface most likely exists in PhuZ<sub>PA3</sub> and PhuZ<sub>KZ</sub> as well, since N299 and Q157 are identical or have conservative substitutions in these proteins. Finally, the putative electrostatic interface between R290 and E225 is conserved in PhuZ<sub>KZ</sub>, and while R290 is missing in PhuZ<sub>PA3</sub>, there is an arginine one helical turn away (R294) that could interact with E225. Thus, based on conservations of critical interactions, we propose that both PhuZ<sub>KZ</sub> and PhuZ<sub>PA3</sub> form similar three-stranded polymers. In support of this, a 2D class average of segments from PhuZ<sub>PA3</sub> filaments shows a pattern characteristic of a three-stranded polymer (Fig. S4C, Fig. 1A). By contrast, the fourth, more evolutionary divergent PhuZ family homologue, PhuZ<sub>EL</sub>, encoded by bacteriophage  $\phi$ EL that does not belong to the “ $\phi$ KZ-like viruses” genus (Lavigne et al., 2009), shows significant variations at the lateral interface, suggestive of a different filament architecture. We had also previously identified a subset of proteins (Cb, Ck, Ca and Cl) belonging to a family of *Clostridial* chromosomal tubulin homologues that also have acidic knuckle sequences (Kraemer et al., 2012). Intriguingly, these tubulins show conservation in a number of the key interactions that define the polymer contacts identified here (Fig. S2), suggesting their filament morphologies may be related.

The structural and kinetic data from this study and the three structures described in previous studies (Kraemer et al., 2012; Aylett et al., 2013) provide insight into the mechanism of PhuZ filament assembly and the role of the  $\gamma$ -phosphate in setting up the metastability required for filament dynamics (Fig. 7). We propose that these structures relate to distinct stages in the assembly process. First, GTP-bound monomers (PhuZ<sub>KZ</sub> 3ZBP) (Aylett et al., 2013) would associate via the extensive interactions between the C-terminal tail of one monomer (#0) and

binding pocket of the #1 monomer forming longitudinal dimers (PhuZ<sub>201</sub> 3r4v) with a relaxed subunit-subunit interface (Kraemer et al., 2012). In the presence of GTP, this state is likely in equilibrium with a compacted form corresponding to a straight tense interface observed within the crystallographic protofilament (PhuZ<sub>KZ</sub> 3ZBQ) (Aylett et al., 2013). The linker allows the longitudinal subunit-subunit interface to elastically transition between these two states: relaxed (47Å) (Kraemer et al., 2012) and tense (~43.5 Å) (Aylett et al., 2013). Three of these dimers then laterally associate further reorganizing the C-termini, twisting and moving out their C-termini to fulfill all of the filament contacts within the hexameric nucleus. The energetically unfavorable loss of longitudinal contacts and strain from the twisting are stabilized by the newly formed lateral interactions and the presence of the  $\gamma$ -phosphate. The filament then grows by further addition of GTP-bound monomers and dimers. We propose that upon GTP hydrolysis, strain resulting from twisting and displacement of C-terminal interactions within each subunit is trapped by cooperative lattice interactions, leading to metastability and highly dynamic filaments.

Previous work had shown that dynamic PhuZ filaments are necessary for clustering and centering phage particles within the host bacterial cell. Interfering with filament dynamics leads to offset fragmented clusters and a significant decrease in phage burst size (Kraemer et al., 2012). Given its conservation among the members of the PhuZ family, the specific choice of a three-stranded architecture must somehow be particularly important for the viral replication cycle. One possibility is that the three-stranded filament morphology could provide a stiffer structure than the more common two-stranded architecture of plasmid-segregating prokaryotic actins in order to move such very large phage particles (200nm+) or their genomes in a crowded cytoplasm. Another intriguing possibility is that the filament's three-stranded architecture might

be a structural adaptation that facilitates interactions directly, or indirectly through an adaptor protein, with three-fold symmetry centers within the capsid or tail.

There are a number of potential protein-protein interaction surfaces in PhuZ that could be functionally important. Of particular note is the acidic C-terminal tail. Within the body of the filament the tail is sequestered in the lateral interface, but it is completely exposed at the plus-end of the filament. Thus, this could provide a unique polar binding site for linkage to DNA or the phage in a manner reminiscent of the interaction between ParM filaments and the end-binding ParRC complexes that connect the filament to plasmid DNA (Garner et al., 2007; Gayathri et al., 2013). Alternatively, among the conserved surfaces exposed along the filament is an acidic patch, defined by D235, D259 and D263, that is in close proximity to the lateral interface formed by the IIDXDD motif and the basic pocket defined by R217 and K238 (Fig. S4B).

The unusual three-stranded architecture of the filament and the novel role of the C-terminus pose intriguing questions about PhuZ filament dynamics and its biological role. Although the filament structure suggests how the energy of GTP is stored within the helical lattice - through the bending of the C-terminus and the supertwist - how this structure defines the dynamic properties of the polymer remains to be explained. Future high-resolution structural studies of PhuZ<sub>201</sub> bound to different nucleotides, both in monomeric and filamentous forms, complemented by kinetic solution and modeling studies are needed to answer this question. Beyond this, the major issues going forward concern the physical and possible regulatory coupling of polymer dynamics to phage maturation and host cell positioning. Whether this only involves phage-encoded proteins or whether host proteins are also recruited remains to be determined.



## **Acknowledgements**

We thank Justin Kollman and Sam Li and for invaluable discussions on image processing, Justin Kollman and Xueming Li for help with image collection, Michael Braunfeld and Bettina Keszthelyi for the help on tomography data collection and processing and Pascal Wassam for maintenance of systems hardware and software. JAK was supported by a Genetech predoctoral fellowship and an ARCS award. This work was supported by HHMI (DAA) and NIH grants GM031627 (DAA), R01GM073898 (JP), and GM104556 (JP and DAA).

## **Accession Codes**

The EM reconstruction and atomic coordinates have been deposited in the Electron Microscopy Data Bank, and the RCSB Protein Data Bank with accession codes EMD-5783 and 3J5V respectively.

## **Materials and Methods**

### **Protein Expression and Purification**

The genes encoding  $\text{PhuZ}_{\text{PA3}}$  and  $\text{PhuZ}_{201}$  were cloned into pET28a (+) with a 6-His tag on the N terminus and expressed in BL21(DE3) cells under an IPTG-inducible T7 promoter. The  $\text{PhuZ}_{201}$  mutants were generated by two primer site-directed mutagenesis PCR. 1 mM IPTG was added once cells reached an  $\text{OD}_{600}$  of 0.7 at 37°C and protein was allowed to express for 8 hr at 16°C before the cells were pelleted. Cells were lysed in a buffer containing 250 mM KCl,

50 mM HEPES pH 7.4, 1 mM MgCl<sub>2</sub>, 10% glycerol, 1mM DTT. EDTA-free protease inhibitor tablets were included during lysis. 250 mM imidazole was added to elute the protein from the Ni-NTA resin. The 6-His tag was cleaved overnight at 4°C by thrombin protease, followed by gel filtration chromatography (Superdex 200) in a buffer as described above, but omitting glycerol.

### **Negative Stain Electron Microscopy**

10 μM PhuZ was polymerized in BRB80 pH7.2 with the addition of 1 mM GMPCPP for 2 min at room temperature. 4 μl of polymerized protein was applied to carbon-coated grids after glow-discharging, unbound sample was washed away with water and grids were stained with 0.75% uranyl formate. Micrographs were collected on Tecnai T12 or T20 microscopes (FEI Co.) using accelerating voltage 120 kV or 200 kV and magnification X52,000 or X50,000 respectively. Images were recorded with a 4k X 4k charge-coupled device (Gatan, Inc.).

### **Sample Preparation and Data Collection for Cryo-Electron Microscopy**

20 μM of PhuZ<sub>201</sub> was polymerized in 50 mM HEPES pH 8, 125 mM KCl, 5 mM MgCl<sub>2</sub>, 5% glycerol and 1 mM GMPCPP for 1 minute at room temperature. 2 μl samples were applied on C-FLAT holey carbon grids and plunge-frozen into liquid ethane using Vitroblot (FEI Co.) Micrographs were collected on Technai F20 operating at 200V. Images were recorded with an 8k X 8k TemCam-F816 camera (TVIPS) at a magnification X62,000, corresponding to a pixel size of 1.204 Å. Total electron dose was in the range of 25-30 e<sup>-</sup> per Å<sup>2</sup> and images were acquired over an underfocus range of 0.7 to 2.5 μm.

### **Image Processing**

CTFFIND was used to determine defocus parameters (Mindell and Grigorieff, 2003). Contrast transfer function (CTF) was corrected by applying Weiner filter to the entire micrograph. 461 cryo-EM micrographs were CTF-corrected, and 460-pixel segments with 40 pixels shift for each segment were extracted from the micrographs. The large segment size was chosen to maximize the accuracy of image alignment in the initial rounds of reconstruction. Reconstructions were determined by iterative helical real space reconstruction (IHRSR) (Egelman, 2000), performed essentially as described by Egelman *et al*, 2000, but following the “gold standard” procedure (Scheres and Chen, 2012) with two models refined independently to optimize resolution estimates and minimize data overfitting. SPIDER (Frank et al., 1996) was used for multireference alignment, projection matching, back projection and hsearch\_lorenz program was used for symmetry search (Egelman, 2000). A preliminary reconstruction (reconstructed without the application of the “gold standard” procedure) of the filament starting from a plain cylinder was carried out. Then, the obtained model was low-pass filtered to 40Å and used as starting references for the reconstruction (with the application of the “gold standard” procedure) of the cryo-EM map shown in this work. Reference projections were generated at 2° intervals perpendicular to the helix axis and up to 12° out-of-plane tilt. The segments were rejected based on the excessive shifts perpendicular to the helix axis and rotations deviating from average rotations for filaments. Filaments containing less than 70% (initial rounds of alignments) or 90% (final rounds of alignment) segments determined as having the same polarity were discarded. After ten initial rounds of alignment, the segments were recentered, applying the determined in the tenth round of refinement shift values, with respect to the helix axis. Then, the segments were masked to 260 pixels along the helix axis, to minimize the effect of filament bending, and 120 pixels perpendicular to the axis with a cosine-edged mask. The initial rounds of

projection matching were carried out using 2X binned data, while the final rounds were performed on unbinned images. An FSC curve was calculated between the two reconstructions at the end of each refinement round and the volumes were low-pass filtered to an estimated resolution, and then these volumes were used as the references for the next round of refinement. At the last round of refinement the half reconstructions were combined to obtain the final cryo-EM model. A total of 69,729 unique PhuZ<sub>201</sub> subunits contributed to the final reconstruction. The map was low-pass filtered to 7.1 Å and sharpened with a -1200 Å<sup>2</sup> B-factor. While this is somewhat large value, even at this level of sharpening the map had very little noise. Molecular graphics and analyses were performed with UCSF Chimera (Pettersen et al., 2004). Noise in the final 3D map was eliminated for display purposes using UCSF Chimera “Hide Dust” option (Pettersen et al., 2004).

### **Light Scattering**

Protein was thawed and spun at 80,000X RPM in a TLA100 rotor (Beckman) at 4° C prior to all light scattering assays. Right-angle light scattering was conducted by mixing PhuZ<sub>201</sub> with BRB80 pH 7.2 (80 mM PIPES, 1 mM MgCl<sub>2</sub>, 1 mM EGTA, pH 7.2 with KOH) containing GTP using a micro-volume stopped-flow system designed in-house. An illumination wavelength of 532 nm was used. Critical concentrations were determined by plotting the maximum intensity versus PhuZ<sub>201</sub> concentration for each mutant. The x-intercept of this plot was used as the critical concentration.

### **Pelleting assay**

Protein samples were spun down for 5 min at 4°C at 80,000X RPM in a TLA100 rotor (Beckman) to remove protein aggregates. 10 µM protein was polymerized in BRB80 pH 7.2, 1mM DTT and 2mM GTP for 2 min at room temperature and spun down at 80,000X RPM for 30 min at 4°C. Supernatant and pellet were analyzed by SDS-PAGE electrophoresis using 12% gel, stained with a Coomassie reagent.

### **Strain Construction**

All mutant strains used (Table 1) were constructed via site-directed mutagenesis PCR on the previously published pME28 (Kraemer et al., 2012), which is the wild type GFP-PhuZ<sub>201</sub> genetic fusion borne in the broad range *Pseudomonad* vector pHERD30T (Qiu et al., 2008). *Pseudomonas chlororaphis* 200B-1 cells were prepared and transformed as in (Howard et al., 2007).

### **Filament Expression Levels in Mutant Strains**

*P. chlororaphis* cells bearing the respective mutant plasmids (Table 1) were grown overnight at 30°C on a Hard Agar plate (Thomas et al., 2008) supplemented with gentamicin sulfate at 25 µg/mL. To prepare the microscope slides, agarose pads were made with 25% LB, 75% distilled H<sub>2</sub>O, 13 mg/mL agarose, 0.1 µL/mL FM4-64 membrane dye, 0.1 µL/mL gentamicin (concentration 25 µg/mL), and the appropriate amount of arabinose. A single colony of cells was then transferred to the slide pad and incubated for 2 hours at 30°C in a humidified chamber. Images of the live cells after 2 hours of incubation were analyzed using ImageJ for total number of cells and number of cells expressing filaments at different arabinose concentrations. Cells were imaged on a Deltavision Deconvolution system (Applied Precision/GE) IX70 Olympus microscope with 100x 1.4 PlanApo lens.

**Table 1 – Strains and plasmids used**

Strain	Organism	Plasmid/Mutation	Citation
ME41	<i>P. chlororaphis</i> 200B-1	pME28/GFP-PhuZ	(Kraemer et al., 2012)
ME91	<i>P. chlororaphis</i> 200B-1	pME57/GFP-PhuZD303A	This paper
ME92	<i>P. chlororaphis</i> 200B-1	pME58/GFP-PhuZD305A	This paper
ME93	<i>P. chlororaphis</i> 200B-1	pME61/GFP-PhuZD303305A	This paper
ME102	<i>P. chlororaphis</i> 200B-1	pME62/GFP-PhuZR217A	This paper
ME103	<i>P. chlororaphis</i> 200B-1	pME63/GFP-PhuZR217D	This paper
ME104	<i>P. chlororaphis</i> 200B-1	pME64/GFP-PhuZD305R	This paper
ME105	<i>P. chlororaphis</i> 200B-1	pME65/GFP-PhuZR217DD305R	This paper

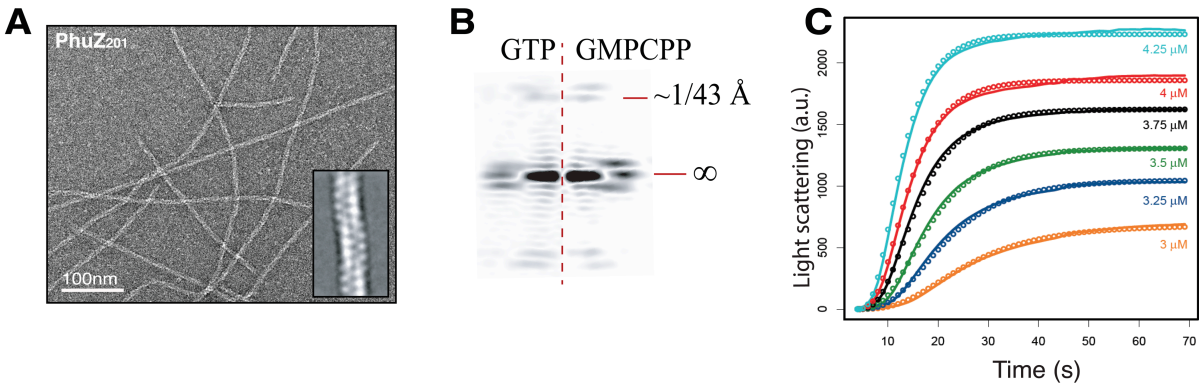


**Figure 1.** PhuZ<sub>201</sub> assembles three-stranded filaments and forms a hexameric nucleus. **(A)** Section of a micrograph of negatively stained PhuZ<sub>201</sub> filaments polymerized in excess GMPCPP. Inset: reference free 2D average of 500 segments of PhuZ<sub>201</sub> polymer. **(B)** Fourier transforms of reference free 2D averages of 500 segments of PhuZ<sub>201</sub> polymerized in 1mM GTP (left) or 1mM GMPCPP (right) show that the pitch of the filament is the same and is  $\sim 43$  Å. (left) GTP is hydrolyzed soon after assembly resulting in PhuZ<sub>201</sub>-GDP filaments. **(C)** Determination of the nucleus size for PhuZ<sub>201</sub>. PhuZ<sub>201</sub> was polymerized at varying concentrations in excess GTP. Solid lines are experimental data and circles are modeling results indicating a hexameric nucleus that grows by monomer and dimer addition.

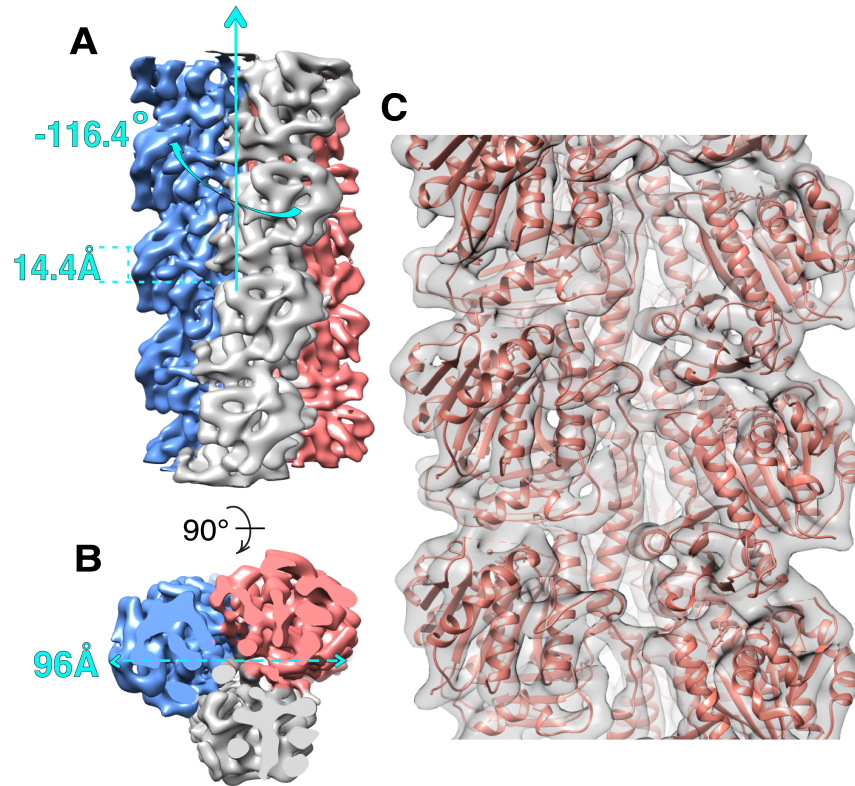


**Figure 2.** Cryo-EM map and pseudo-atomic model of PhuZ<sub>201</sub> filament. **(A)** and **(B)** Cryo-EM map of PhuZ<sub>201</sub> filament with each protofilament presented in a different color. **(A)** Map has helical symmetry of  $-116.4^\circ$  rotation and  $14.4 \text{ \AA}$  rise per subunit. **(B)** End-on view of the filament shows that it is a trimer with  $96 \text{ \AA}$  diameter. **(C)** Pseudo-atomic model of PhuZ<sub>201</sub> filament. In gray surface is the cryo-EM density fitted with the atomic models of PhuZ<sub>201</sub> in salmon. See also Figure S1 and Movie S1.



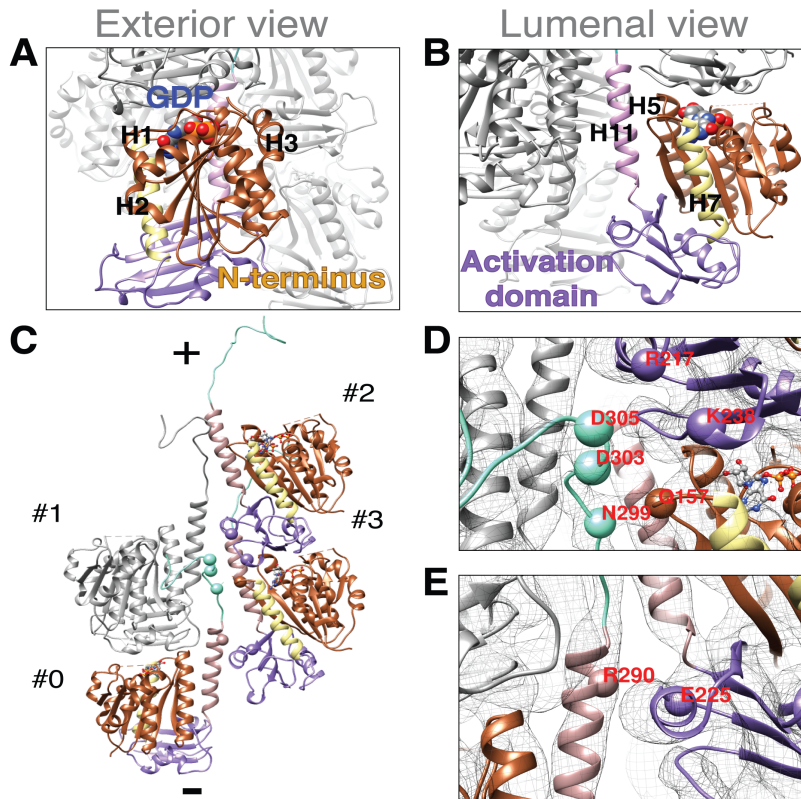


**Figure 3.** PhuZ<sub>201</sub> subunit is uniquely oriented within the filament and makes lateral contacts via a set of conserved residues. (A)-(E) PhuZ<sub>201</sub> subunit is colored by the following scheme: brown, N-terminal domain; yellow, H7; violet, activation domain; rosy brown, H11; cyan, C-terminal tail; GDP:Mg<sup>2+</sup> is colored by element. Cryo-EM map density is represented as a gray mesh (D) and (E). (A) Exterior and (B) luminal views of a subunit within the filament. (C)-(E) Lateral contacts within the three-stranded filament. Alpha carbons of the residues predicted to mediate lateral contacts are shown as spheres. (C) C-terminus of a subunit #0 makes contacts with the longitudinal subunit #1 and with the subunits #2, and #3 of a lateral dimer. Filament ends are designated as (+) end with the C-termini and (-) end with the activation domains. (D) D303 and D305 of #0 contact K238 and R217 of #2 respectively; N299 of #0 contacts Q157 of #3; (E) R290 of #0 contacts E225 of #3. See also Figure S2.

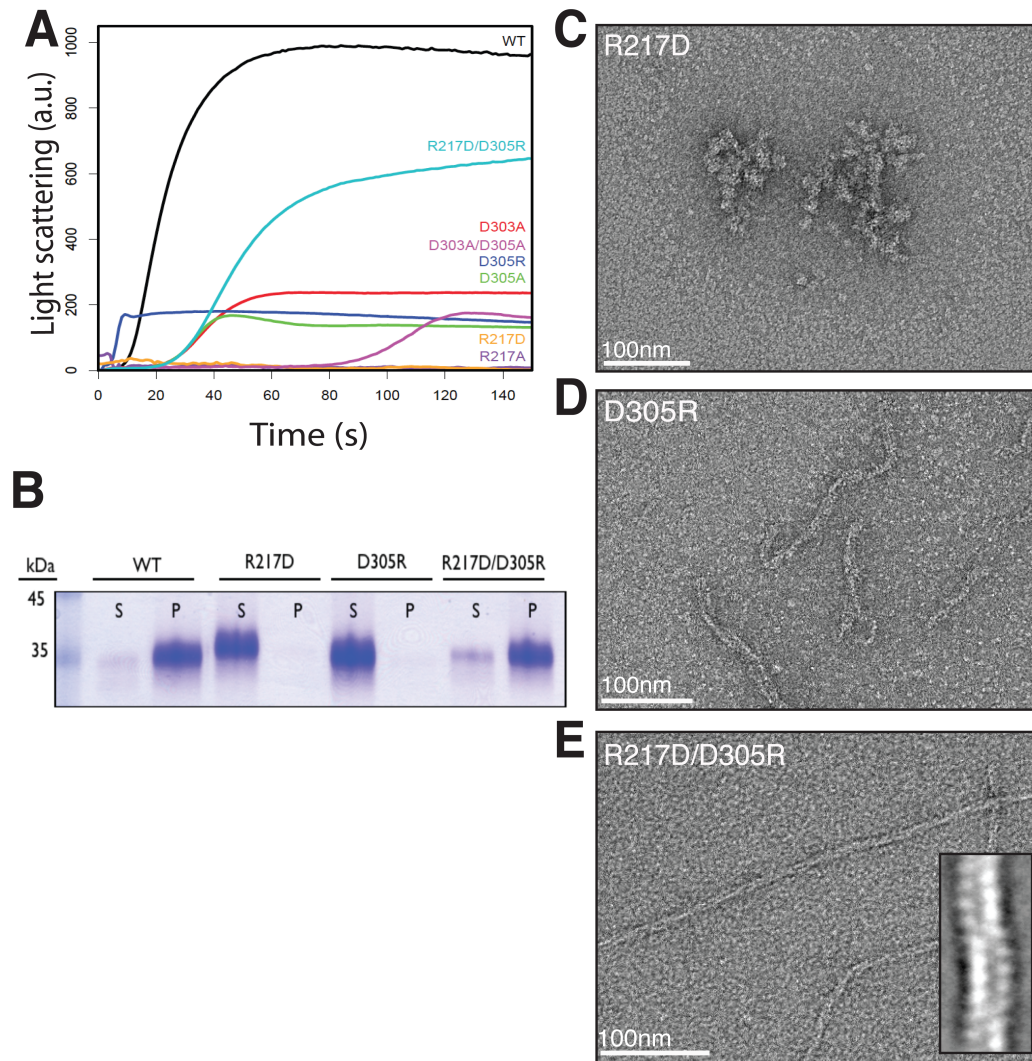


**Figure 4.** Mutations to residues predicted to mediate lateral contacts disrupt PhuZ<sub>201</sub> assembly *in vitro*. **(A)** Right-angle light-scattering traces of PhuZ<sub>201</sub> wild type (WT) and mutants polymerized in 1mM GTP. The following concentrations were used: 3 μM WT in black, 5 μM D303A in red, 7 μM D305A in green, 9 μM D305R in dark blue, 30 μM R217A in purple, 30 μM R217D in orange, 10 μM D303A/D305A in violet, and 6 μM R217D/D305R in cyan. **(B)** Polymerization of PhuZ<sub>201</sub> mutants in excess GTP was assayed by high-speed pelleting assay as described under “Experimental Procedures” with supernatant (S) and pellet (P) fractions analyzed by SDS-

PAGE. **(A)** and **(B)** Charge reversal mutant R217D/D305R partially restores the ability to form filaments. **(C)-(E)** Sections of micrographs of negatively stained PhuZ<sub>201</sub> mutants polymerized in excess GMPCPP. PhuZ<sub>201</sub> single mutants R217D **(C)** and D305R **(D)** are unable to form three-stranded filaments, but the double mutant R217D/D305R **(E)** assembles three-stranded filaments (inset). See also Table S1 and Figure S3.

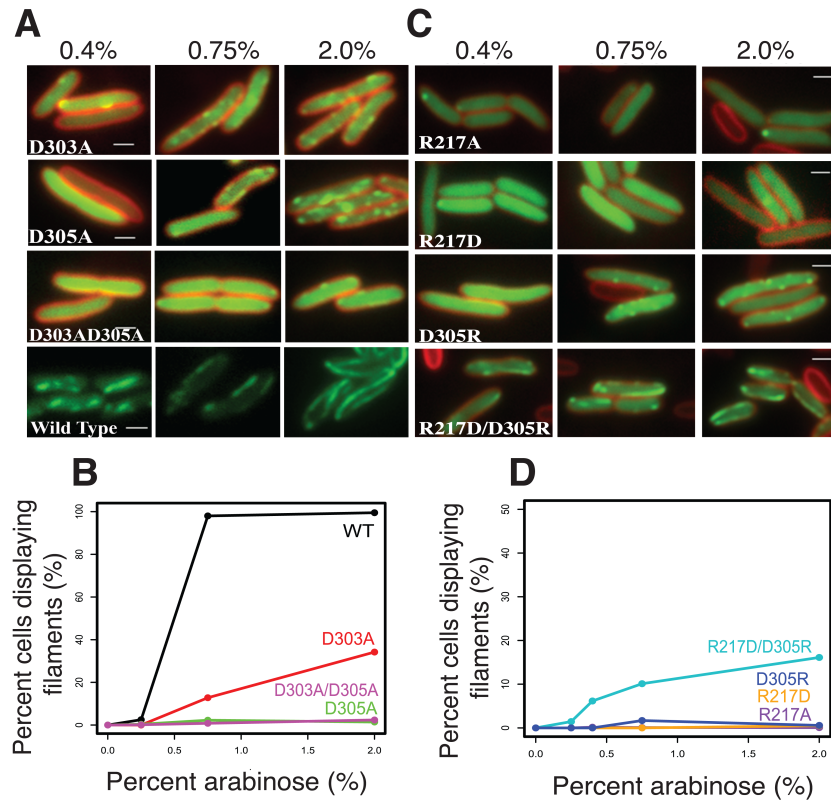


**Figure 5.** PhuZ<sub>201</sub> assembles via the same set of lateral surfaces *in vivo* as *in vitro*. **(A)** and **(C)** Fluorescent micrographs of uninfected *P. chlororaphis* cells expressing various GFP-PhuZ<sub>201</sub> mutant constructs. **(A)** Shown are the three tail mutants D303A, D305A and the double mutant D303A/D305A at 0.4%, 0.75%, and 2% arabinose induction. Wild type PhuZ<sub>201</sub> is in the last strip for comparison. All mutants have compromised filament formation. **(B)** Quantitation of data in **(A)** indicating that of the three mutants, only D303A shows any appreciable polymerization at 2% arabinose. **(C)** Shown are the four tail mutants R217A, R217D, D305R and the double mutant R217D/ D305R at 0.4%, 0.75% and 2% arabinose induction. The single mutants are unable to make filaments, but the charge reversal in the double mutant partially restores filament formation. **(D)** Quantitation of the concentration data from **(C)**. All scale bars = 1 micron.

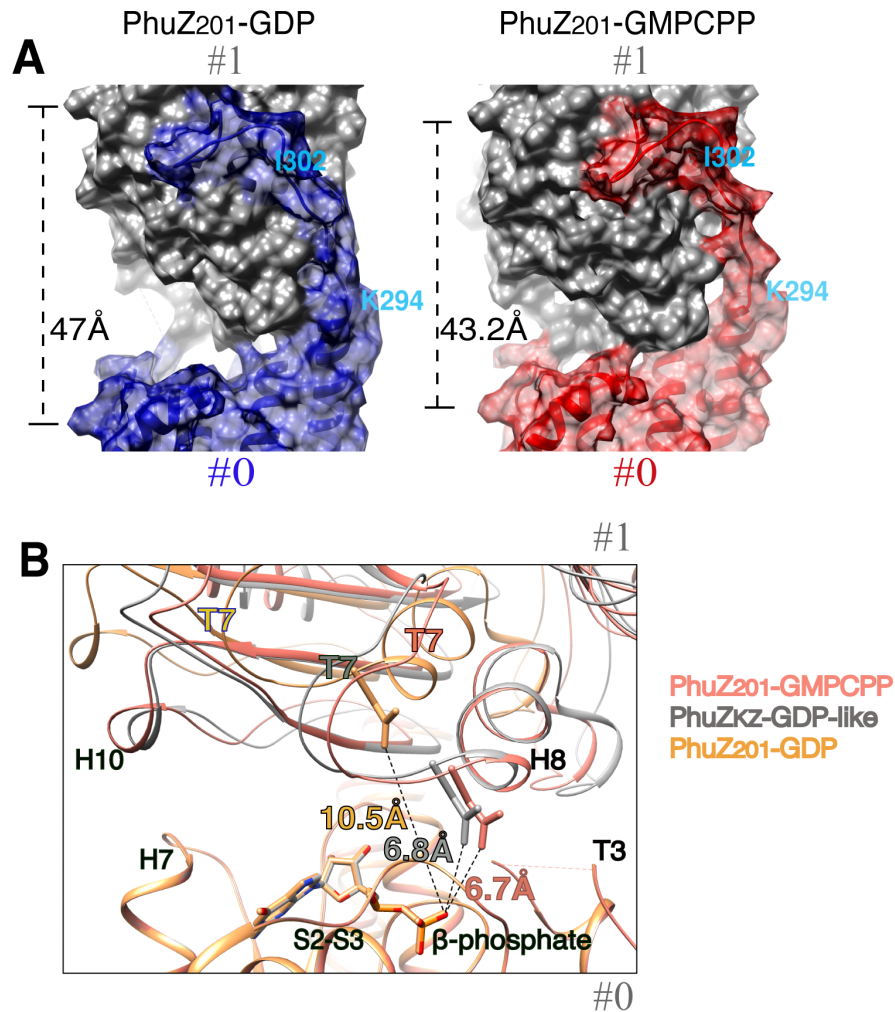


**Figure 6.** Comparison of the longitudinal packing between PhuZ<sub>201</sub>-GDP, PhuZ<sub>KZ</sub>-GDP-like and the three-stranded filament. **(A)** and **(B)** Longitudinal subunits within a dimer are labeled as #0 and #1. **(A)** PhuZ<sub>201</sub> dimers representative of the packing within the crystal (3r4v) (Kraemer et al., 2012) (left) vs the three-stranded filament (right) are shown as molecular surfaces. (left) PhuZ<sub>201</sub> subunit packing within the crystal: the C-terminal tail of the subunit #0 in blue forms extensive interactions with the side of the subunit #1 in gray. The dimer has a relaxed longitudinal interface with 47 Å spacing. (right) PhuZ<sub>201</sub> subunit packing within the three-

stranded filament: the C-terminal tail of the subunit #0 in red forms weak longitudinal contacts with the side of the subunit #1 in gray. The dimer has a tense canonical tubulin/FtsZ longitudinal interface with 43.2 Å spacing. **(B)** Magnified view of the longitudinal interfaces in: PhuZ<sub>201</sub>-GMPCPP dimer in salmon, PhuZ<sub>201</sub> mimicking subunit packing as in a PhuZ<sub>KZ</sub>-GDP dimer (3ZBQ) (Aylett et al., 2013) in gray and a PhuZ<sub>201</sub>-GDP dimer (3r4v) (Kraemer et al., 2012) in yellow. The dimers were superimposed via the residues (2-271) corresponding to the N-terminal domains and the activation domains, but excluding the residues corresponding to the C-termini, of the subunits at minus ends. Measured distances from the catalytic Asp on the T7 loop to the β-phosphate are: 6.7 Å the three-stranded filament, 6.8 Å in PhuZ<sub>KZ</sub>-GDP-like state, and 10.5 Å in PhuZ<sub>201</sub>-GDP. See also Movie S2.

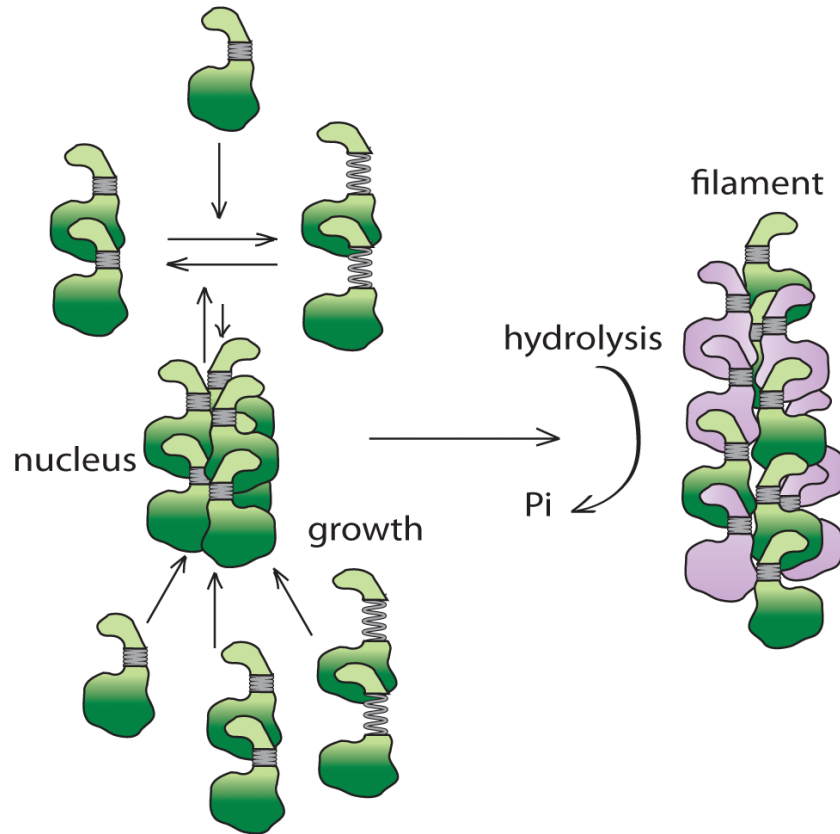


**Figure 7.** Model for PhuZ assembly. GTP-bound PhuZ is in green and GDP-bound is in purple. PhuZ monomers as seen in the crystal (3ZBP) (Aylett et al., 2013) assemble dimers with a tense longitudinal interface as in the crystal structure (3ZBQ) (Aylett et al., 2013) or the relaxed interface as in the crystal structure (3r4v) (Kraemer et al., 2012). Three dimers form a hexameric nucleus with subunits displaying the intramolecular contacts as seen in the pseudo-atomic model described in this work. The nucleus grows by the addition of dimers and monomers. GTP is hydrolyzed soon after filament assembly.

## References

- Aylett, C.H., Izore, T., Amos, L.A., and Lowe, J. (2013). Structure of the Tubulin/FtsZ-Like Protein TubZ from Pseudomonas Bacteriophage PhiKZ. *Journal of molecular biology*.
- Aylett, C.H., Lowe, J., and Amos, L.A. (2011). New insights into the mechanisms of cytomotive actin and tubulin filaments. *International review of cell and molecular biology* 292, 1-71.
- Aylett, C.H., Wang, Q., Michie, K.A., Amos, L.A., and Lowe, J. (2010). Filament structure of bacterial tubulin homologue TubZ. *Proceedings of the National Academy of Sciences of the United States of America* 107, 19766-19771.
- Bramhill, D., and Thompson, C.M. (1994). GTP-dependent polymerization of Escherichia coli FtsZ protein to form tubules. *Proceedings of the National Academy of Sciences of the United States of America* 91, 5813-5817.
- Egelman, E.H. (2000). A robust algorithm for the reconstruction of helical filaments using single-particle methods. *Ultramicroscopy* 85, 225-234.
- Egelman, E.H. (2007). The iterative helical real space reconstruction method: surmounting the problems posed by real polymers. *Journal of structural biology* 157, 83-94.
- Flyvbjerg, H., Jobs, E., and Leibler, S. (1996). Kinetics of self-assembling microtubules: an "inverse problem" in biochemistry. *Proceedings of the National Academy of Sciences of the United States of America* 93, 5975-5979.
- Fokine, A., Battisti, A.J., Bowman, V.D., Efimov, A.V., Kurochkina, L.P., Chipman, P.R., Mesyanzhinov, V.V., and Rossmann, M.G. (2007). Cryo-EM study of the Pseudomonas bacteriophage phiKZ. *Structure* 15, 1099-1104.



Frank, J., Radermacher, M., Penczek, P., Zhu, J., Li, Y., Ladjadj, M., and Leith, A. (1996). SPIDER and WEB: processing and visualization of images in 3D electron microscopy and related fields. *Journal of structural biology* *116*, 190-199.

Garner, E.C., Campbell, C.S., Weibel, D.B., and Mullins, R.D. (2007). Reconstitution of DNA segregation driven by assembly of a prokaryotic actin homolog. *Science* *315*, 1270-1274.

Gayathri, P., Fujii, T., Namba, K., and Lowe, J. (2013). Structure of the ParM filament at 8.5Å resolution. *Journal of structural biology*.

Howard, G.T., Mackie, R.I., Cann, I.K., Ohene-Adjei, S., Aboudehen, K.S., Duos, B.G., and Childers, G.W. (2007). Effect of insertional mutations in the pueA and pueB genes encoding two polyurethanases in *Pseudomonas chlororaphis* contained within a gene cluster. *J Appl Microbiol* *103*, 2074-2083.

Kraemer, J.A., Erb, M.L., Waddling, C.A., Montabana, E.A., Zehr, E.A., Wang, H., Nguyen, K., Pham, D.S., Agard, D.A., and Pogliano, J. (2012). A phage tubulin assembles dynamic filaments by an atypical mechanism to center viral DNA within the host cell. *Cell* *149*, 1488-1499.

Krylov, V.N., Dela Cruz, D.M., Hertveldt, K., and Ackermann, H.W. (2007). "phiKZ-like viruses", a proposed new genus of myovirus bacteriophages. *Archives of virology* *152*, 1955-1959.

Lavigne, R., Darius, P., Summer, E.J., Seto, D., Mahadevan, P., Nilsson, A.S., Ackermann, H.W., and Kropinski, A.M. (2009). Classification of Myoviridae bacteriophages using protein sequence similarity. *BMC microbiology* *9*, 224.

Li, Z., Trimble, M.J., Brun, Y.V., and Jensen, G.J. (2007). The structure of FtsZ filaments in vivo suggests a force-generating role in cell division. *The EMBO journal* *26*, 4694-4708.

Lowe, J., and Amos, L.A. (1999). Tubulin-like protofilaments in Ca<sup>2+</sup>-induced FtsZ sheets. *The EMBO journal* *18*, 2364-2371.

Lu, C., Reedy, M., and Erickson, H.P. (2000). Straight and curved conformations of FtsZ are regulated by GTP hydrolysis. *Journal of bacteriology* *182*, 164-170.

Mindell, J.A., and Grigorieff, N. (2003). Accurate determination of local defocus and specimen tilt in electron microscopy. *Journal of structural biology* *142*, 334-347.

Ni, L., Xu, W., Kumaraswami, M., and Schumacher, M.A. (2010). Plasmid protein TubR uses a distinct mode of HTH-DNA binding and recruits the prokaryotic tubulin homolog TubZ to effect DNA partition. *Proceedings of the National Academy of Sciences of the United States of America* *107*, 11763-11768.

Nogales, E., Downing, K.H., Amos, L.A., and Lowe, J. (1998a). Tubulin and FtsZ form a distinct family of GTPases. *Nature structural biology* *5*, 451-458.

Nogales, E., Whittaker, M., Milligan, R.A., and Downing, K.H. (1999). High-resolution model of the microtubule. *Cell* *96*, 79-88.

Nogales, E., Wolf, S.G., and Downing, K.H. (1998b). Structure of the alpha beta tubulin dimer by electron crystallography. *Nature* *391*, 199-203.

Oliva, M.A., Martin-Galiano, A.J., Sakaguchi, Y., and Andreu, J.M. (2012). Tubulin homolog TubZ in a phage-encoded partition system. *Proceedings of the National Academy of Sciences of the United States of America* *109*, 7711-7716.

Pettersen, E.F., Goddard, T.D., Huang, C.C., Couch, G.S., Greenblatt, D.M., Meng, E.C., and Ferrin, T.E. (2004). UCSF Chimera--a visualization system for exploratory research and analysis. *Journal of computational chemistry* *25*, 1605-1612.

Qiu, D., Damron, F.H., Mima, T., Schweizer, H.P., and Yu, H.D. (2008). PBAD-based shuttle vectors for functional analysis of toxic and highly regulated genes in *Pseudomonas* and *Burkholderia* spp. and other bacteria. *Appl Environ Microbiol* *74*, 7422-7426.

Scheres, S.H., and Chen, S. (2012). Prevention of overfitting in cryo-EM structure determination. *Nature methods* *9*, 853-854.

Sui, H., and Downing, K.H. (2010). Structural basis of interprotofilament interaction and lateral deformation of microtubules. *Structure* *18*, 1022-1031.

Thomas, J.A., Rolando, M.R., Carroll, C.A., Shen, P.S., Belnap, D.M., Weintraub, S.T., Serwer, P., and Hardies, S.C. (2008). Characterization of *Pseudomonas chlororaphis* myovirus 201varphi2-1 via genomic sequencing, mass spectrometry, and electron microscopy. *Virology* *376*, 330-338.

Weisenberg, R.C. (1972). Microtubule formation in vitro in solutions containing low calcium concentrations. *Science* *177*, 1104-1105.

## Supplemental Data

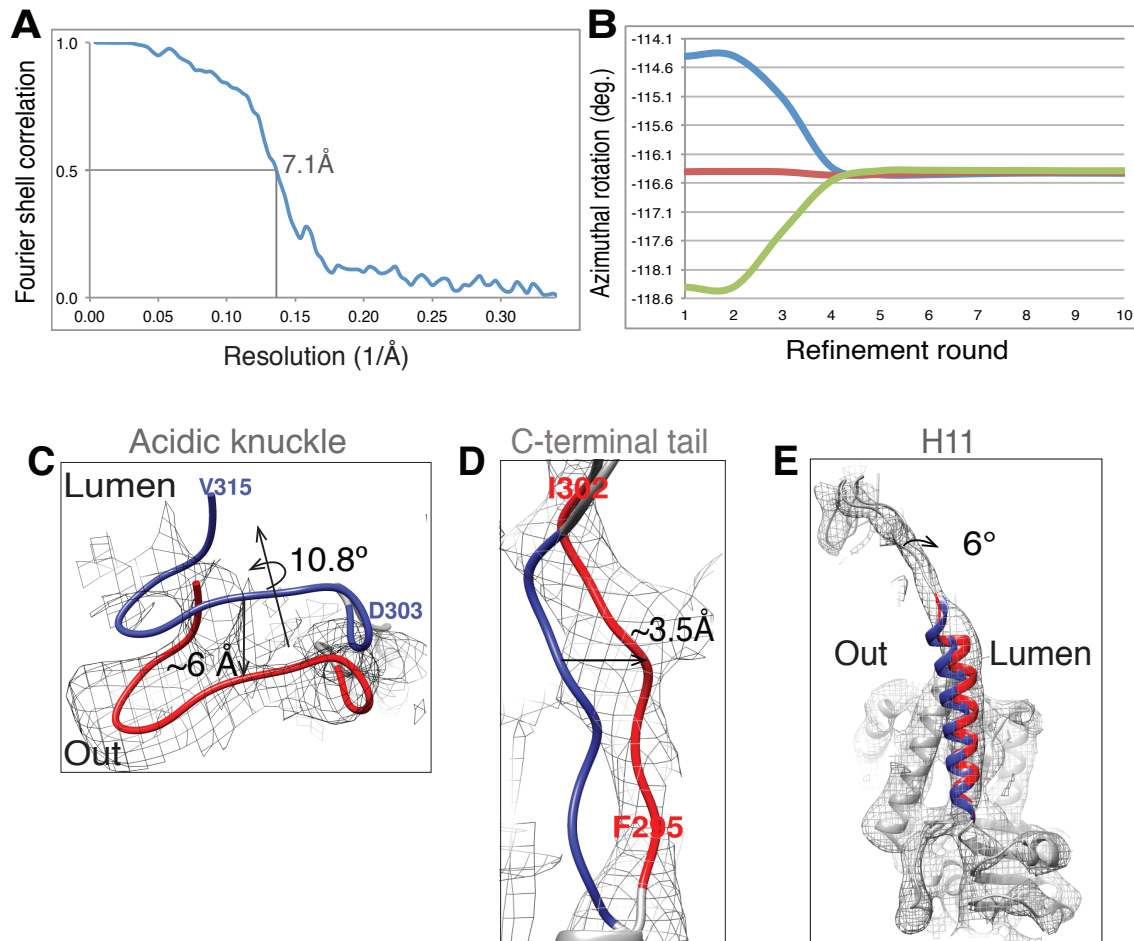


**Figure S1, related to Figure 2.** Resolution estimation and helical parameter validation test for the cryo-EM reconstruction. Flexible fitting of the atomic model into the cryo-EM map. **(A)** Resolution estimate for the cryo-EM reconstruction of the PhuZ<sub>201</sub> filament. FSC indicates the resolution of the reconstruction is 7.1 Å by the FSC 0.5 criterion and likely better as “gold standard” refinement was performed. **(B)** Convergence of azimuthal rotation per subunit from different starting symmetries. Three independent reconstructions were performed starting from different values (-118.4°, -116.4° or -114.4°) for the azimuthal rotation angle per subunit. In the fourth round of refinement the value for the angle converged to -116.4°, indicating a stable and

consistent solution for the helical symmetry. **(C)-(E)** Atomic model is colored by the scheme: C-terminus (H11 and the C-terminal tail) is in blue and red; N-terminal and activation domains, and H7 are in gray. Cryo-EM map density is represented as a gray wire mesh. Out is the outer surface and Lumen is the inside of the filament. In blue is the conformation of the C-terminus as in the crystal packing (3r4v) (Kraemer et al., 2012) and in red is the conformation as in the three-stranded filament. Flexible fitting: **(C)** The C-terminal tail was rotated  $10.8^\circ$  counterclockwise together with the longitudinal subunit and translated by  $3.5 \text{ \AA}$  towards the adjacent strand **(D)**; **(E)** H11 was tilted  $6^\circ$  towards the lumen.

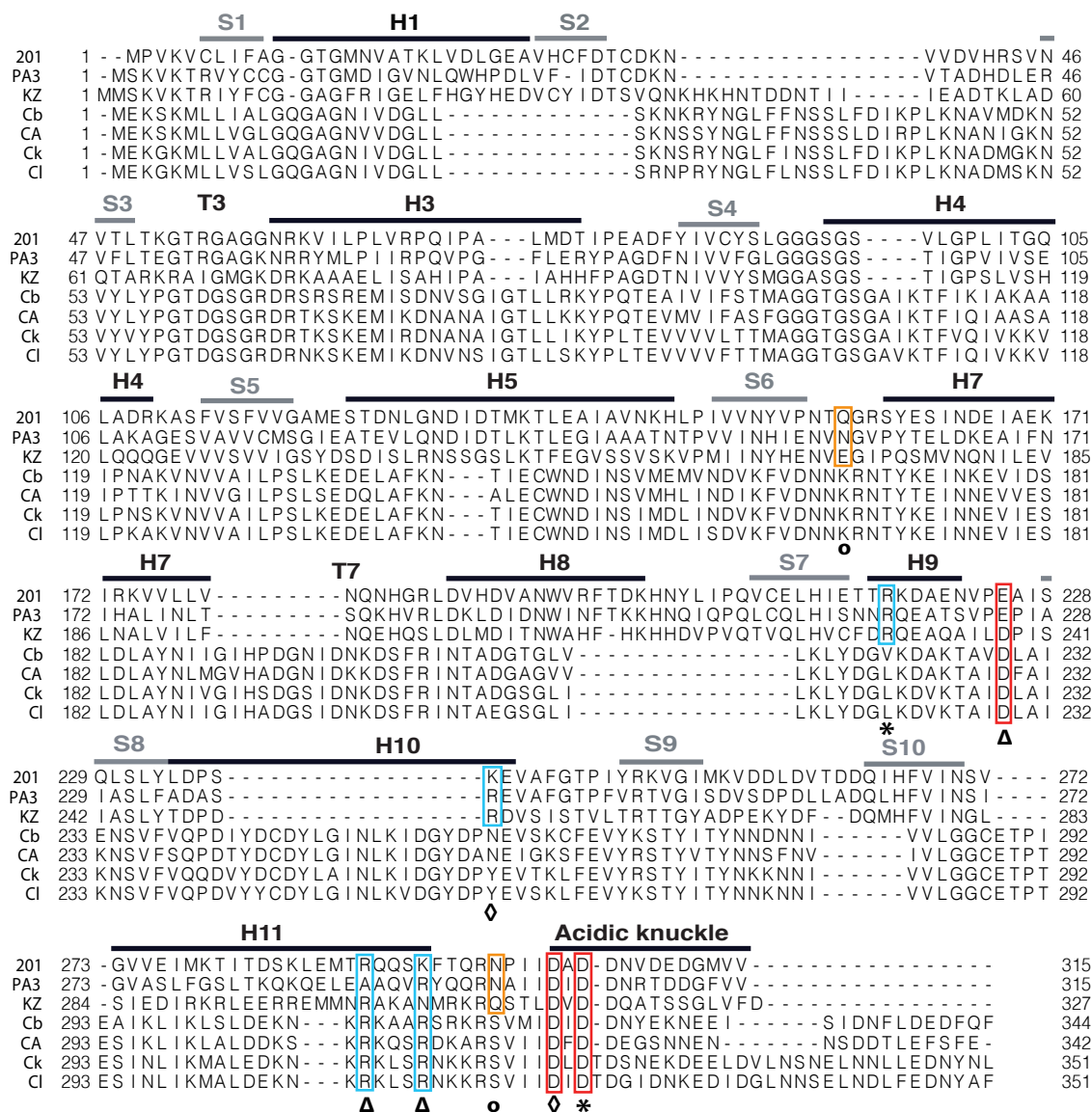


**Figure S2, related to Figure 3.** Conservation of residues predicted to form lateral contacts among the PhuZ family and *Clostridial* chromosomal tubulin homologues. Alignment of amino acid sequences was performed using Mafft with default settings in Jalview (Waterhouse et al., 2009). The amino acid positions are indicated at the beginning and at the end of each line. Secondary structural elements of PhuZ<sub>201</sub> are abbreviated as: a-helices (H), b-strands (S) and loops/turns (T). Conserved residues, predicted to form the lateral interface, are highlighted:

negatively charged (red), positively charged (blue), and polar (orange). D303 contacts K238 (◇), D305 contacts R217 (\*), N299 contacts Q157 (●); R290 or R294 (PhuZ<sub>PA3</sub>) contacts E225 (▲). Abbreviations for sequences encoding tubulin homologues: 201 (phage 201Φ2-1); PA3 (phage ΦPA3); KZ (phage ΦKZ); Cb (*C. butyricum* 5521); CA (*C. acetobutylicum* ATCC824); Ck (*C. kluyveri* DSM555) and Cl (*C. cellulovorans* 743B).

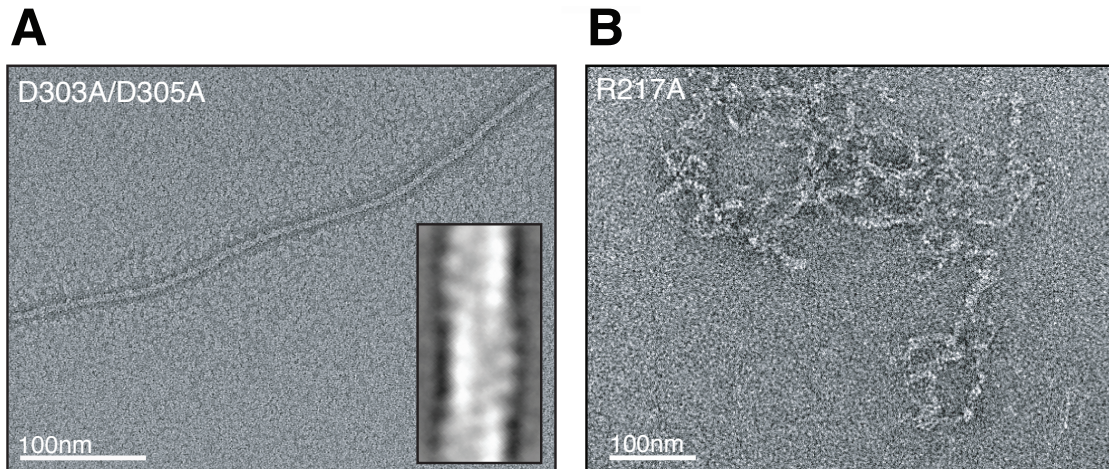


**Figure S3, related to Figure 4.** Mutations to residues predicted to mediate lateral contacts disrupt PhuZ<sub>201</sub> assembly *in vitro*. Sections of micrographs of negatively stained PhuZ<sub>201</sub> double mutant (D303A/D305A) (**A**) and single mutant (R217A) (**B**). (**A**) D303A/D305A forms rare three-stranded filaments as indicated by the reference-free 2D average in the inset. (**B**) R217A forms amorphous structures in a nucleotide-dependent manner.



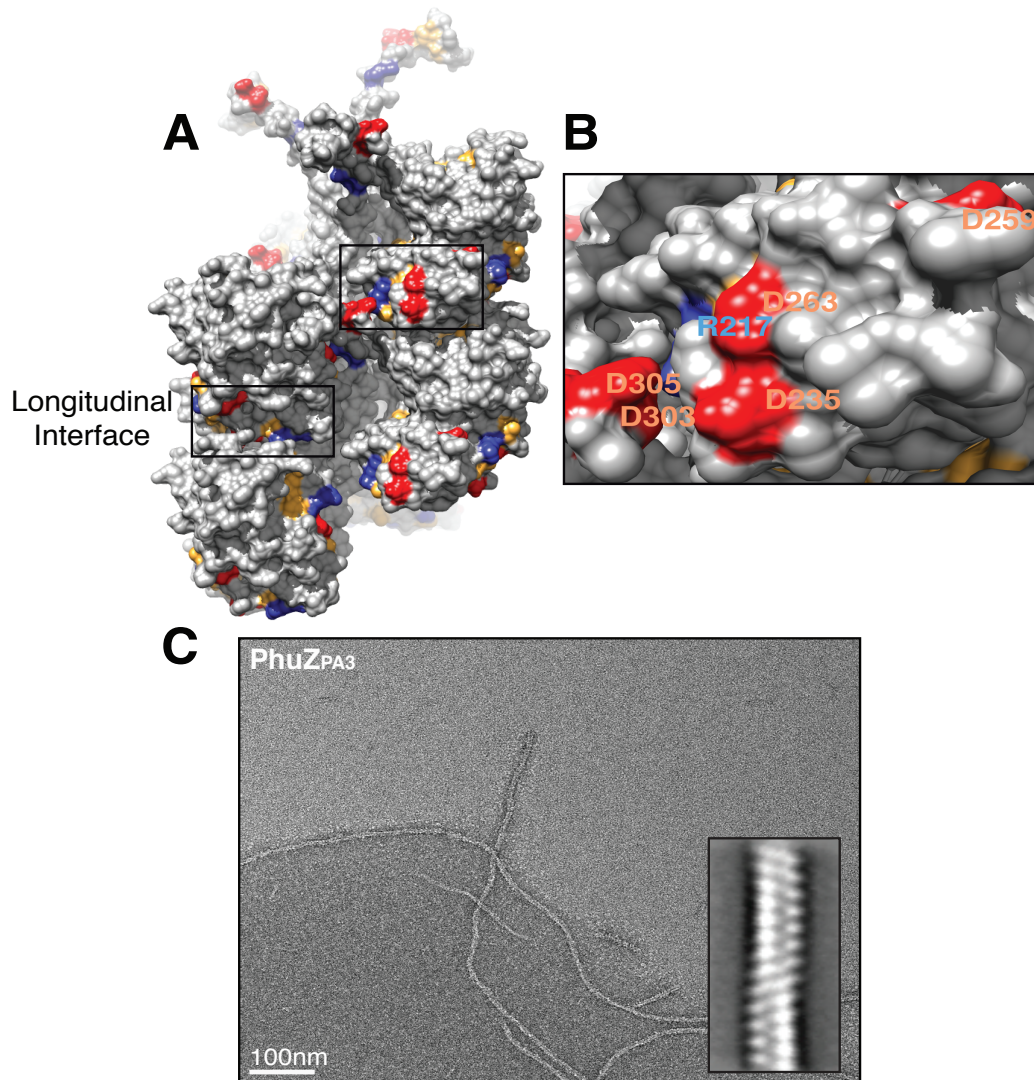


**Figure S4.** PhuZ family tubulins assemble three-stranded filaments. (A) and (B) In yellow (hydrophobic and polar), red (negatively charged) and blue (positively charged) surfaces having 100% amino acid sequence conservation among PhuZ<sub>201</sub>, PhuZ<sub>PA3</sub> and PhuZ<sub>KZ</sub>. Non-conserved surfaces are in gray. Amino acid sequences of PhuZ<sub>201</sub>, PhuZ<sub>PA3</sub> and PhuZ<sub>KZ</sub> were aligned using Jalview Mafft option (Waterhouse et al., 2009) and molecular surfaces of the PhuZ<sub>201</sub> filament atomic model were “rendered by conservation” using UCSF Chimera (Pettersen et al., 2004). The conserved surfaces are outlined on the atomic structure (A) and some are magnified in the

inset **(B)**. In addition to the conservation of the longitudinal and lateral surfaces, there is a negatively charged surface formed by D235, D259 and D263 **(B)** that may mediate protein-protein interactions. **(C)** Section of a micrograph of negatively stained PhuZ<sub>PA3</sub> filaments polymerized in 1mM GMPCPP. Inset: reference free 2D average of 500 segments of PhuZ<sub>PA3</sub> polymer indicates that PhuZ<sub>PA3</sub> forms three-stranded filaments.

<b>Mutations</b>	<b>Critical concentration <math>\pm</math> error, (<math>\mu\text{M}</math>)</b>
<b>Wild type</b>	$2.5 \pm 0.1$
<b>R217A</b>	$> 30$
<b>D303A</b>	$3.7 \pm 0.2$
<b>D305A</b>	$4.1 \pm 0.4$
<b>D303A/D305A</b>	$9.4 \pm 0.3$
<b>R217D</b>	$> 30$
<b>D305R</b>	$8.0 \pm 0.2$
<b>R217D/D305R</b>	$5.9 \pm 0.3$

**Table S1, related to Figure 4.** Critical concentrations of PhuZ<sub>201</sub> wild type and mutant constructs.

**Movie S1, related to Figure 2. Pseudo-atomic model of PhuZ<sub>201</sub> filament.** Gray wire mesh represents 3D cryo-EM density map fitted with the atomic model of PhuZ<sub>201</sub> in red. Flexible fitting was applied to the C-terminus before docking the atomic model into the map. The movie rotates the pseudo-atomic model around an axis parallel to the long axis of the PhuZ<sub>201</sub> filament.

**Movie S2, related to Figure 6. PhuZ dimer rearranges upon incorporation into the filament lattice.** Morph movie shows differences between packing of the PhuZ<sub>201</sub>-GDP dimer (3r4v) (Kraemer et al., 2012) versus PhuZ<sub>KZ</sub>-GDP (3ZBQ) (Aylett et al., 2013) and the three-stranded GMPCPP filament. To make the morph longitudinal dimers from the three structures were aligned using the N-terminal domains of the subunits at the minus ends of the dimers. Alpha carbons of the residues, predicted to mediate lateral contacts, are shown as spheres. In the presence of the  $\gamma$ -phosphate (GMPCPP filament) a tense inter-subunit interface is formed. Both inter-subunit twisting and C-terminal bending towards the laterally adjacent dimer are required to establish the lateral interface.

## **Supplemental Methods**

### **Molecular Fitting**

To optimize the fit of the PhuZ<sub>201</sub> atomic model (Kraemer et al., 2012) into the cryo-EM map, the atomic model was initially docked into the map using “Fit in Map” option in UCSF Chimera (Pettersen et al., 2004), and the fit of H11 and the C-terminal tail were further optimized using Coot (Emsley and Cowtan, 2004). Next, the helical parameters (-116.4° rotation and 14.4 Å axial rise per subunit) were applied to the atomic structure to obtain a pseudo-atomic model of the filament. The cross-correlation coefficients for the atomic model, before and after the application of the flexible fitting, with the segment of the cryo-EM reconstruction, corresponding to a single subunit, was measured using “Fit in Map” option in UCSF Chimera (Pettersen et al., 2004).

### **Structure Analysis and Comparison**

Visualization and comparative analysis were performed using UCSF Chimera (Pettersen et al., 2004). Buried surface area values were measured using CCP4 “areaimol” (Lee and Richards, 1971) (E.B.Saff and A.B.J.Kuijlaars, *The Mathematical Intelligencer*, **19**, 5-11 (1997) <http://www.math.vanderbilt.edu/~esaff/texts/161.pdf>).

## **Supplemental References**

Emsley, P., and Cowtan, K. (2004). Coot: model-building tools for molecular graphics. *Acta crystallographica Section D, Biological crystallography* 60, 2126-2132.

Lee, B., and Richards, F.M. (1971). The interpretation of protein structures: estimation of static accessibility. *Journal of molecular biology* 55, 379-400.

Waterhouse, A.M., Procter, J.B., Martin, D.M., Clamp, M., and Barton, G.J. (2009). Jalview Version 2--a multiple sequence alignment editor and analysis workbench. *Bioinformatics* 25, 1189-1191.

## Chapter Four

### **A bacteriophage tubulin harnesses dynamic instability to center DNA in infected cells**

Marcella L Erb<sup>1,\*</sup>, James A Kraemer<sup>2,\*</sup>, Joanna K.C. Coker<sup>1</sup>, Vorrapon Chaikeeratisak<sup>1</sup>, Poochit Nonejuie<sup>1</sup>, David A Agard<sup>2</sup>, and Joe Pogliano<sup>1</sup>

<sup>1</sup>Division of Biological Sciences, University of California, San Diego, CA 92093

<sup>2</sup>Department of Biochemistry and Biophysics and the Howard Hughes Medical Institute,  
University of California, San Francisco, CA 94158

\*These authors contributed equally

This work is being currently prepared for submission for submission for publication to Elife and is reprinted here with permission.

## Abstract

Dynamic instability, polarity, and spatiotemporal organization are hallmarks of the microtubule cytoskeleton that allow formation of complex regulated structures such as the eukaryotic spindle. No similar structure has been identified in prokaryotes. A recently discovered bacteriophage-encoded tubulin, PhuZ, is required to position DNA at the cell center, without which infectivity is compromised. Here, we show that PhuZ filaments, like microtubules, stochastically switch from growing in a distinctly polar manner to rapid and catastrophic depolymerization (dynamic instability) both *in vitro* and *in vivo*. Moreover, the minus ends of PhuZ filaments are stably anchored near the cell pole to form a spindle-like array that orients the growing ends toward the replicating phage nucleoid so as to position it near mid-cell. Our results demonstrate how a bacteriophage can harness the dynamic instability of a tubulin-like cytoskeleton for efficient propagation. This represents the first identification of a prokaryotic tubulin with the properties of microtubules and a simplified bipolar spindle.



## Introduction

Tubulins are universally conserved GTPases that polymerize in a head to tail fashion to form filaments. They have evolved properties that allow them to assemble into a wide variety of structures with various functions and dynamic properties. In eukaryotes,  $\alpha/\beta$ -tubulin forms large, dynamically unstable microtubules (MTs), composed of 13 protofilaments (Downing and Nogales, 1998). MTs are the essential component of many cell biological processes; one of the most familiar and well studied is the mitotic spindle required for the faithful segregation of sister chromatids in all eukaryotic cells.

MTs have a distinct growth polarity in which growing (plus) ends elongate substantially faster than minus ends (Allen and Borisy, 1974; Downing and Nogales, 1998). They are often anchored by their minus ends at specific locations in the cell known as microtubule organizing centers to facilitate mitosis, directional transport, and motility. This anchoring significantly stabilizes the MTs and lends a consistent organization to these structures (Mitchison and Kirschner, 1984b). The polarity of the filament becomes key in its ability to specifically interact with binding partners, such as the kinetochore, and for the regulation of the filaments by microtubule accessory proteins (MAPs) (Euteneuer and McIntosh, 1981; Kitamura et al., 2010). These two features allow for the rapid and effective search and capture of the sister chromatids by the MTs via dynamic instability.

Dynamic instability is defined as the stochastic switching between states of polymerization and rapid depolymerization (Mitchison and Kirschner, 1984a, b). The biomechanical source of this dynamic instability is the differential between the addition of new monomers into the MT lattice and the hydrolysis of the GTP bound into the beta subunit of the heterodimer. While GTP bound to the subunits in the middle of the lattice has been hydrolyzed

to GDP, the tip of the growing MT is crowned by a cap of GTP-bound heterodimers (Mitchison and Kirschner, 1984a). The loss of this GTP cap facilitates a conformational change in the filaments and subsequent depolymerization and, possibly, catastrophe (Downing and Nogales, 1998).

Until now, these properties of tubulins have appeared to be unique hallmarks of eukaryotes. Some plasmid encoded bacterial actins, such as ParM and Alp7A, display dynamic instability (Derman et al., 2009; Garner et al., 2004); however, unlike MTs, ParM filaments elongate bidirectionally (Garner et al., 2004) and assemble only transiently during the relatively brief process of pushing plasmid DNA molecules apart (Campbell and Mullins, 2007). Furthermore, they are not spatially organized and assemble at random positions in the cell. Several families of bacterial tubulins have been identified that participate in cell division, DNA segregation, and viral DNA positioning (Larsen et al., 2007; Meier and Goley, 2014; Oliva et al., 2012). While TubZ has been shown to treadmill<sup>8</sup>, for most, the type of motion the filament undergoes *in vivo* remains unclear. None of the bacterial tubulins have been shown to exhibit dynamic instability or other critical properties of a microtubule-based spindle.

We recently identified a family of bacteriophage tubulins, PhuZ, that play a role in spatially organizing DNA during lytic growth and thereby contribute to efficient phage production (Kraemer et al., 2012). PhuZ from *Pseudomonas chlororaphis* phage 201Φ2-1 contains a tubulin fold and an extended C-terminus that forms extensive longitudinal and lateral contacts required to stabilize a unique triple stranded filament (Kraemer et al., 2012; Zehr et al., 2014). Catalytically defective PhuZ mutants lacking GTPase activity generate stable filaments and disrupt correct positioning of clusters of DNA during lytic growth (Kraemer et al., 2012).

While this suggested the importance of filament dynamics, it has remained unclear how PhuZ polymers might facilitate this organization.

Here we present the first example of a prokaryotic tubulin that undergoes dynamic instability both *in vitro* and *in vivo*. In addition, the PhuZ cytoskeleton has many of the properties of eukaryotic MTs, including polarity, a GTP cap, and anchoring. These shared properties extend to the ability of both PhuZ and MTs to build a bipolar spindle for the movement of DNA. We further characterize replication of this bacteriophage, demonstrating that the infection nucleoid contains only replicating phage DNA and that nucleoid centering is independent of replication.

## Results

### PhuZ Filaments are Highly Dynamic *in Vitro*

To gain insight into the mechanism of phage centering by PhuZ, we investigated the properties of PhuZ filaments assembled *in vitro* and *in vivo*. First, we used total internal reflection (TIRF) microscopy to visualize dynamics of purified PhuZ (Fig. 1a). In the presence of GTP and a crowding agent to minimize filament diffusion, 2.5  $\mu\text{M}$  PhuZ (20% Cy3-labeled, 80% unlabeled) that was otherwise unattached to PEG-coated coverslips, formed short dynamic filaments that translocated across the coverslip (Fig. 1a, Movie 1). Many of these filaments displayed non-uniform intensity, and annealing and severing events were observed (Movie 2), implying that many of these structures consist of at least two PhuZ filaments. The apparent motion could be the result of either diffusion near the surface or treadmilling, that is, growth at one end and depolymerization at the other. This ambiguity could be resolved by using the naturally occurring intensity variations along each filament to allow growth and shrinkage rates at each end to be quantified (n=10) independent of any overall filament motion. This revealed that the filaments treadmill in a coordinated manner (Fig. 1a), with new filament growth at one end and depolymerization at the other. Thus like MTs and actin, PhuZ filaments must be polar, with one end growing faster than the other. In a manner reminiscent of MT catastrophe, filaments were also observed to occasionally fully depolymerize (Movie 3).

### PhuZ Filaments Exhibit Dynamic Instability and Distinct Polarity *in Vitro*

To better assess the dynamics and polarity of individual growing filaments, we performed two-color TIRF microscopy of Cy3-labeled PhuZ (green) growing off of Cy5-labeled and biotinylated seeds (red) in the absence of crowding agent. To make stable seeds, 2  $\mu\text{M}$  PhuZ

(20% Cy5, 5% biotin, 75% unlabeled) was polymerized with the non-hydrolyzable GTP analogue GMPCPP for 5 minutes and attached to PEG-biotin-coated coverslips via streptavidin. After 2 minutes, the flow chamber was subsequently washed with TIRF buffer (see Materials and Methods) to remove unattached filaments, free monomers, and GMPCPP. Cy3-labelled PhuZ (20% Cy3, 80% unlabeled) and GTP were then added to the chamber to initiate dynamic filament formation, and dynamics were monitored at a 0.25 second interval for 100 seconds (Fig. 1b-d, Movie 4). To ensure that Cy3-PhuZ filaments would only grow from the preformed Cy5-PhuZ seeds, Cy3-PhuZ was added to the flow chamber at a concentration (1.5  $\mu$ M) below the critical concentration (2.5  $\mu$ M). The movies indicate that PhuZ filaments possess a distinct kinetic polarity, with growth only seen from one end, highlighted in Fig 1. This is similar to, but more asymmetric than MTs (Bergen and Borisy, 1980). The Cy3-PhuZ filaments elongated at a rate of  $1.9 \pm 0.1$   $\mu$ m/min at 1.5  $\mu$ M, (n=40). This rate, when normalized for concentration, is equivalent to the growth rate of ParM filaments (Garner et al., 2004), and about 6-fold faster than growing MTs (Hyman et al., 1992). After a random period of time, growing PhuZ filaments were observed to switch to rapid disassembly (Fig. 1c,d, Supplementary Video 4) and completely depolymerize. The remaining stabilized GMPCPP Cy5-PhuZ seed could then nucleate another round of polymerization. As shown in the kymographs (Fig. 1D), filament depolymerization always (n=40) went to completion and proceeded at an average rate of  $108 \pm 20$   $\mu$ m/min. This rate of catastrophic depolymerization is comparable to rates observed for yeast tubulin, but is an order of magnitude faster than that of either mammalian tubulin or ParM (13, 9.4  $\mu$ m/min, respectively) (Garner et al., 2004; Hyman et al., 1992). The GMPCPP Cy5-seeds formed stable filaments that never disassembled (Fig. 1c,d Supplementary Video 4), showing that, as with

MTs, dynamic instability of PhuZ filaments requires the energy of GTP hydrolysis. PhuZ is thus the first prokaryotic tubulin known to display dynamic instability.

### Nucleotide Hydrolysis Drives PhuZ Dynamic Instability

The dynamic instability observed by TIRF suggests that filament behavior is tightly coupled to nucleotide hydrolysis. Examination of the polymerization kinetics of a catalytically inactive mutant (D190A-PhuZ) by right-angle light scattering (Fig. 2a) revealed that the critical concentration ( $320 \pm 20$  nM) was about 10-fold lower than the 2.5  $\mu$ M previously measured for wild-type PhuZ (Kraemer et al., 2012; Zehr et al., 2014). This difference is likely due to the competition between the rate of hydrolysis during transient association of longitudinal dimers (proportional to  $[\text{PhuZ}]^2$ ) with the rate of assembly of hexameric nuclei (proportional to  $[\text{PhuZ}]^6$ ) as well as contributions from filament turnover at steady-state due to nucleotide hydrolysis by wild-type PhuZ. Unlike wild-type PhuZ, D190A-PhuZ polymerization curves also show a linear phase after the initial growth phase (Fig. 2a), likely due to increased bundling of these non-dynamic filaments. Compared with tubulin whose GDP critical concentration is about 10x higher than with GTP (Caplow et al., 1994; Mitchison and Kirschner, 1984a), PhuZ is even more discriminating, with no polymerization detectable in GDP at PhuZ concentrations as high as 200  $\mu$ M (Fig. 2c). D190A-PhuZ also requires GTP for polymerization (Fig. 2d).

While the polymer cannot form with GDP, GTP is rapidly hydrolyzed in the filament body to GDP. To test the stability of the GDP-PhuZ lattice, excess GDP was spiked into wild-type or D190A-PhuZ polymerization reactions having 100  $\mu$ M GTP (Fig. 2b). Upon addition of GDP, wild-type PhuZ rapidly depolymerized, with no observable polymer detected  $\sim$ 1 min post GDP addition, while no appreciable depolymerization was observed with D190A-PhuZ (Fig. 2b).

Because GTP is rapidly hydrolyzed to GDP within the lattice, only the most recently added monomers at the plus-end of the filament contain GTP. Thus, the observed rapid depolymerization after adding GDP implies the existence of a stabilizing GTP-cap that is lost upon GDP addition. The stability observed with D190A-PhuZ demonstrates that the nucleotide state of the penultimate PhuZs must be determining filament stability and not the state of the exchangeable most plus-end monomer. These observations help explain the catastrophic depolymerizations observed in our movies as the result of stochastic loss of the cap due to nucleotide hydrolysis in one or more plus end monomers.

#### PhuZ Filaments Display Dynamic Instability *in Vivo*

To determine if PhuZ displays the microtubule-like properties *in vivo* that were observed *in vitro* (unidirectional growth, dynamic instability), we visualized GFP-PhuZ filaments in *Pseudomonas chlororaphis* cells using rapid time-lapse microscopy. To permit fluorescent labeling, *P. chlororaphis* cells were grown on agar pads containing arabinose to induce production of GFP tagged PhuZ expressed from a plasmid. When GFP-PhuZ was expressed in the absence of phage infection, but at concentrations comparable to that occurring during an infection, short filaments were formed (average length of 0.9  $\mu\text{m}$ , n=1260) at random positions throughout the cell (Fig. 3a,i). In time-lapse microscopy, these filaments displayed dynamic instability, undergoing periods of polymerization and depolymerization (Fig. 3g; Movie 5). Overall, the dynamic properties of the *in vivo* assembled filaments of uninfected cells were similar to the results obtained *in vitro*.

By contrast, upon infection of *P. chlororaphis* cells with phage 201 $\Phi$ 2-1, PhuZ assembled long filaments that extended approximately half the length of the cell, with an average

length of 2.0  $\mu\text{m}$  (n=780). As shown in Fig. 3b-f and Movie 6, PhuZ formed a spindle-like structure in which a pair of bundled filaments emanated from a single location at each cell pole and extended toward the infection nucleoid at midcell. Filaments of the phage spindle were highly dynamic and could be observed to polymerize and depolymerize (Fig. 3h,j; Movie 6). Depolymerization always occurred from the nucleoid side, suggesting that the filaments are oriented with the minus end at the cell pole and the plus end extending toward the nucleoid. While filaments in uninfected cells were located at random positions throughout the cell (Fig. 3i, n=110), the spindle vertex was always (95%, n=60) stably associated with the extreme pole of the cell (Fig. 3i), indicating that minus ends are specifically anchored at the cell pole during phage infection.

#### The Infection Nucleoid is Composed Solely of Phage DNA

To further understand how PhuZ participates in development and centering of the infection nucleoid and to determine the composition of the DNA in this structure, we followed infection nucleoid formation using fluorescence *in situ* hybridization (FISH). Using probes complementary to either phage DNA (Cy3) or host chromosomal DNA (Cy5) (Fig. 4), we showed that host chromosomal DNA is degraded by 20 minutes post infection and that the nucleoid formed during phage infection is composed entirely of phage DNA. We never observed co-localization of the two probe signals.

To assess the dynamics of the phage DNA in live cells, we used the nonspecific vital DNA stain Syto16. Infected wild type (WT) cells were grown on agar pads containing Syto16. We observed that upon phage infection, host DNA disappears concomitant with the appearance of a focus of phage DNA, which first appears near one cell pole 75% of the time (n= 155



infected cells) (Fig. 5a and Movies 7 and 8). Over time, the small circular mass of phage DNA increases in size and migrates toward the cell midpoint (Fig. 5a & b). After arrival at midcell, the phage nucleoid oscillates slightly about the central axis (Fig. 5c & d), suggesting that the nucleoid continues to experience positioning forces. This oscillatory movement is reminiscent of eukaryotic chromosomes lined up at midcell by the mitotic spindle. In contrast to eukaryotes, where DNA replication is temporally separated from segregation, the phage nucleoid continued to increase in mass as it moved toward midcell, suggesting that DNA replication and positioning occur simultaneously. In time-lapse co-localization microscopy experiments, we simultaneously visualized CFP-PhuZ filaments and Syto16 stained phage nucleoids during infection (Fig. 5e & f). As the phage nucleoid migrated toward midcell, it was associated with the end of the growing PhuZ filament, consistent with a model in which PhuZ filaments center phage DNA by applying pushing forces.

#### Phage Nucleoid Positioning is Independent of DNA replication

To test whether replication was a requirement for phage DNA movement, we added a potent DNA gyrase inhibitor (ciprofloxacin) that blocks replication of DNA to WT cells at various points during infection. While ciprofloxacin reduced nucleoid size as expected, indicating a reduced accumulation of DNA, it had no effect on its positioning at midcell, suggesting that DNA replication was not required for the centering function of the PhuZ spindle (Fig. 6). By contrast, interfering with PhuZ filament dynamics has a marked effect on phage DNA positioning (Kraemer et al., 2012).

## Discussion

The ability of intrinsically polarized and dynamically unstable MTs to be anchored, stabilized, and regulated allows these filaments to be harnessed by the eukaryotic cell to perform key organizational tasks. It has been argued that the spatiotemporal organization of the cytoskeleton by organizing centers may be a defining characteristic of eukaryotes (Theriot, 2013). However, the prokaryotic cell also utilizes cytoskeletal proteins to organize its internal space and efficiently execute essential life processes. Now we show that even entities often considered “non-living,” such as bacteriophage, also exploit the advantages of a well-defined cytoskeletal organization to faithfully propagate themselves.

We have shown that the PhuZ tubulin polymerizes into a filament that is intrinsically polar and dynamically unstable and that *in vivo* it is anchored, and stabilized. Furthermore, it assembles into a bipolar spindle that more than superficially resembles its eukaryotic counterpart. The PhuZ spindle appears to play a key role in organizing viral reproduction by positioning the phage nucleoid at midcell (Fig. 7). Early during infection, dynamically unstable PhuZ polymers specifically interact with and move the replicating phage DNA, presumably by applying pushing forces, although this movement is independent of replication.

Tubulins in bacteria have been studied intensively for nearly 25 years. To date, prokaryotic tubulins have either been demonstrated to treadmill (TubZ) or the relevant filament movement remains an unresolved matter (FtsZ). This apparent switch in the type of functional movement displayed by prokaryotic tubulins versus eukaryotic ones had posed an intriguing question – why don't bacterial tubulins undergo dynamic instability? We now know that some of them do and this particular type of biomechanics may inherently lend itself to the formation of complex structures for the search and capture of large masses of DNA.

All eukaryotic cells are thought to utilize a mitotic spindle to ensure accurate inheritance of sister chromatids to the daughter cells, but it has long been a mystery how such a complicated structure might have evolved. The first function of the eukaryotic spindle is to line up replicated chromatids at the midline of the dividing cell. Our discovery of a bacteriophage that assembles a similar structure raises the possibility that bipolar spindles arose more than once by convergent evolution taking advantage of the unique properties of tubulin polymers. Alternatively, it is also possible that phage hijacked the mitotic spindle from an ancient eukaryotic cell. However, since bacteria and phage are thought to predate eukaryotic life, an intriguing possibility is that the mitotic spindle first evolved in a bacteriophage for the purpose of positioning viral DNA during lytic growth and was later co-opted for positioning chromosomal DNA in the progenitor of the first eukaryotic cell. One can imagine that a primordial tubulin evolved to form filaments of increasing biochemical, structural, and functional complexity, beginning with single stranded protofilaments (FtsZ) required for cell division (Erickson et al., 1996; Meier and Goley, 2014). These then evolved into multi-stranded filaments capable of segregating plasmid DNA (TubZ) (Aylett et al., 2010; Chen and Erickson, 2008; Larsen et al., 2007; Montabana and Agard, 2014; Oliva et al., 2012) and centering viral DNA (PhuZ). The increased structural and biochemical complexity, including increases in the number of protofilaments would allow the lattice to become more cooperative, allowing a greater difference between growth and nucleation rates. This in turn would allow the lattice to become more metastable, thereby storing the greater energy necessary for more complex functions within the lattice.

Bacterial tubulin homologs have proven as essential to prokaryotic cell biology as to eukaryotes, and as such, it is not totally unexpected that the advantages conferred upon a cell or

virus by the ability to build complex tubulin based structures would also be selected for and shared across kingdoms.

## **Materials and Methods**

### **Protein Expression and Purification**

Wild-type and KCK-PhuZ were expressed and purified as previously reported (Kraemer et al., 2012). D190A-PhuZ was purified by an altered protocol to minimize polymerization. Cultures were lysed in a buffer containing 500 mM KCl, 2 mM EDTA, 10 % glycerol, 15 mM thioglycerol, and 50 mM HEPES, pH 8 and cleared at 35k xg. 0.1 volumes of DOWEX resin were then added to the clarified lysate to remove nucleotide. The sample was then spun at 38k XRPM in a Ti45 rotor (Beckman) to remove the resin and residual aggregates. D190A-PhuZ was then purified by Ni-affinity chromatography using an EDTA-resistant Ni-resin (Roche). The 6x His-tag was cleaved with thrombin protease and EDTA was dialyzed out, and the protein was subsequently purified by gel filtration (Superdex 200) in a buffer containing 250 mM KCl, 1 mM MgCl<sub>2</sub>, 10% glycerol, 15 mM thioglycerol, and 50 mM HEPES, pH 8. Prior to experiments, all constructs were spun at 80,000 RPM in a TLA100 rotor (Beckman) at 4°C for 20 min.

### **Dye and Biotin Labeling of PhuZ**

Thioglycerol was removed from KCK-tagged protein by a Zeba column (Pierce) equilibrated with buffer with no reducing agent. A 2-fold molar excess of dye, Cy3- or Cy5-maleimide (GE), or biotin-maleimide (Sigma) was added and incubated for 15 min at 25°C. 50 mM DTT was added to quench the reaction and the reaction was spun at 80,000 RPM in a TLA100 rotor (Beckman) to remove aggregates. To remove excess dye and non-functional

protein, labeled PhuZ was exchanged into BRB80 pH 7.2 in by a Zeba column (Pierce), polymerized by the addition of 5 mM GTP, and pelleted at 80k XRPM in a TLA100 rotor (Beckman). Non-polymerized protein was removed, and the pellet was resuspended in a depolymerization buffer (500 mM KCl, 1 mM MgCl<sub>2</sub>, 15 mM thioglycerol, 10% glycerol, 50 mM HEPES pH 8) on ice for 1.5 hours. Labeled protein was buffer exchanged into BRB80 pH 7.2 and stored.

### **Preparation of PEG-coated Glass Slides**

Slides were prepared using a modified protocol from Bieling et al (Bieling et al., 2007). 24 x 40 mm coverslips (VWR) were sonicated in 2 M KOH for 30 min. Slides were then washed three times with H<sub>2</sub>O and sonicated in piranha solution (2 parts 30% H<sub>2</sub>O<sub>2</sub>, 3 parts H<sub>2</sub>SO<sub>4</sub>) for 30 min. Slides were subsequently washed three times with H<sub>2</sub>O and spun dry. Slides were silanized by making sandwiches with a drop of GOPTS (Sigma) and baked for 1 hour at 75 °C. Sandwiches were separated and washed in dry isopropanol (Sigma), and spun dry. 30 µl of a saturated PEG-SEV acetone solution (1% biotin-PEG-SEV) (Laysan) were added to silanized slides, and sandwiches were baked for 4 hours at 75 °C. Sandwiches were separated in H<sub>2</sub>O, sonicated for 5 min, spun dry, and stored in the dark.

### **Total Internal Reflection Fluorescence (TIRF) Microscopy**

Flow chambers were made using double-sided tape. For single color experiments, the chamber was washed three times with imaging buffer (BRB80 pH 7.2 supplemented with 100 mM KCl, 0.5% BSA, 0.5% methylcellulose, and 40 mM βme). 4 mM GTP was added to 2.5 µM

Cy3-PhuZ (80% wild-type, 20% Cy3-labeled) in imaging buffer, flowed into the chamber, and subsequently imaged. Images were acquired at a 0.5 sec interval on an Andor CCD camera.

For two-color imaging, chambers were washed three times with imaging buffer (supplemented with a GLOX system to minimize photobleaching), followed by 5 min incubation with neutravidin. Chambers were then washed three more times with imaging buffer to remove unbound neutravidin. 200  $\mu$ M GMPCPP was added to 2  $\mu$ M Cy5-PhuZ (75% wild-type, 20% Cy5, 5% biotin) to induce polymerization. After 5 min on ice, Cy5-PhuZ-GMPCPP seeds were added to the chamber. After 2 min, the chamber was washed three times with imaging buffer to remove any seeds not adhered to the cover slip. 4 mM GTP was added to 1.5  $\mu$ M Cy3-PhuZ (80% wild-type, 20% Cy3), added to the chamber, and imaged at a 0.25 sec interval.

### **Light Scattering**

Right angle light scattering was conducted by mixing D190A-PhuZ with BRB80 pH7.2 containing GTP using a stop-flow system designed in-house. An excitation wavelength of 530 nm was used. The critical concentration was determined by plotting the maximum intensity versus PhuZ concentration. The x-intercept of this plot was used as the critical concentration.

For nucleotide spiking experiments, protein and buffer were mixed 1:1 (150  $\mu$ l reactions) by hand and polymerization was followed by right angle light scattering. Upon reaching plateau, 10  $\mu$ l of GDP or buffer was added.

### **Pelleting**

5 mM GDP or GTP was added to PhuZ constructs and, after 5 min, samples were spun at 80k XRPM in a TLA100 rotor (Beckman) for 20 min at 25°C. Supernatants were carefully

removed and the pellet was resuspended in 1X gel loading buffer. Samples from the supernatant and pellet were then run on a 10% SDS-PAGE gel and stained with Simple Blue (Life Technologies).

### **Live cell microscopy**

*Pseudomonas chlororaphis* cells were grown on 1% agarose pads supplemented with 25% Luria broth, 1 µg/ml FM4-64, and when appropriate, either 0.5µM Syto 16 or 5µg/ml DAPI as described (1). For phage infections, 5 µl of phage lysate ( $10^8$  pfu/ml) was applied to the cells, a coverslip was added, and images were captured using a DeltaVision Spectris Deconvolution microscope (Applied Precision, Issaquah, WA). GFP-PhuZ was expressed in strain ME41 (1) from the arabinose promoter by including arabinose within the pad at a concentration ranging from 0 to 2%, as indicated.

### **Fluorescence in situ hybridization (FISH)**

*P. chlororaphis* cells were grown on a 1% agarose pad, infected with 5 µl of phage 201phi2-1 lysate ( $10^8$  pfu/ml) and at various times (8, 20, 40 70 minutes) after infection fixed with glutaraldehyde (0.025%) and paraformaldehyde (16%). Fixed cells were processed for hybridization as described (Ho et al., 2002). Briefly, cells were washed in PBS, blocked at 75°C for 2 min with 70% formamide, 2X SSC, 1 mg/ml Salmon sperm DNA, washed one time each with 70%, 90%, and 100% ethanol, and allowed to dry. Cells were then treated with 50% formamide, 2XSSC for 5 minutes at 23°C, probe was added, and then heated at 94°C for 2 minutes, and then hybridized at 42°C overnight. DNA probes specific for the host *P. chlororaphis* chromosomal DNA or phage 201phi2-1 DNA were prepared by first digesting total

*P. chlororaphis* chromosomal DNA or total phage 201phi2-1 DNA with a set of enzymes (*DNA* with *Bsp1286 I*, *HhaI*, *HpyCH4 III*, *Hpy188 I*, *Nla III*), and then labeling the ends of with Cy3-dCTP or Cy5-dCTP using terminal deoxynucleotidyl transferase.

### **Plasmid construction**

The *phuZ* gene was amplified from pME28 plasmid (1) by standard PCR using the primer VC091 and VC094, while the CFP tag was amplified from pMutin-CFP using the primer VC092 and VC093. To generate CFP-PhuZ fusion, the CFP tag was then fused at the 5' end of the *phuZ*-PCR product by the overlapping PCR method. The PCR fusion was constructed into the pHERD30T vector under the control of the arabinose promoter by the Gibson assembly cloning kit (New England Biolab) using the following primers: VC095, VC096, VC097 and VC098. This yields an N-terminal fusion of cyan fluorescent protein with PhuZ with an 11 amino acid linker in between, named as pVC01. This construct was introduced into *E.coli* to test whether it is able to be expressed and to confirm that PhuZ filaments can be made. After that, this recombinant plasmid was transformed into *P. chlororaphis* and the clone was designated as strain VC085.

### **Primer list**

VC091: 5'- ACTACCCTGCAGGTCAAACCTACCATGCCGTCTT -3'

VC092: 5'-

GTAGTTCTAGATTGATAAGAAGGAGATATACATACATGGTGAGCAAGGGCGAGGA -  
3'



VC093: 5'-

CAGGCATTTTTGGCTGCCTCCTGCAGCGGCCGCTCCGGACTTGTACAGCTCGTCCA  
TGC -3

VC094: 5'-

GTACAAGTCCGGAGCGGCCGCTGCAGGAGGCAGCCAAAAAATGCCTGTAAAGTCT  
GTCT -3'

VC095: 5'- CCTGCAGGCATGCAAGCTTGGCACT -3'

VC096: 5'- TCTAGAGGATCCCCGGGTACCGAGCT -3'

VC097: 5'- AGCTCGGTACCCGGGGATCCTCTAGATTGATAAGAAGGAG -3'

VC098: 5'- GCCAGTGCCAAGCTTGCATGCCTGCAGGTCAAACCTACCAT -3'

### **DNA replication inhibition by ciprofloxacin**

*Pseudomonas chlororaphis* cells were grown on 1% agarose pads supplemented with 25% Luria broth, 1 µg/ml FM4-64, and 5µg/ml DAPI. After 2 hours of cell growth at 30°C, 5 µl of phage lysate ( $10^8$  pfu/ml) was applied to the cells, and infection was allowed to proceed for 80 minutes at 30°C. 5µl of ciprofloxacin (2µg/ml) was added 10 minutes before infection, or 10, 20, 40, and 50 minutes after infection. After 80 minutes of infection, cells were fixed on the pad with glutaraldehyde (0.025%) and paraformaldehyde (16%) and then coverslips were added and the cells imaged using a DeltaVision Spectris Deconvolution microscope (Applied Precision, Issaquah, WA). As a control, a set of infections was performed in which only buffer (1N HCl) but no ciprofloxacin was added. In addition, we also examined cells treated with ciprofloxacin but without the addition of phage. Images were analyzed using Image J software to quantitate

DAPI intensity of the infection nucleoids and to determine the position of infection nucleoids relative to cell lengths.

### **Acknowledgements**

We thank members of the Agard and Pogliano labs for invaluable discussions, especially Daniel Elnatan for TIRF microscopy assistance. We also thank members of the Mullins lab for TIRF advice. The OMX and Light Microscopy Facility at UCSD is funded by grant NS047101. We thank Jennifer Santini for her invaluable help with the OMX. J.A.K. was supported by the Genentech Foundation Predoctoral Fellowship and the Achievement Rewards for College Scientists Foundation Award. This work was supported by the Howard Hughes Medical Institute (D.A.A.) and National Institutes of Health grants R01GM073898 (J.P.), GM031627 (D.A.A.), and GM104556 (J.P. and D.A.A.).

### **Author Contributions**

M.L.E., J.A.K., D.A.A., and J.P. designed experiments. M.L.E., J.A.K., V.C., and J.K.C.C. conducted experiments. M.L.E., J.A.K., J.K.C.C., V.C., and P.N. analyzed the data. M.L.E., J.A.K., D.A.A., and J.P. wrote the paper.

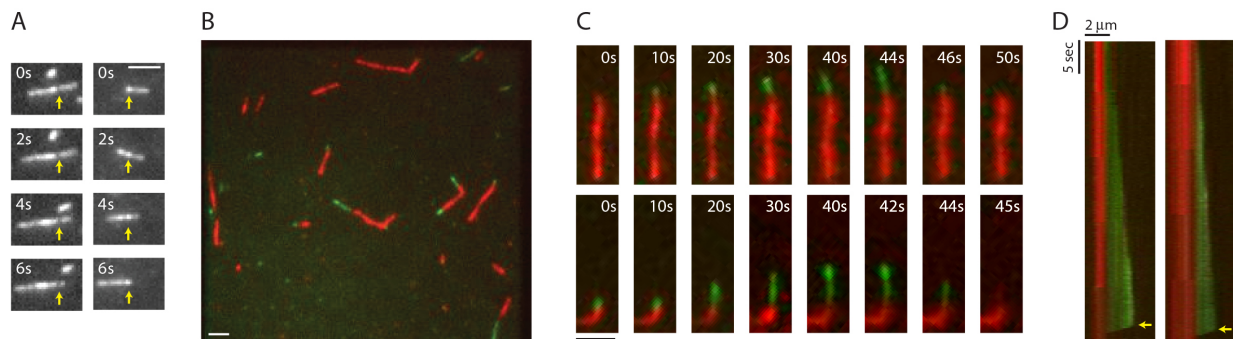


**Figure 1. TIRF microscopy reveals polarity and dynamic instability in PhuZ filaments. (A)** Cy3 labeled PhuZ filaments exhibit treadmilling, in the presence of GTP. Many filaments displayed non-uniform intensity (highlighted by arrows), which moved directionally toward the shrinking end of filaments. **(B-D)** Polymerization of GTP-PhuZ filaments (green) off of GMPCPP stabilized PhuZ seeds (red) (see supplemental methods). **(B)** Wide-field still image of PhuZ filaments growing unidirectionally off of GMPCPP stabilized seeds. **(C)** Montages of two representative PhuZ filaments undergoing dynamic instability. Periods of filament growth are followed by rapid disassembly back to the GMPCPP seed. **(D)** Kymographs of filaments from **(B)**. Arrow indicates catastrophe event. Scale bars equal 2  $\mu\text{m}$ .

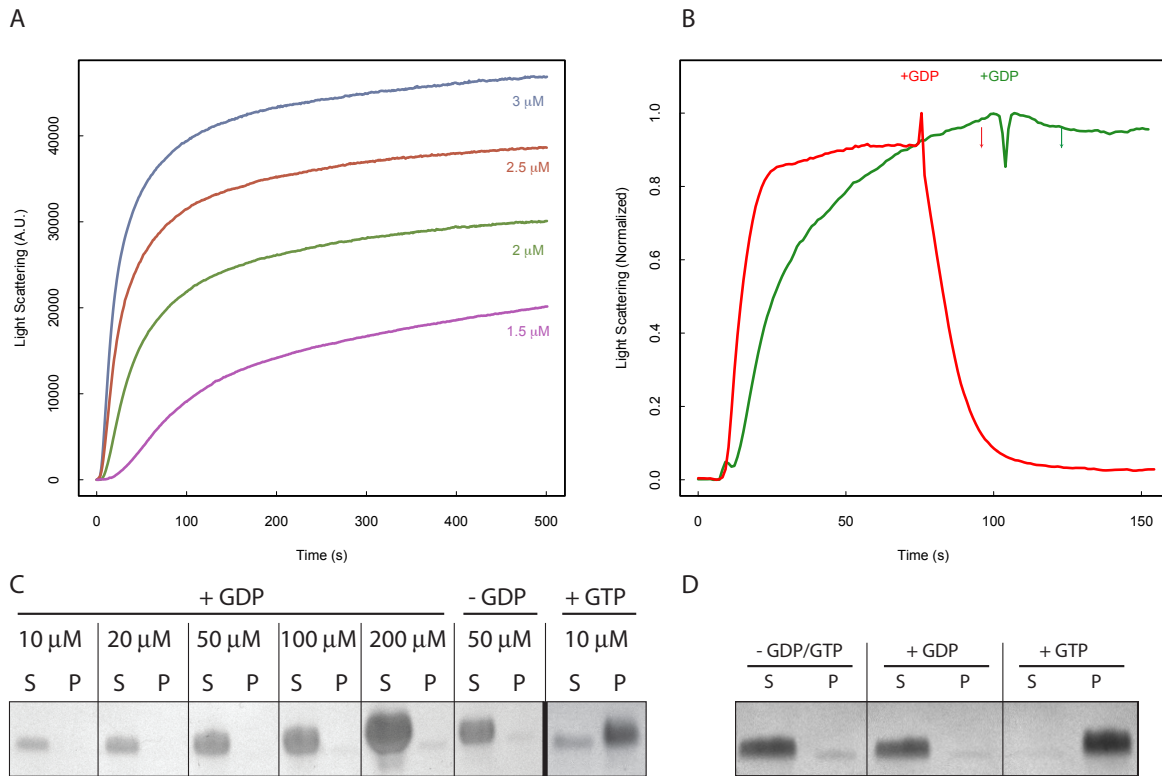


**Figure 2. Nucleotide hydrolysis destabilizes PhuZ filaments. (A)** Right-angle light scattering traces of D190A-PhuZ polymerization at 1.5 (purple), 2 (green), 2.5 (red), and 3 (blue)  $\mu\text{M}$  upon addition of 1 mM GTP. **(B)** Right-angle light scattering traces of PhuZ (red) or D190A-PhuZ (green) polymerized in 100  $\mu\text{M}$  GTP. 3 mM GDP was added at once polymerization reached steady state (arrow +GDP), and subsequent depolymerization was monitored. **(C)** Testing PhuZ polymerization by pelleting (see Supplemental Methods). Supernatants (S) and pellets (P) were analyzed by SDS-PAGE. No detectable PhuZ polymer formed at concentrations as high as 200  $\mu\text{M}$ . No detectable polymer formed in the absence of nucleotide (second from right), and PhuZ filaments were readily detected in the presence of 5 mM GTP (10  $\mu\text{M}$  shown right). **(D)** Pelleting of D190A-PhuZ in the presence of GDP, GTP, or no nucleotide as in (C). Nucleotide was added to 10  $\mu\text{M}$  D190A-PhuZ and spun 80000X RPM for 20 min at 25 °C. Supernatants (S) and pellets

(P) were analyzed by SDS-PAGE. No detectable polymer was formed in the presence of GDP. In contrast, almost all of the protein was found in the pellet in the presence of GTP.

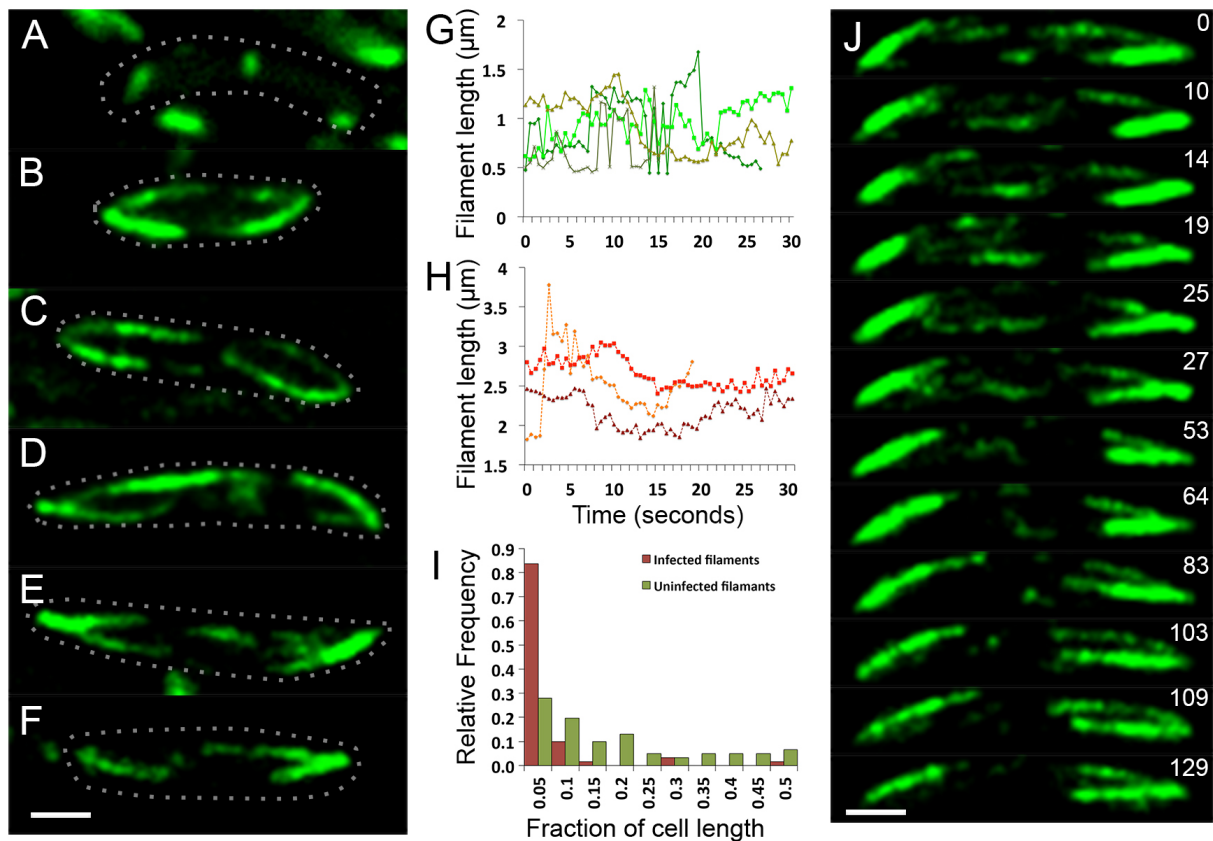


**Figure 3. PhuZ forms a bipolar spindle composed of dynamically unstable filaments *in vivo*.**

(A) GFP-PhuZ expressed by itself (in the absence of phage infection) assembles relatively short filaments in *P. chlororaphis*. A single cell (outlined) with three filaments is shown. (B-F) Five examples of *P. chlororaphis* cells (outlined) that have been infected with phage 201phi2-1 for approximately 60 minutes have bipolar GFP-PhuZ spindles. (G) Filament length versus time (seconds) is plotted for 3 filaments from uninfected cells, revealing alternating periods of growth and shrinkage (dynamic instability). (H) Filament length versus time (seconds) is plotted for 3 spindle filaments assembled during infection. (I) Relative position of filament ends (closest to the cell pole) are expressed as fraction of cell length in uninfected (green, n=110) or infected

(red, n=60) cells plotted as a frequency distribution (fraction of population). **(J)** Time-lapse sequence showing a single cell with a bipolar spindle over the course of 129 seconds. The filaments of the spindle can be observed to grow and shrink (Movie S6). The white scale bar equals 1 micron. For A-F and J, GFP-PhuZ was expressed at physiologically relevant levels (near the critical concentration for assembly) from the arabinose promoter with 0.25% arabinose for uninfected cells and below the critical concentration for assembly (0.15% arabinose) for infected cells to avoid overexpression.

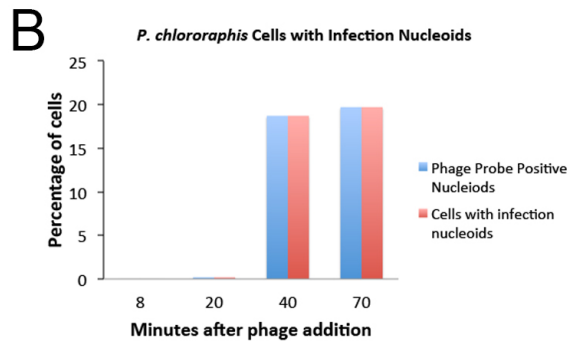
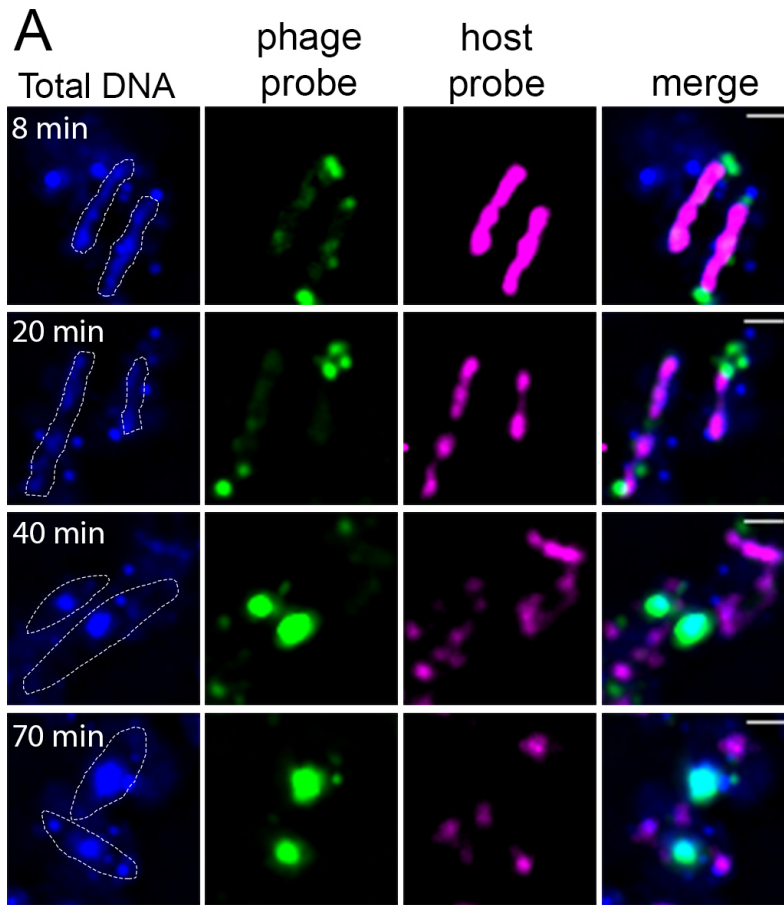


**Figure 4. Fluorescence in situ hybridization (FISH) during phage infection.**

(a) *P. chlororaphis* cells were grown on a 1% agarose pad, infected with 5  $\mu$ l of phage 201phi2-1 lysate ( $10^8$  pfu/ml) and at various times (8, 20, 40 70 minutes) after infection fixed with glutaraldehyde (0.025%) and paraformaldehyde (16%). Fixed cells were hybridized with DNA probes specific for the host *P. chlororaphis* chromosomal DNA (pink, labeled with Cy3) or



phage 201phi2-1 DNA (green, labeled with Cy3) as further described in the methods. Total DNA was stained with DAPI. The white scale bar equals 1 micron. Cells outlines are indicated with a white dotted line. By 40 minutes post infection, host DNA was mostly degraded in the cells such that only small remnants of *P. chlororaphis* DNA was detectable, typically near the cell poles.

**(b)** The percentage of cells containing an infection nucleoid was quantitated (red) over time and compared to the percentage of nucleoids staining positive for probe. All (100%, n>50) of the infection nucleoids stained brightly with phage specific probes, but had no detectable staining with *P. chlororaphis* chromosomal DNA probe.

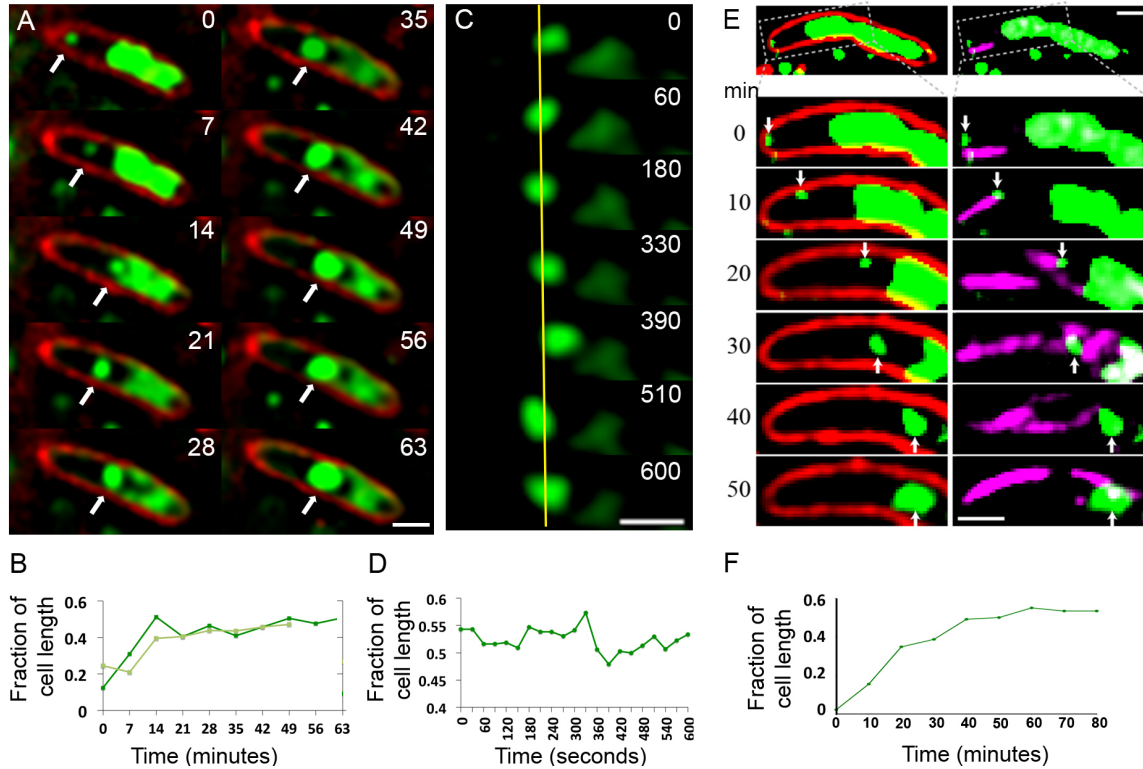


**Figure 5. Observation of phage nucleoid migration by time-lapse microscopy.**

**(A)** Time-lapse sequence showing development of a phage nucleoid (arrows) in a single cell over the course of 63 minutes. Membranes are stained red with FM 4-64 and the DNA is stained green with Syto16. At time zero, a small phage nucleoid (small green focus, arrow) is observed near the cell pole in *P. chlororaphis* infected with phage 201phi2-1. Over time the phage nucleoid moves to midcell and increases in size. The host chromosome, which fills half of the cell at time zero (large green mass), is degraded during infection (Movie S7). The scale bar equals 1 micron.

**(B)** Position of the phage nucleoid in panel A (dark green) is recorded as fraction of cell length and plotted versus time. A second example of nucleoid migration is plotted in light green and is shown in Movie S8. **(C)** Time-lapse showing nucleoid oscillation over the course of 600 seconds. **(D)** Position (expressed as fraction of cell length) of the phage nucleoid in panel C plotted versus time shows nucleoid movement. **(E)** Time-lapse sequence showing CFP-PhuZ

together with movement of a phage nucleoid (arrows) in a single cell over the course of 50 minutes. At time zero, a small phage nucleoid is observed near the cell pole in *P. chlororaphis* infected with phage 201phi2-1. One region of the cell (white box) is enlarged in the time sequence. Over time (minutes) the nucleoid moves to midcell and increases in size (note that for clarity only one-half of the cell is enlarged in the time sequence). Midway through its migration (10 minutes), the nucleoid is associated with the end of the PhuZ polymer. **(F)** Position (expressed as fraction of cell length) of the phage nucleoid in panel E plotted versus time shows nucleoid movement.

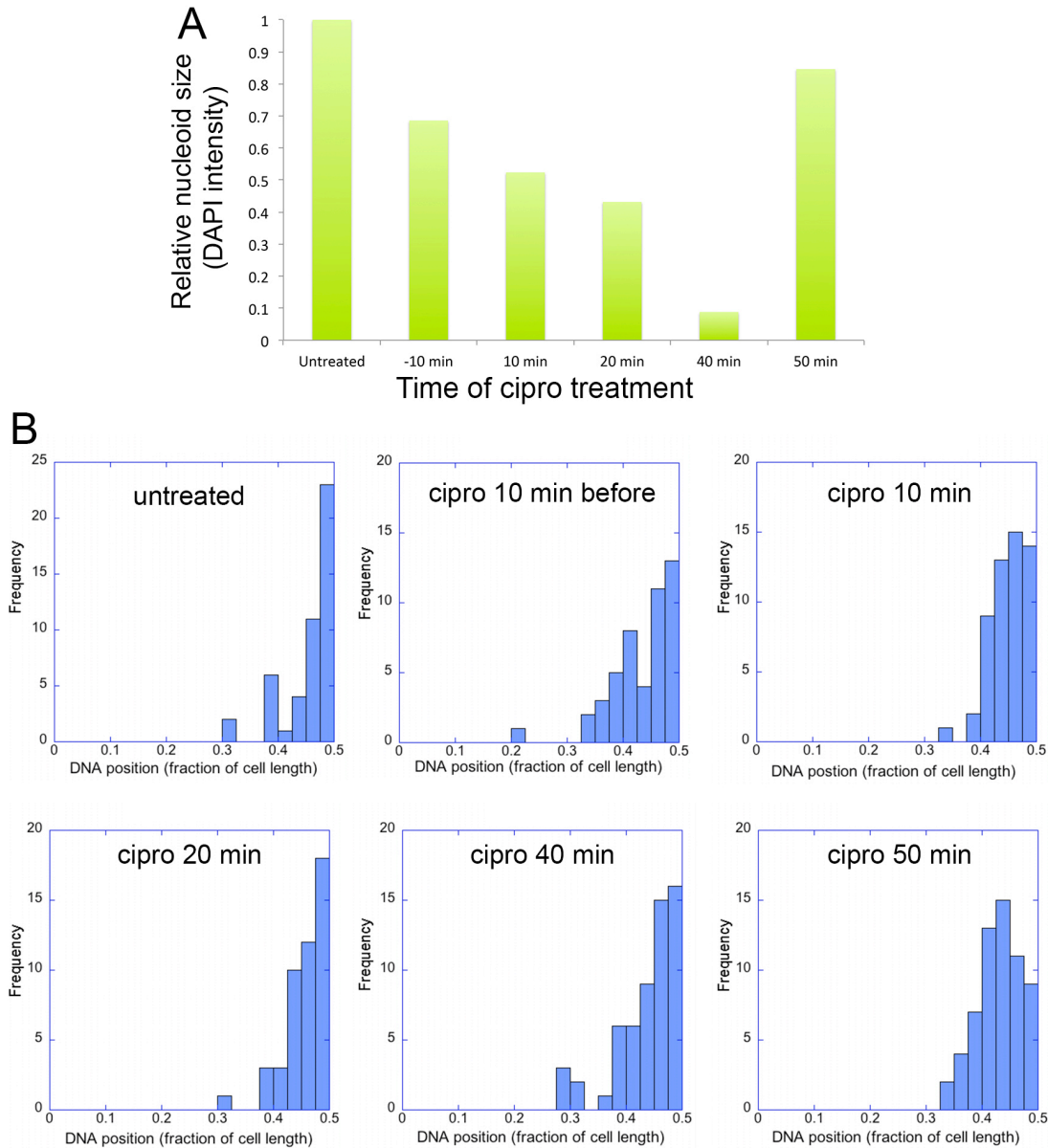


**Figure 6. Infection Nucleoid Centering is Independent of DNA replication.**

a) DNA content of infection nucleoids was measured by DAPI staining. Cells were grown on an agarose pad and infected with phage 201phi2-1. Ciprofloxacin was applied to cells either 10 minutes before infection or at various times (10, 20, 40, and 50 minutes) after infection. After 80 minutes of infection, cells were fixed and images were collected. Total DAPI intensity was measured for approximately 300 cells for each time point. The average total DAPI intensity was

normalized to the value for untreated cells. The addition of ciprofloxacin inhibited phage nucleoid (DAPI intensity) growth when added during the first 40 of minutes phage infection, but had little effect on replication when added at 50 minutes, suggesting that by 50 minutes DNA replication was mostly completed or no longer dependent on DNA gyrase. **b)** Histograms showing the position of phage DNA within the cell plotted as a fraction of cell length versus the percentage of the population (frequency) for each time point in A. Although ciprofloxacin treatment inhibited phage DNA replication, it had no effect on phage DNA positioning.

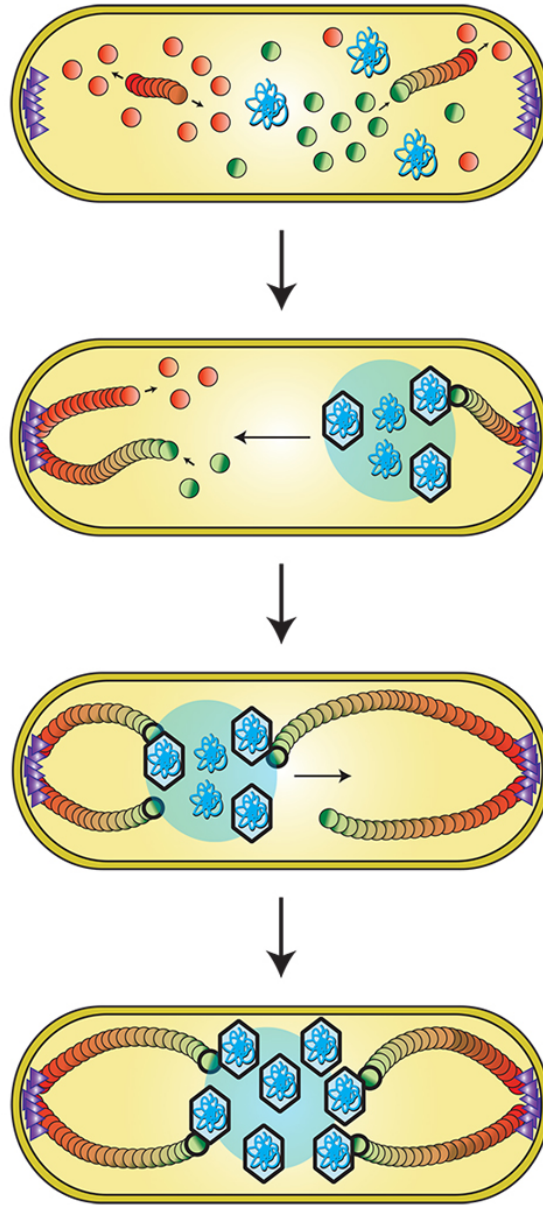


**Figure 7. Model of PhuZ bipolar spindle formation during lytic growth.** PhuZ is expressed early in lytic growth and forms dynamically unstable polymers anchored at the cell poles.

Filaments polymerize unidirectionally, with GTP-bound (green) subunits adding to one end, to center the replicating phage DNA at midcell. Capsids assemble on the phage nucleoid for DNA packaging.

## Legends to Supplemental Movies

**Movie S1.** TIRF microscopy of 2.5  $\mu\text{M}$  Cy3-PhuZ (20% Cy3) filaments reveals PhuZ filaments are dynamic and translocate around the field of view. Filaments treadmill and undergo catastrophic depolymerization. Images were acquired every 250 ms for 75 seconds. Scale bar equals 2  $\mu\text{m}$ .

**Movie S2.** Close up of Cy3-labelled PhuZ showing annealing, severing, and depolymerization events. Images were acquired every 500 ms for 100 sec. Scale bar equals 2  $\mu\text{m}$ .

**Movie S3.** Close up of Cy-labelled PhuZ filaments demonstrating a full depolymerization event. Zoom in from Movie S1. Scale bar equals 2  $\mu\text{m}$ .

**Movie S4.** Dynamic instability and polarity of PhuZ filaments revealed by two-color TIRF microscopy. GMPCPP stabilized PhuZ seeds (20% Cy5, 5% biotin, red) were attached to biotin-PEG coated glass, and 1.5  $\mu\text{M}$  Cy3-PhuZ (20% Cy3, green) and GTP were added. Green filaments are observed to grow from only one end of the seeds and exhibit dynamic instability. Images were acquired every 250 ms for 100 seconds. Scale bar equals 2  $\mu\text{m}$ .

**Movie S5.** A time-lapse movie of uninfected *P. chlororaphis* cells expressing GFP-PhuZ shows that PhuZ filaments display dynamic instability *in vivo*. Time points were taken 1 second apart for 1 minute. Cells were grown on an agarose pad and GFP-PhuZ was expressed from the arabinose promoter with 0.25% arabinose.

**Movie S6.** Time-lapse movie of *P. chlororaphis* cells expressing GFP-PhuZ and infected with phage 201phi2-1 shows that PhuZ filaments form a spindle in which the centrally located ends of the filaments display dynamic instability. Images were captured 0.5 second apart for 2.5 minutes. Cells were grown on an agarose pad with 0.15% arabinose to express GFP-PhuZ from the arabinose promoter and then infected with phage.

**Movie S7.** Time-lapse movie corresponding to the cell in Fig 4A showing development of a phage nucleoid in a single infected cell over the course of 63 minutes. The phage nucleoid first appears as a small green focus at the cell pole that migrates to the cell midpoint and develops into a very large infection nucleoid. Images were captured 7 minutes apart for 63 minutes. Cells were grown on an agarose pad containing Syto16 and then infected with phage.

**Movie S8.** Time-lapse movie showing development of a phage nucleoid in a single infected cell over the course of 49 minutes. This example of nucleoid formation and movement corresponds to one of the nucleoids reported in the graph in Figure 4C. The phage nucleoid first appears at the cell pole and then migrates to cell midpoint. Images were captured 7 minutes apart for 49 minutes. Cells were grown on an agarose pad containing Syto16 and then infected with phage.



## References

- Allen, C., and Borisy, G.G. (1974). Structural polarity and directional growth of microtubules of *Chlamydomonas* flagella. *Journal of molecular biology* *90*, 381-402.
- Aylett, C.H., Wang, Q., Michie, K.A., Amos, L.A., and Lowe, J. (2010). Filament structure of bacterial tubulin homologue TubZ. *Proceedings of the National Academy of Sciences of the United States of America* *107*, 19766-19771.
- Bergen, L.G., and Borisy, G.G. (1980). Head-to-tail polymerization of microtubules in vitro. Electron microscope analysis of seeded assembly. *The Journal of cell biology* *84*, 141-150.
- Bieling, P., Laan, L., Schek, H., Munteanu, E.L., Sandblad, L., Dogterom, M., Brunner, D., and Surrey, T. (2007). Reconstitution of a microtubule plus-end tracking system in vitro. *Nature* *450*, 1100-1105.
- Campbell, C.S., and Mullins, R.D. (2007). In vivo visualization of type II plasmid segregation: bacterial actin filaments pushing plasmids. *The Journal of cell biology* *179*, 1059-1066.
- Caplow, M., Ruhlen, R.L., and Shanks, J. (1994). The free energy for hydrolysis of a microtubule-bound nucleotide triphosphate is near zero: all of the free energy for hydrolysis is stored in the microtubule lattice. *The Journal of cell biology* *127*, 779-788.
- Chen, Y., and Erickson, H.P. (2008). In vitro assembly studies of FtsZ/tubulin-like proteins (TubZ) from *Bacillus* plasmids: evidence for a capping mechanism. *The Journal of biological chemistry* *283*, 8102-8109.
- Derman, A.I., Becker, E.C., Truong, B.D., Fujioka, A., Tucey, T.M., Erb, M.L., Patterson, P.C., and Pogliano, J. (2009). Phylogenetic analysis identifies many uncharacterized actin-like proteins (Alps) in bacteria: regulated polymerization, dynamic instability and treadmilling in Alp7A. *Molecular microbiology* *73*, 534-552.

Downing, K.H., and Nogales, E. (1998). Tubulin and microtubule structure. *Current opinion in cell biology* 10, 16-22.

Erickson, H.P., Taylor, D.W., Taylor, K.A., and Bramhill, D. (1996). Bacterial cell division protein FtsZ assembles into protofilament sheets and minirings, structural homologs of tubulin polymers. *Proceedings of the National Academy of Sciences of the United States of America* 93, 519-523.

Euteneuer, U., and McIntosh, J.R. (1981). Structural polarity of kinetochore microtubules in PtK1 cells. *The Journal of cell biology* 89, 338-345.

Garner, E.C., Campbell, C.S., and Mullins, R.D. (2004). Dynamic instability in a DNA-segregating prokaryotic actin homolog. *Science* 306, 1021-1025.

Ho, T.Q., Zhong, Z., Aung, S., and Pogliano, J. (2002). Compatible bacterial plasmids are targeted to independent cellular locations in *Escherichia coli*. *The EMBO journal* 21, 1864-1872.

Hyman, A.A., Salser, S., Drechsel, D.N., Unwin, N., and Mitchison, T.J. (1992). Role of GTP hydrolysis in microtubule dynamics: information from a slowly hydrolyzable analogue, GMPCPP. *Molecular biology of the cell* 3, 1155-1167.

Kitamura, E., Tanaka, K., Komoto, S., Kitamura, Y., Antony, C., and Tanaka, T.U. (2010). Kinetochores generate microtubules with distal plus ends: their roles and limited lifetime in mitosis. *Developmental cell* 18, 248-259.

Kraemer, J.A., Erb, M.L., Waddling, C.A., Montabana, E.A., Zehr, E.A., Wang, H., Nguyen, K., Pham, D.S., Agard, D.A., and Pogliano, J. (2012). A phage tubulin assembles dynamic filaments by an atypical mechanism to center viral DNA within the host cell. *Cell* 149, 1488-1499.

Larsen, R.A., Cusumano, C., Fujioka, A., Lim-Fong, G., Patterson, P., and Pogliano, J. (2007). Treadmilling of a prokaryotic tubulin-like protein, TubZ, required for plasmid stability in *Bacillus thuringiensis*. *Genes & development* *21*, 1340-1352.

Meier, E.L., and Goley, E.D. (2014). Form and function of the bacterial cytokinetic ring. *Current opinion in cell biology* *26C*, 19-27.

Mitchison, T., and Kirschner, M. (1984a). Dynamic instability of microtubule growth. *Nature* *312*, 237-242.

Mitchison, T., and Kirschner, M. (1984b). Microtubule assembly nucleated by isolated centrosomes. *Nature* *312*, 232-237.

Montabana, E.A., and Agard, D.A. (2014). Bacterial tubulin TubZ-Bt transitions between a two-stranded intermediate and a four-stranded filament upon GTP hydrolysis. *Proceedings of the National Academy of Sciences of the United States of America*.

Oliva, M.A., Martin-Galiano, A.J., Sakaguchi, Y., and Andreu, J.M. (2012). Tubulin homolog TubZ in a phage-encoded partition system. *Proceedings of the National Academy of Sciences of the United States of America* *109*, 7711-7716.

Theriot, J.A. (2013). Why are bacteria different from eukaryotes? *BMC biology* *11*, 119.

Zehr, E.A., Kraemer, J.A., Erb, M.L., Coker, J.K.C., Montabana, E.A., Pogliano, J., and Agard, D.A. (2014). The structure and assembly mechanism of a novel three-stranded tubulin filament that centers phage DNA. *Structure* *22*.

## **Chapter Five**

### **Preliminary Studies of High-Resolution GTP-binding and Hydrolysis**

## **Introduction**

In the previous chapters, we have detailed PhuZ dynamics, and their structural and molecular origins. This chapter covers further work aimed at gaining a high-resolution understanding of the role of GTP binding to polymerization and a biochemical understanding of its interaction to and hydrolysis by PhuZ. Although the high-resolution crystal structure of full-length PhuZ-GDP (Chapter 2) and cryo-EM structure of PhuZ-GMPCPP (Chapter 3) provided many insights into the mechanism of PhuZ polymerization, many questions were still left unanswered. For instance, a high-resolution insight into the molecular origins of how GTP drives polymerization was still a mystery. Various attempts to answer this question by crystallization of PhuZ and PhuZ mutants bound to different nucleotides and nucleotide analogs are detailed in this chapter.

In addition to attempts at high-resolution studies of PhuZ bound to GTP, this chapter also details initial studies of PhuZ as a GTPase. As shown in previous chapters, PhuZ dynamics are closely tied to nucleotide state. Understanding of nucleotide binding, discrimination, and hydrolysis is paramount for a full molecular understanding of how nucleotide state related to PhuZ filament dynamics. Preliminary studies of these behaviors are outlined in this chapter.

## **Results and Discussion**

### **Crystallization of wild-type PhuZ with GMPCPP or GTP $\gamma$ S**

Inspired by the prior success of crystalizing filaments of TubZ in the presence of GTP $\gamma$ S (Aylett et al., 2010), I tried to crystallize PhuZ in the presence of GTP $\gamma$ S or GMPCPP. With the help of a talented summer undergraduate student, we obtained crystals with drops containing 1 mM GTP $\gamma$ S in the same condition as the PhuZ-GDP crystals (see Chapter 2 methods). GTP $\gamma$ S

does not support PhuZ polymerization, so this result was not surprising. We hoped that these crystals could provide insight into GTP coordination by PhuZ. However, when we solved the structure from these crystals, PhuZ was bound to GDP, implying that the GTP $\gamma$ S was all hydrolyzed, either in the crystal lattice, or prior to crystal formation.

Initial attempts to crystallize PhuZ in the presence of GMPCPP (using 1 mg/ml protein as with GDP and GTP $\gamma$ S) yielded no crystal hits in initial screens. Hits were obtained by raising the protein concentration to 10 mg/ml. Initial hits were observed in three conditions: 1) 200 mM NaOAc, 100 mM Tris pH 8.5, 30% PEG4000; 2) 1 M LiCl, 100 mM MES pH 6, 20% PEG6000; and 3) 200 mM NaCl, 100 mM Tris pH 7, 30% PEG3000 (Figure 1). Optimized crystals were obtained based on the first condition (200 mM NaOAc, 200 mM Tris pH 8.5, 21% PEG4000, 875 mM AmOAc). Crystals were not obtained in scale ups of the other conditions.

Unfortunately, as was the case with the GTP $\gamma$ S crystals, optimized PhuZ crystals set in the presence of GMPCPP contained GDP (Figure 2).

### **Crystallization and structure of tailless PhuZ**

To find if tail binding as in the GDP-PhuZ crystal structure (Chapter 3) allosterically affected PhuZ confirmation, I created a tail deletion mutant of PhuZ where the C-terminal 20 residues had been removed ( $\Delta$ tail-PhuZ). In initial crystallography screens,  $\Delta$ tail-PhuZ (10 mg/ml) readily formed crystals in the presence of GDP (100 mM Tris pH 8.5, 2 M Am<sub>2</sub>SO<sub>4</sub>, 1 mM GDP) (Figure 3). Unlike wild-type PhuZ,  $\Delta$ tail-PhuZ required gel filtration after thawing in order to form crystals. Additionally, in scaling up drop size (2  $\mu$ l handset drops), pH needed to be lowered to 7.5, and addition of 1% PEG400 was required to produce high quality crystals. Final crystallization conditions used were 100 mM HEPES pH 7.5, 1.9 M (NH<sub>4</sub>)<sub>2</sub>SO<sub>4</sub>, 1% PEG400.

I solved the structure of  $\Delta$ tail-PhuZ-GDP by molecular replacement to 1.46 Å (Figure 4), using a tailless model of PhuZ as a model. The structure was refined to an  $R_{\text{work}} = 0.17$  and  $R_{\text{free}} = 0.19$ .  $\Delta$ tail-PhuZ crystalized in  $P4_3$ , with two monomers in the asymmetric unit (Figure 4). Even though no polymer-like crystal packing was observed (Figure 5), and the C-terminal tail is not present, the conformation of the PhuZ monomers is almost identical to the wild-type PhuZ-GDP structure (Figure 6). The only slight difference is a bend in the C-terminal helix, H11 (Figure 6), which could be attributed to relaxation of the helix from the position observed for optimal tail binding.

Of note, crystals did not form in the presence of GMPCPP or GMPPNP, suggesting the potential for a different conformation when bound to these nucleotide analogs.  $\Delta$ tail-PhuZ crystals did form when drops were set with GTP $\gamma$ S in the same condition as for GDP above. However, these crystals were of irregular shape, suggesting that they formed as the GTP $\gamma$ S was hydrolyzed and did not form in as ordered a fashion as the  $\Delta$ tail-PhuZ-GDP crystals.

### **Nucleotide Soaks of $\Delta$ tail-PhuZ**

Even though crystallization of  $\Delta$ tail-PhuZ in the presence of GMPCPP or GTP $\gamma$ S was unsuccessful, I wanted to see if I could learn about the molecular consequences of GTP-binding to PhuZ monomers by soaking GTP or a GTP-analog into the  $\Delta$ tail-PhuZ-GDP crystals. Crystals were grown in drops prepared the same way as above (see Materials and Methods), and transferred to new hanging drops supplemented with 10 mM GTP, GTP $\gamma$ S, or 1 mM GMPCPP and 10 mM MgCl<sub>2</sub>. Crystals were soaked in these drops overnight, and then frozen in liquid N<sub>2</sub> for data collection. Crystals soaked in any of the three nucleotide diffracted well ( $\sim$ 1.7 Å), and their structures were solved by molecular replacement. Although all crystals contained the tri-

phosphate (or analog) (example Figure 7A, no conformational changes were observed compared to the original  $\Delta$ tail-PhuZ-GDP structure (Figure 7B). Since the crystals did not crack or dissolve, I did not expect a large conformational change.

The structures did reveal the coordination of the  $\gamma$ -phosphate within the nucleotide-binding pocket (Figure 8A), as well as allow for the resolution of the three residues of the T3 loop that were unstructured in the wild-type PhuZ-GDP structure (Figure 8A; Chapter 2, Figure 4). Residues G93 and S94 from the conserved G-box in the T4 loop hydrogen bond to the  $\gamma$ -phosphate. Though expected to make a hydrogen bond with the  $\gamma$ -phosphate based on the  $\gamma$ -tubulin-GTP $\gamma$ S crystal structure (Rice et al., 2008), G58 in the T3 loop is too far away to make any contacts with the  $\gamma$ -phosphate (Figure 8A,B). Like the  $\gamma$ -tubulin-GTP $\gamma$ S crystal structure (Rice et al., 2008), the  $\gamma$ -phosphate also contacts the Mg<sup>2+</sup> ion coordinated in the nucleotide-binding pocket.

### **Crystallization of Wild-type or $\Delta$ tail-PhuZ with GMPCPP and Seeds**

Since attempts to crystallize wild-type or  $\Delta$ tail-PhuZ in the presence of GMPCPP *de novo* either failed or resulted in GDP-bound crystals, I attempted to grow crystals off of PhuZ crystal seeds in the presence of GMPCPP. Wild-type or  $\Delta$ tail-PhuZ-GDP crystals were grown as described previously (Chapter 2, this chapter). Crystals were harvested from these drops, and seeds were made using a Seed Bead (Hampton Research) following their standard protocol in a buffer containing no nucleotide; seeds were frozen and stored at -20°C. PhuZ crystal seeds were then used in initial screens, using the same protein concentrations used for initial, GDP, crystals (wild-type 1 mg/ml,  $\Delta$ tail-PhuZ 10 mg/ml). Drops were made with a 1:1:2 ratio of protein to seeds to mother liquor.



Many initial hits were found for  $\Delta$ tail-PhuZ (Figure 9) and optimized. Unfortunately, when these crystals were shot at the beam line, all of them were salt crystals and not protein. Two initial hits were found for wild-type-GMPCPP crystals (Figure 10), which were promisingly in quite different conditions than the other wild-type crystals (i.e. did not contain AmOAc). Initial hits were: 1) 200 mM  $\text{Am}_2\text{SO}_4$ , 100 mM Tris pH 8.5, 25% PEG3350 and 2) 200 mM  $\text{Li}_2\text{SO}_4$ , 100 mM Tris pH 8.5, 25% PEG3350. These hits were optimized and structures were solved from them. Unfortunately, although these crystals were PhuZ, the protein was bound to GDP and not GMPCPP. The nucleotide either was hydrolyzed during the crystallization time, or only a small subset of protein in the drop containing GDP, and not GMPCPP, could be incorporated into crystals grown off of the initial GDP crystals.

### **Attempts to get PhuZ dimer bound to GMPCPP**

We wanted to gain an atomic level understanding of how GTP facilitates interaction between PhuZ molecules, so I generated mutants that should interact with each other, but not themselves and not hydrolyze GTP. This idea is similar to the method used by Chen et al. to obtain the crystal structure of an actin filament nucleus bound to Cobl (Chen et al., 2013). The mutants generated were 1)  $\Delta$ tailbinding-PhuZ (R60A, K61A, R68A, E138A) to eliminate C-terminal tail interactions and 2)  $\Delta$ tail-PhuZD190A to prevent further filament growth and nucleotide hydrolysis. These mutants were unable to polymerize alone or mixed in a 1:1 ratio as measured by right-angle light scattering (Figure 11A). This result was promising, as it showed that the mutants were incapable of making large structures in the presence of GTP as I had hoped. However, preliminary attempts to glutaraldehyde crosslink the mutants together proved inconclusive (Figure 11B).

Despite the crosslinking results being inconclusive, I went forward with crystal trials, using a 1:1 molar ratio of the two mutants. Initial screening resulted in one good hit and two hits with very small crystals (Figure 12). The conditions were all different from any of the other PhuZ crystals produced previously: 1) 200 mM MgOAc<sub>2</sub>, 20% PEG3350; 2) 50 mM MgCl<sub>2</sub>, 100 mM HEPES pH 7.5m 30% PEG550MME; and 3) 200 mM Li<sub>2</sub>SO<sub>4</sub>, 100 mM Bis-Tris pH 6.5, 25% PEG3350 (Figure 12). The large crystal hit grown in condition 3 diffracted to ~3.4 Å resolution (Figure 13A). However, indexing of the crystal was difficult, possibly due to multiple lattices within the crystal. I attempted to solve the structure from this data set, but the R<sub>symm</sub> for all potential space groups (C2, C222, and P3) was always approximately 20%, and no structures were solved. The best result was a molecular replacement attempt in C2, which was clearly wrong (Figure 13B), with R<sub>work</sub> = 0.49 and R<sub>free</sub> = 0.51. Running the data through Xtrriage (Phenix) suggested attempting P622, but the data were unable to be processed in this space group. Unfortunately, attempts to reproduce these crystals all proved futile and no more data were collected.

### **Structure of D303A/D305A-PhuZ**

D303A/D305A-PhuZ (introduced in Chapter 3), lacks important residues for proper lateral interactions, and forms highly unstable filaments with a high critical concentration. These filaments are stabilized upon the addition of the D190A mutation, and no longer have an exaggerated lag phase (Figure 14). This makes the D303A/D305A-PhuZ mutant an intriguing construct to crystallize.

In a further attempt to solve a crystal structure of PhuZ bounding to GMPCPP, I tried crystallizing the D303A/D305A double mutant discussed in Chapter 3. Nice initial hits were

obtained using 10 mg/ml D303A/D305A-PhuZ (Figure 15A) in 200 mM Li<sub>2</sub>SO<sub>4</sub>, 100 mM Tris•HCl pH 8.5, and 30% PEG4000. These crystals were optimized in a condition containing 200 mM Li<sub>2</sub>SO<sub>4</sub>, 100 mM Bis-Tris pH 7, and 30% PEG4000 and appeared to be hexagonal rods (Figure 15B). Even though very nice looking crystals were obtained, they only diffracted to moderate (3.2 Å) resolution (Figure 15C). Although the data were of moderate resolution, they were of high enough quality to accurately integrate and scale in space group P65.

The Δtail-PhuZ monomer structure was used as a molecular replacement model with the 3.2 Å data set to solve the structure of D303A/D305A-PhuZ. The final model had good statistics, with an  $R_{\text{work}} = 0.22$  and  $R_{\text{free}} = 0.26$ . Surprisingly, D303A/D305A-PhuZ crystallized as a continuous, curving filament in the shape of a tube with the filament wrapping around in a helical fashion (Figure 16). We have not observed a structure like this by EM, as this mutant is still capable of forming three-stranded filaments in the presence of GMPCPP (Chapter 3), so it is unclear if this is a relevant filament state. The unit cell contains two monomers making longitudinal contacts (Figure 17A). Unfortunately, both nucleotide-binding pockets contain GDP and not GMPCPP, so no insight about the role of the  $\gamma$ -phosphate can be inferred. The dimer exists in an extremely bent conformation compared to the wild-type PhuZ-GDP crystal structure (Figure 17B), and is not twisted like the PhuZ-GMPCPP filament (Figure 17C). Also perplexing is that the C-terminal tail is unstructured within the dimer, but is still bound at the vertex between the dimer and the next dimer within the twisted filament. The longitudinally buried surface at this interface is extremely small, and it is unclear why the intradimer C-terminal tail would have become unbound. Taken together, it is unclear what true insight can be gained from this interesting crystal structure of a tube of D303A/D305A-PhuZ bound to GDP.

## Initial GTP and GDP Binding Experiments

In order to get binding affinities of PhuZ for GTP and GDP respectively, I attempted to measure their binding by ITC (see Materials and Methods) with 10  $\mu\text{M}$  PhuZ in the chamber and 100  $\mu\text{M}$  nucleotide in the needle. Since PhuZ polymerization and nucleotide hydrolysis will lead to a change in enthalpy,  $\Delta\text{tail-D190A-PhuZ}$  was used to attempt to get a GTP binding constant. Although the data look qualitatively good, and a  $K_D$  of  $1.4 \pm 0.1 \mu\text{M}$  was measured, the model that fit the data best included only half of a binding site for the nucleotide (Figure 18A). For attempting to get the GDP binding constant, wild-type PhuZ was used, as polymerization was not a worry. The results for the GDP were very similar to what I found for GTP (Figure 18B): a measured  $K_D$  of  $2.7 \pm 0.3 \mu\text{M}$ , with a model that fits having only half of a binding site. If these values are in the right ballpark, it is surprising how close they are, and how relatively poorly PhuZ binds GTP compared to other tubulins (Huecas et al., 2007; Ni et al., 2010; Zeeberg and Caplow, 1979).

These results indicate that something is not quite right with the sample. Neither of these proteins was purified with EDTA or DOWEX resin to attempt to strip away the nucleotide during purification. It is likely that PhuZ purifies bound to residual GDP, and this preloaded nucleotide could be having a profound effect on the ITC experiment. It is also possible that the protein and/or nucleotide concentrations are suboptimal for the affinity regime of the nucleotides to get a better binding curve and more accurate  $K_D$ . There is also the unlikely possibility that removing the C-terminal tail had an effect on the ability of PhuZ to bind GTP.

## Measurement of PhuZ GTP Hydrolysis

From the work discussed in previous chapters, it is clear that PhuZ filament dynamics are closely tied to nucleotide hydrolysis. GTP should be rapidly hydrolyzed to GDP once PhuZ monomers are incorporated into the filament. To gain understanding of the rate at which PhuZ hydrolyses GTP and turns over nucleotide, and hopefully correlate these values to filament depolymerization, I attempted several different experiments: 1) measuring steady-state phosphate release by  $^{32}\text{P}$ , 2) measuring steady-state phosphate release by an enzyme-coupled adsorption assay, and 3) nucleotide turnover by GDP regeneration to GTP in an enzyme-coupled assay (see Materials and Methods).

First attempts to get a steady-state PhuZ GTPase rate were done using a well-established assay for measuring accumulating amounts of phosphate with  $^{32}\text{P}$  (see Materials and Methods) (Figure 19). PhuZ GTP hydrolysis was measured to be approximately 1 GTP/(min\*PhuZ). This number is surprisingly low, as other tubulins hydrolyze GTP faster (Chen and Erickson, 2008; Erickson and O'Brien, 1992; Mukherjee and Lutkenhaus, 1998). However, this value is not so slow as to be completely unreasonable. GTP hydrolysis was also monitored by use of an enzyme-coupled system for monitoring free phosphate and found to be approximately 3 GTP/(min\*PhuZ) by this assay (Figure 20)

In order to attempt to gain an understanding of nucleotide release (and some insight into filament turnover) by PhuZ, I performed an established enzyme-coupled GTP regeneration assay established by Ingerman and Nunnari (Ingerman and Nunnari, 2005) (Figure 21). Of note, PhuZ filaments appear to be quite sensitive to salt. Initial experiments (not shown) used pyruvate kinase in an  $\text{Am}_2\text{SO}_4$  slurry. The resulting high concentration of salt prevented filament polymerization. Results from these experiments agreed with the phosphate release experiments, yielding a GDP turnover rate of approximately 1 GDP-regenerated/(min\*PhuZ).

## **Materials and Methods**

### **Protein Cloning, Expression, and Purification**

In order to generate  $\Delta$ tail-PhuZ, inverse PCR performed to remove the C-terminal 21 residues from the PhuZ gene as it was cloned into pET28a. All point mutants were generated using primers designed for QuikChange PCR. All constructs were expressed and purified as described earlier (Chapter 2 for hydrolysis competent constructs, Chapter 4 for hydrolysis-dead).

### **Protein Crystallization**

All initial screens were conducted on a Mosquito (TTP) using Qiagen 96 well crystallography screens. For wild-type PhuZ in the presence of GTP $\gamma$ S, trays were set as described in Chapter 2. For wild-type PhuZ in the presence of GMPCPP, 1 mM GMPCPP was added to 10 mg/ml on ice for 5 minutes, and screens were set.

For  $\Delta$ tail-PhuZ, prior to crystallization protein was thawed and freshly freshly gel filtered on a S200 10/30 in a low HEPES gel filtration buffer (10 mM HEPES pH 8, 250 mM KCl, 1 mM MgCl<sub>2</sub>, 15 mM thioglycerol). The elution peak was then concentrated to 10 mg/ml and used for setting crystal trays. 1 mM GDP was added to the protein, and it was mixed 1:1 with 100 mM HEPES pH 7.5, 1.9 M (NH<sub>4</sub>)<sub>2</sub>SO<sub>4</sub>, 1% PEG400 in 2  $\mu$ l drops. For soaks, crystals were looped from these drops and moved into drops containing the mother liquor supplemented with 10 mM MgCl<sub>2</sub> and 10 mM GTP or GT $\gamma$ S, or 1 mM GMPCPP overnight. Soaked crystals were then looped and frozen for data collection.

For seeding experiments, wild-type or  $\Delta$ tail-PhuZ crystals were grown as described. Crystals were then harvested and crushed using a Seed Bead (Hampton Research). Seeds were stored at -20°C. Seeded drops were set in a 1:2:1 ratio of seeds:mother liquor: protein.

PhuZ mutant dimer proteins were mixed in a 1:1 ratio at 5 mg/ml each with 1 mM GMPCPP, for 10 mg/ml total PhuZ protein, prior to mixing 1:1 with mother liquor for both screening and hit optimization.

For the D303A/D305A-PhuZ mutant crystals, 10 mg/ml protein was mixed 1:1 with mother liquor. Initial crystals grew in 200 mM Li<sub>2</sub>SO<sub>4</sub>, 100 mM Tris•HCl pH 8.5, and 30% PEG4000. Scaled up and optimized crystals were grown in 200 mM Li<sub>2</sub>SO<sub>4</sub>, 100 mM Bis-Tris pH 7, and 30% PEG4000.

All crystallography data were collected at LBNL BL8.2.2 and BL8.3.1.

### **Isothermal Titration Calorimetry**

For ITC, protein (either wild-type or  $\Delta$ tail-PhuZ) was dialyzed overnight into gel filtration buffer without reducing agent (250 mM KCl, 1 mM MgCl<sub>2</sub>, 50 mM HEPES pH 8). GTP or GDP were dissolved directly into this buffer to make sure buffers matched. All samples were degassed at 16°C prior to the ITC experiment. 100  $\mu$ M GTP or GDP was titrated into 10  $\mu$ M protein at 16°C, with injections occurring every 5 minutes for 400 minutes. The injections and change of enthalpy were monitored by a VP-ITC instrument. Data were analyzed with the Origin 5.0 software package.

### **Measurement of GTP Hydrolysis**

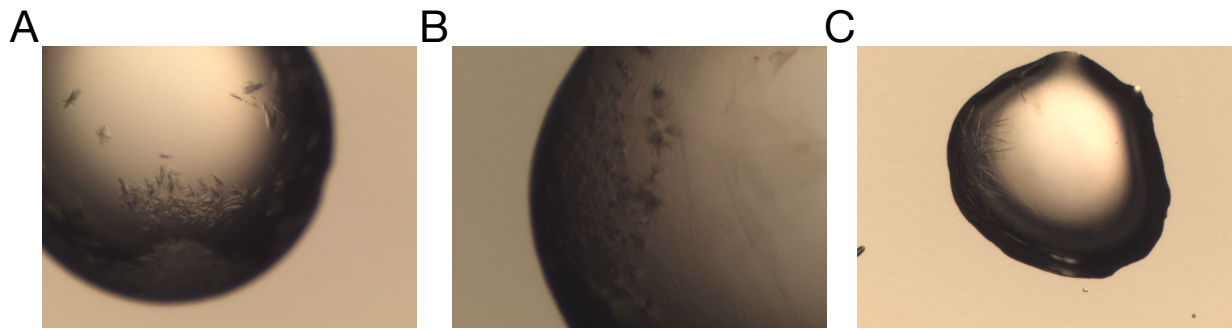
Radioactive GTPase experiments were performed as follows: A fresh TLC plate was washed with water and allowed to air dry. A specific concentration of PhuZ in a polymerization buffer was then mixed with 1 mM GTP spiked with 10 mCi/ml  $\gamma$ -<sup>32</sup>P-GTP at room temperature (10  $\mu$ l reaction volume). 1  $\mu$ l aliquots were removed every 5 or 10 minutes and mixed 1:1 with

quenching buffer (59 mM EDTA, 0.5 mg/ml proteinase K). In parallel, reactions containing no protein were run to control for spontaneous GTP hydrolysis. 1.5  $\mu$ l of quenched time points was spotted onto the TLC plate and air-dried. Free phosphate was separated from GTP in a TLC chamber containing 6% formic acid and 0.5 M LiCl. Reactions were visualized on a Typhoon (GE) and quantified using ImageJ. The amount of GTP hydrolyzed was corrected to account for the concentration of PhuZ present in the experiment.

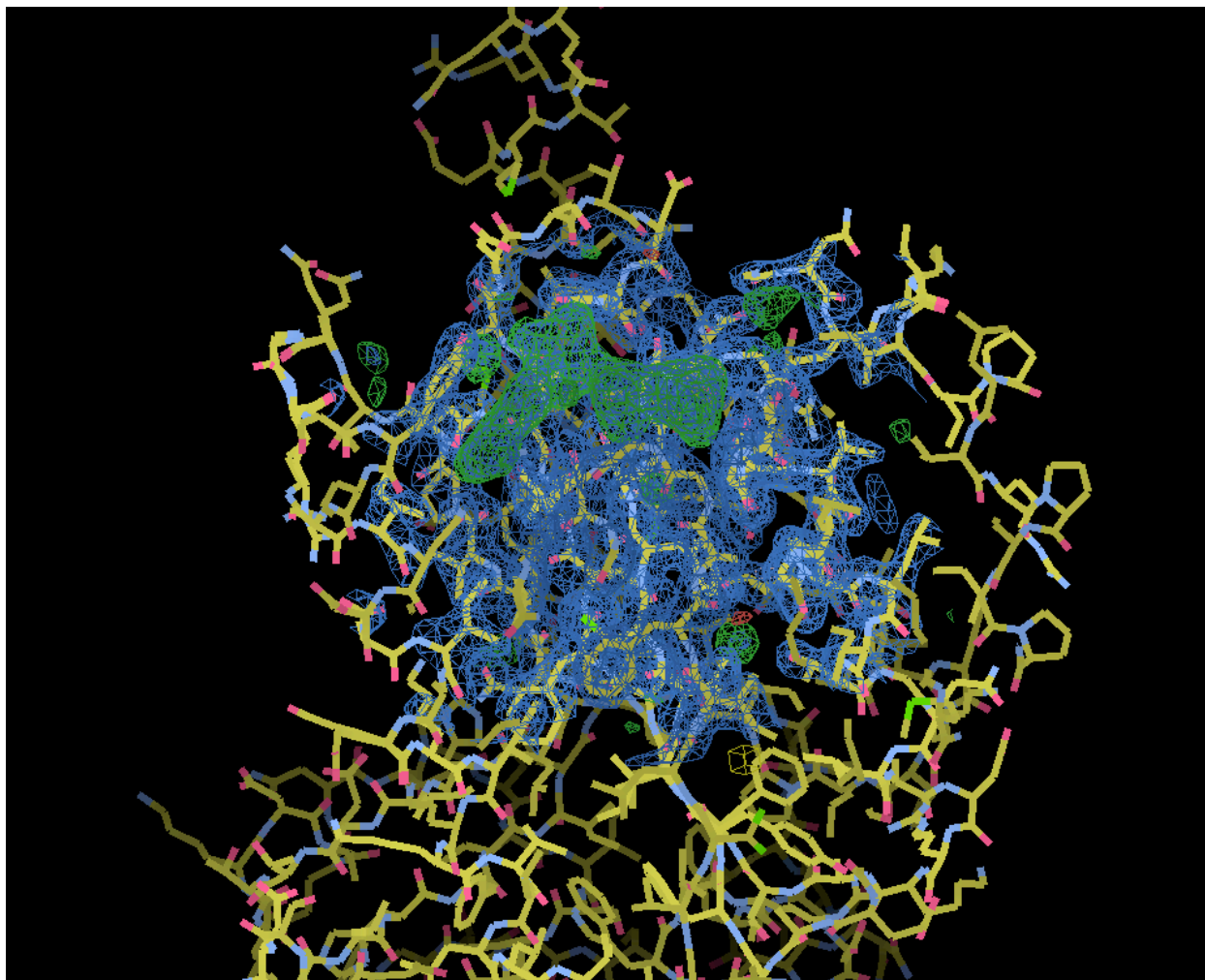
The phosphate release assay was performed using an EnzChek phosphate assay kit (Life Technologies), polymerizing PhuZ in BRB80 pH 7.2 and monitoring absorbance at 360 nm. Absorbance was converted to concentration of phosphate by a phosphate standard and standardized for the PhuZ concentration in the experiment.

The continuous GTP regeneration GTPase assay was performed similar to previously (Ingerman and Nunnari, 2005). Various concentrations of PhuZ were used and the regeneration system contained 0.2 mM NADH, 1 mM PEP, 2 mM GTP, 200 U/ml pyruvate kinase, and 200 U/ml LDH. Loss of absorbance at 340 nm as NADH was converted to NAD<sup>+</sup> was monitored, and GTPase rate calculated from the slope of this line.

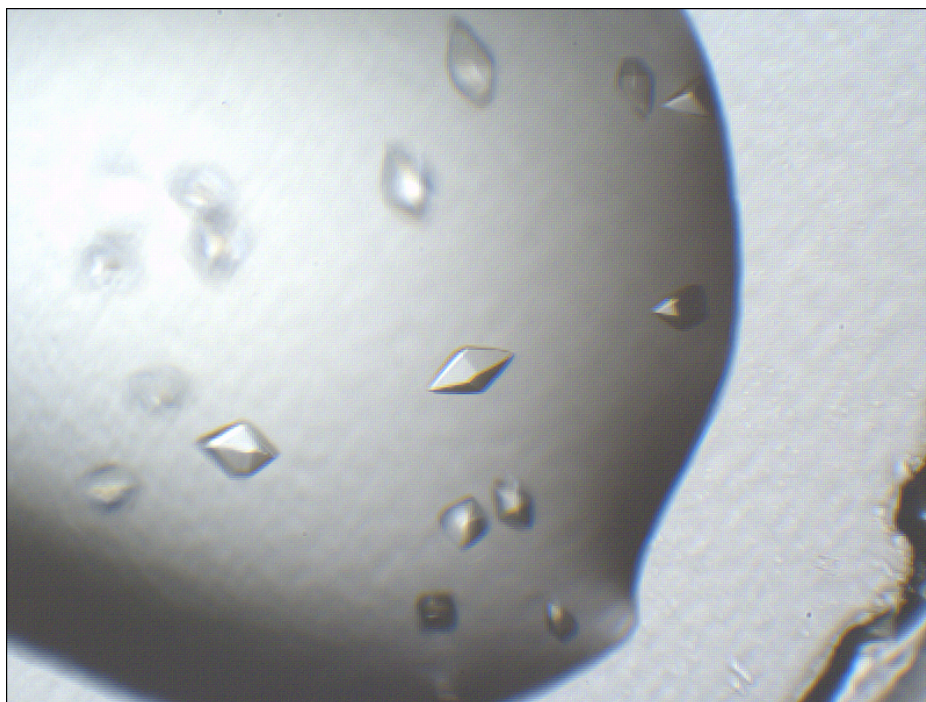




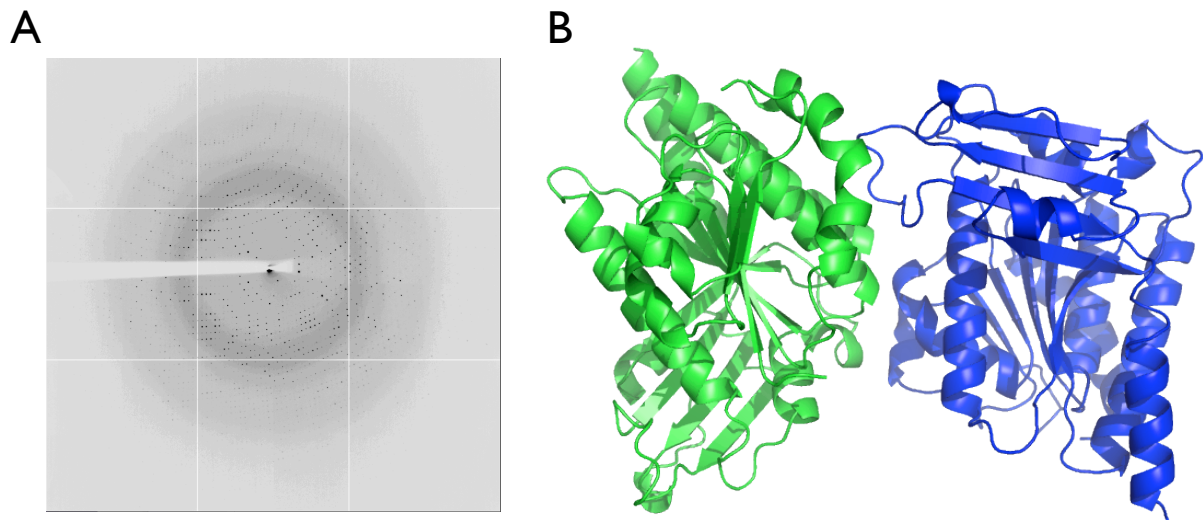
**Figure 1.** Initial crystal hits of wild-type PhuZ in the presence of GMPCPP. **A)** Hit in 200 mM NaOAc, 100 mM Tris pH 8.5, 30% PEG4000; **B)** 1 M LiCl, 100 mM MES pH 6, 20% PEG6000; and **C)** 200 mM NaCl, 100 mM Tris pH 7, 30% PEG3000.



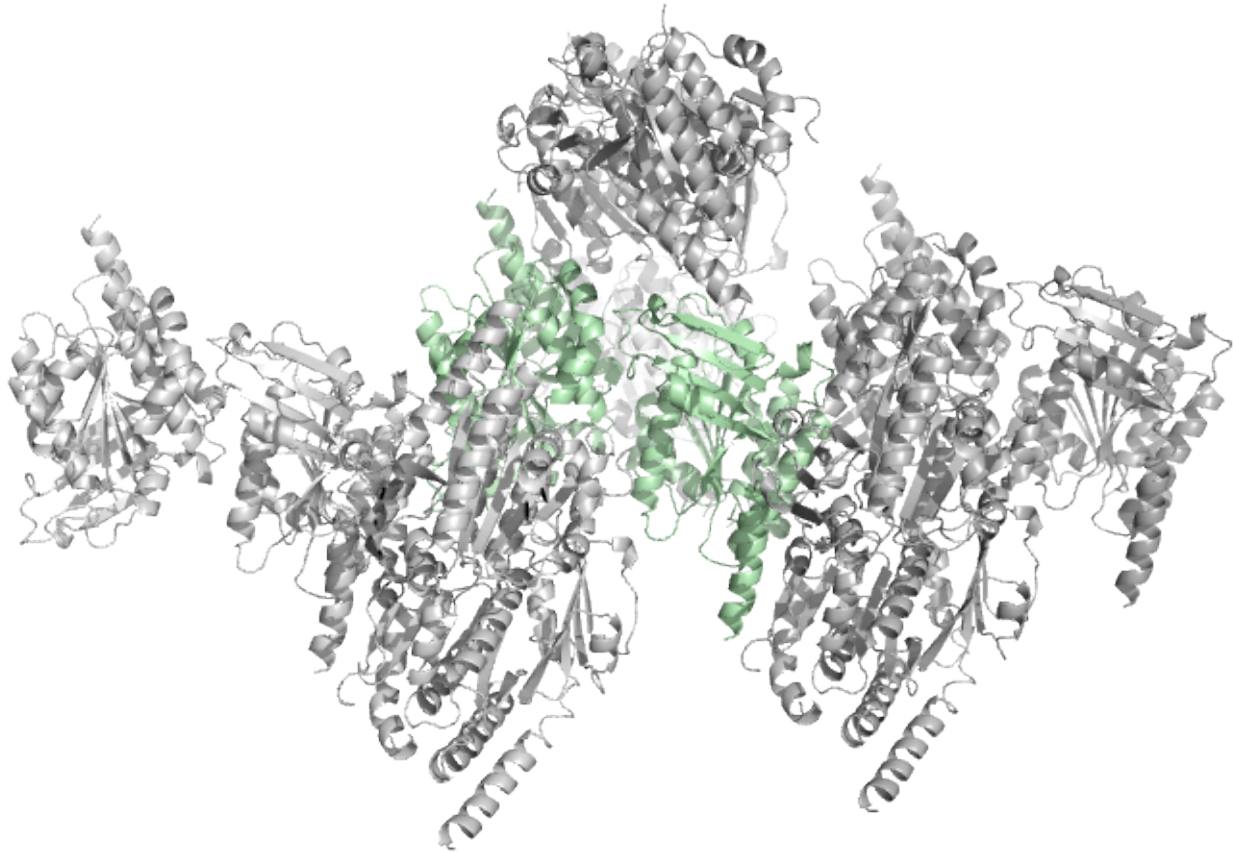
**Figure 2.** Wild-type PhuZ crystallized in GMPCPP only contains GDP. Crystals grown in the presence of GMPCPP only shows strong density ( $2F_o - F_c$  – blue,  $F_o - F_c$  – green) for GDP.  $F_o - F_c$  shown at  $3 \sigma$  and  $2F_o - F_c$  shown at  $1.5 \sigma$ .



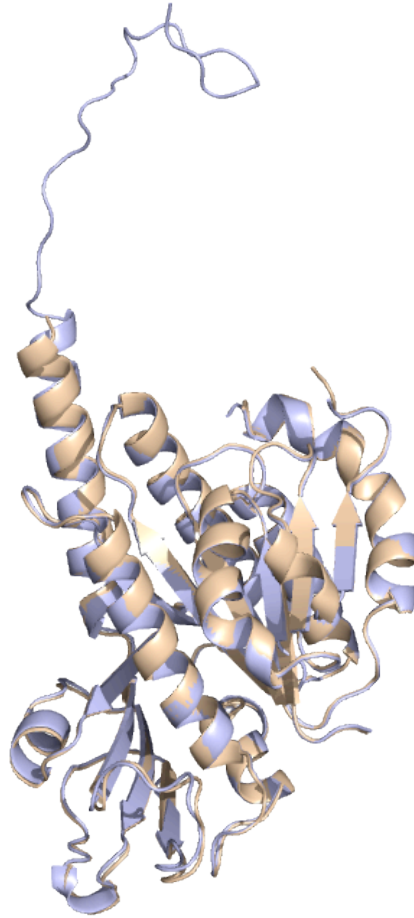
**Figure 3.** Initial crystal hit of  $\Delta$ tail-PhuZ in GDP. Crystals appeared in a condition containing 100 mM Tris pH 8.5, 2 M  $\text{Am}_2\text{SO}_4$ , and 1 mM GDP.



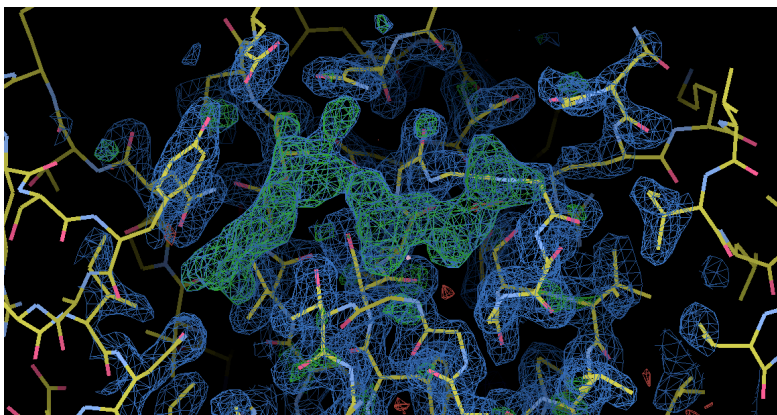
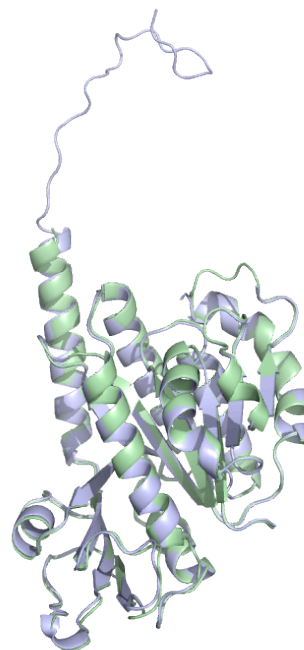
**Figure 4.** Crystal structure of  $\Delta$ tail-PhuZ to 1.46 Å. **A)** 1.46 Å diffraction from a  $\Delta$ tail-PhuZ crystal. **B)** The structure of  $\Delta$ tail-PhuZ has two monomers per asymmetric unit. The absence of the tail leads to a slight bending of H11 compared to the wild-type structure.



**Figure 5.** The crystal packing of the  $\Delta$ tail-PhuZ crystals contains no protofilament-like contacts. In contrast to the wild-type PhuZ crystals (Chapter 2), there are no signs of filament-like contacts in the  $\Delta$ tail-PhuZ crystals.



**Figure 6.** Overlay of  $\Delta$ tail-PhuZ with wild-type PhuZ.  $\Delta$ tail-PhuZ (wheat) is in the exact same conformation as wild-type PhuZ (slate). Only a slight bend in H11 can be observed, most likely due to a lack of C-terminal tail interactions in the protofilament.

**A****B**

**Figure 7.**  $\Delta$ tail-PhuZ crystal soaks have GTP, but no conformational change. **A)** The crystals show clear density for GTP when soaked overnight in 10 mM GTP and 10 mM MgCl<sub>2</sub>. Strong density ( $2F_o - F_c$  - blue,  $F_o - F_c$  - green) for GTP is shown with  $F_o - F_c$  shown at 3  $\sigma$  and  $2F_o - F_c$  shown at 1.5  $\sigma$ .

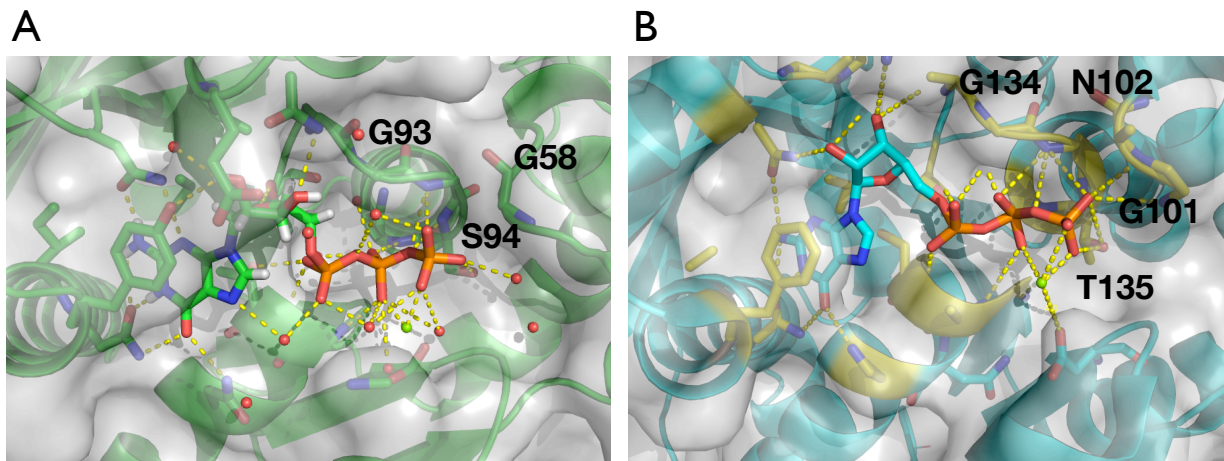


**Figure 8.** Comparison of GTP coordination between PhuZ and  $\gamma$ -tubulin. **A)** Coordination of GTP in the PhuZ nucleotide-binding pocket from  $\Delta$ tail-PhuZ GTP soak crystal structure. Important conserved residues are highlighted. **B)** Coordination of GTP in the  $\gamma$ -tubulin nucleotide-binding pocket.



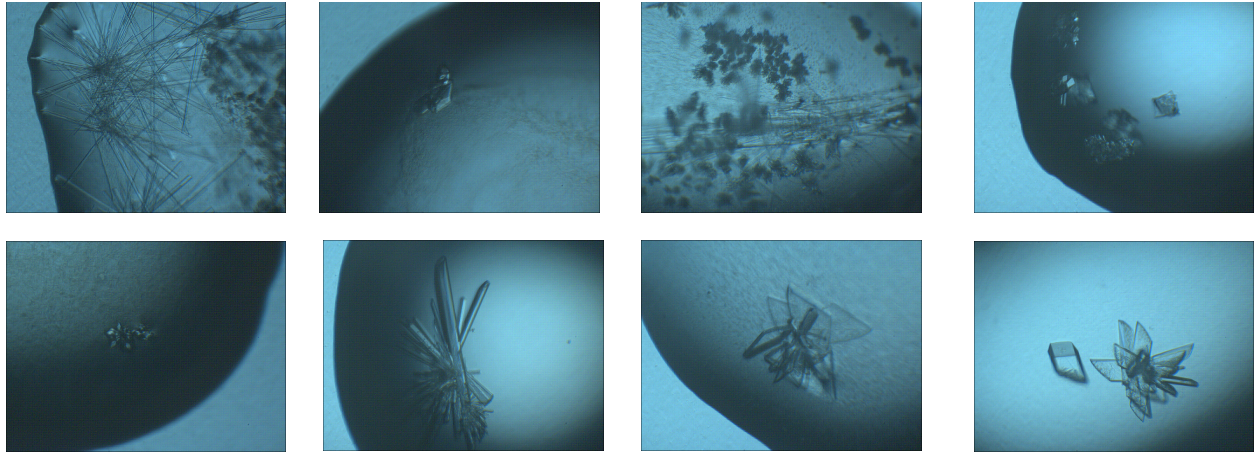


**Figure 9.** Gallery of crystal hits from  $\Delta$ tail-PhuZ grown in GMPCPP off of seeds. All of the above hits turned out to be salt.

**A****B**

**Figure 10.** Crystal hits of wild-type PhuZ crystals grown in the presence of GMPCPP and seeds.

**A)** Condition contains 200 mM  $\text{Am}_2\text{SO}_4$ , 100 mM Tris pH 8.5, 25% PEG3350, and 1 mM

**B)** Condition contains 200 mM  $\text{Li}_2\text{SO}_4$ , 100 mM Tris pH 8.5, 25% PEG3350, and 1 mM GMPCPP.

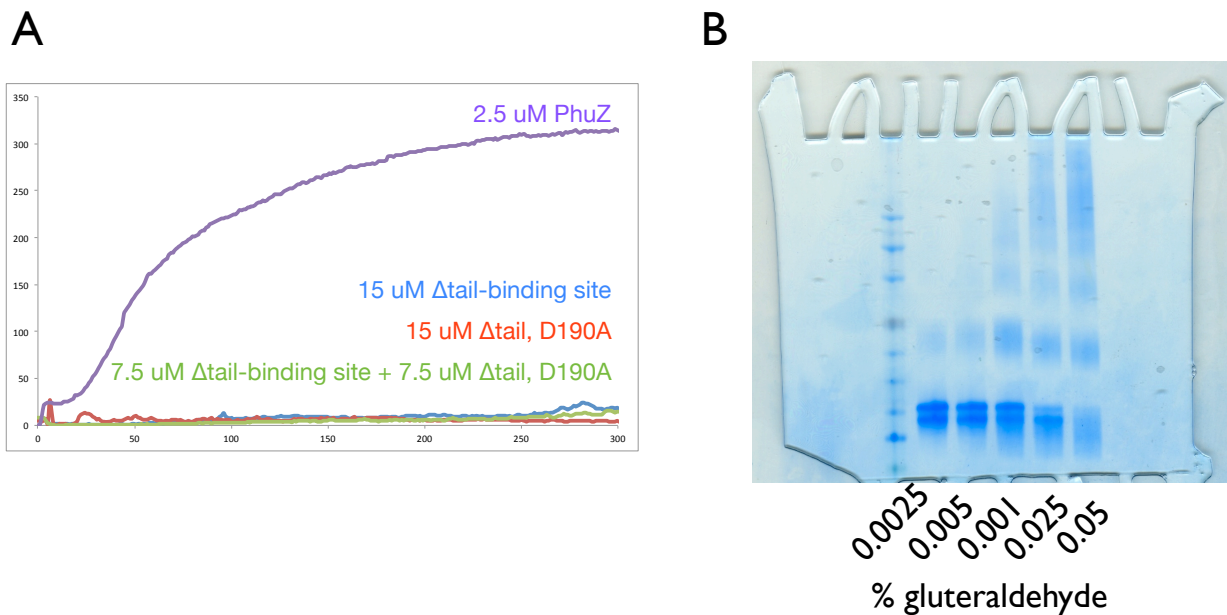


**Figure 11.**  $\Delta$ tailbinding- and  $\Delta$ tail-PhuZ do not copolymerize and may interact. **A)** Neither  $\Delta$ tailbinding- nor  $\Delta$ tail-PhuZ can polymerize on their own or together as shown by right-angle light scattering. A wild-type PhuZ growth curve is shown for comparison. **B)** Glutaraldehyde crosslinking of 20  $\mu$ M  $\Delta$ tailbinding- and  $\Delta$ tail-PhuZ. Large order structures may be being made. However, at low enough levels of glutaraldehyde, it appears that maybe dimers are being formed. It is unclear if they are the desired heterodimers or not.

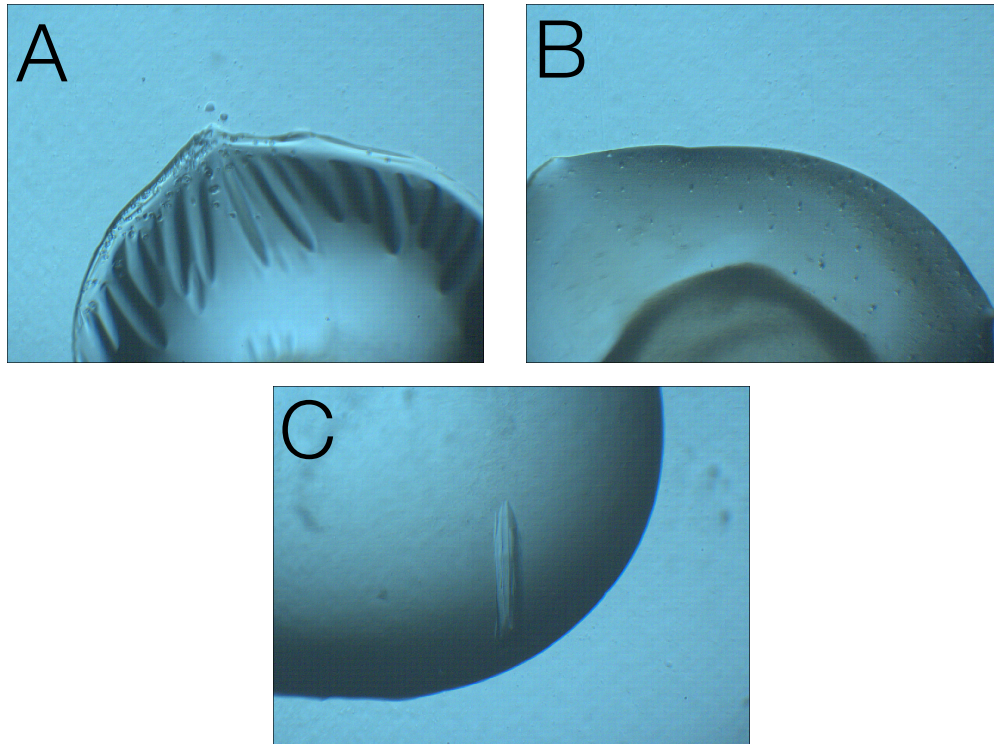


**Figure 12.** Initial hits of  $\Delta$ tailbinding- and  $\Delta$ tail-PhuZ in the presence of GMPCPP. **A)** Crystals formed in 200 mM  $\text{MgOAc}_2$ , 20% PEG3350; **B)** 50 mM  $\text{MgCl}_2$ , 100 mM HEPES pH 7.5m 30% PEG550MME; and **C)** 200 mM  $\text{Li}_2\text{SO}_4$ , 100 mM Bis-Tris pH 6.5, 25% PEG3350.

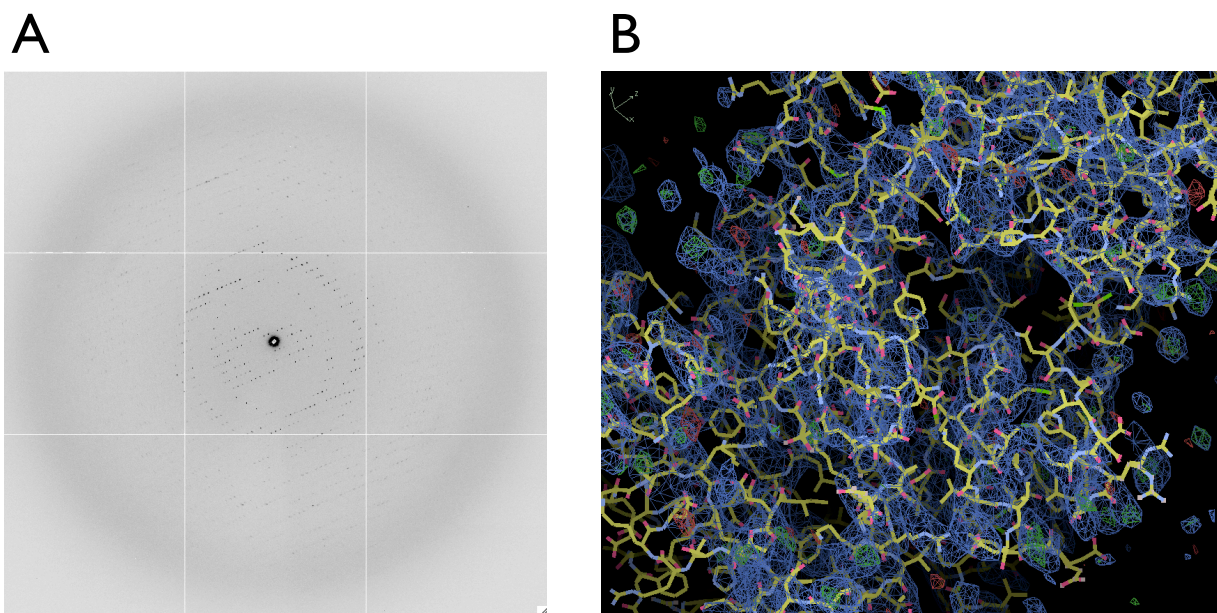


**Figure 13.** Crystal C from Figure 12 diffracted, but the structure could not be solved. **A)** Diffraction pattern from Crystal C in Figure 12. The crystal diffracted to 3.4 Å resolution, but was hard to index. **B)** The best molecular replacement solution using the data from A in space group C2. The R values were about 0.5, and the density clearly does not correspond to the protein.

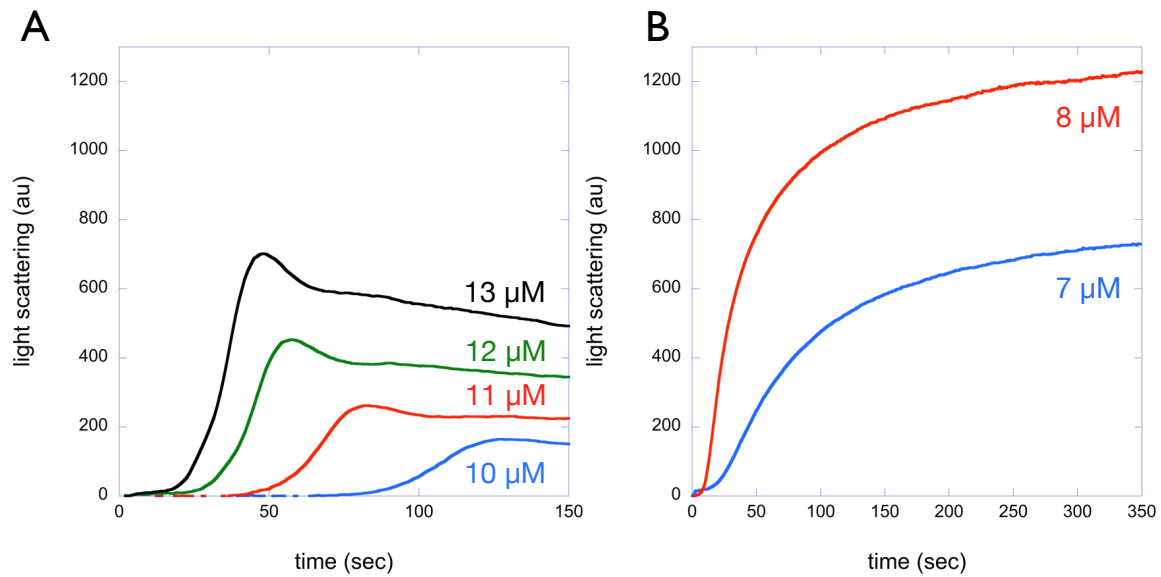


**Figure 14.** Right-angle light scattering of D303A/D305A-PhuZ and D303A/D305A/D190A-PhuZ. **A)** Titration of D303A/D305A-PhuZ concentrations so that its polymerization has a radically increased lag phase, and that the filaments are unstable. **B)** D303A/D305A/D190A-PhuZ no longer has an exaggerated lag phase and forms stable filaments.

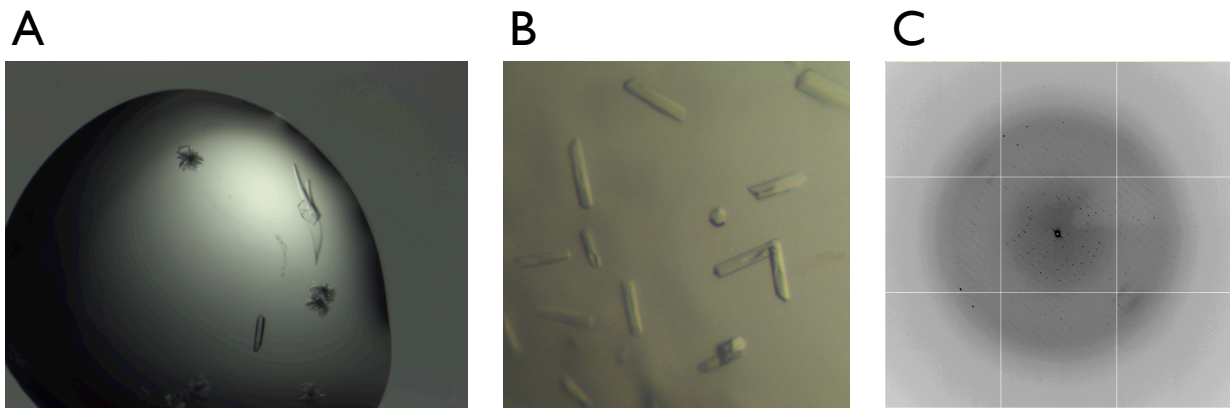


**Figure 15.** Crystals of D303A/D305A-PhuZ in the presence of GMPCPP. **A)** Initial hit of D303A/D305A-PhuZ in 200 mM  $\text{Li}_2\text{SO}_4$ , 100 mM Tris•HCl pH 8.5, and 30% PEG4000. **B)** Optimized crystals grown in 200 mM  $\text{Li}_2\text{SO}_4$ , 100 mM Bis-Tris pH 7, and 30% PEG4000. **C)** Diffraction pattern of crystals from B to 3.2 Å resolution.

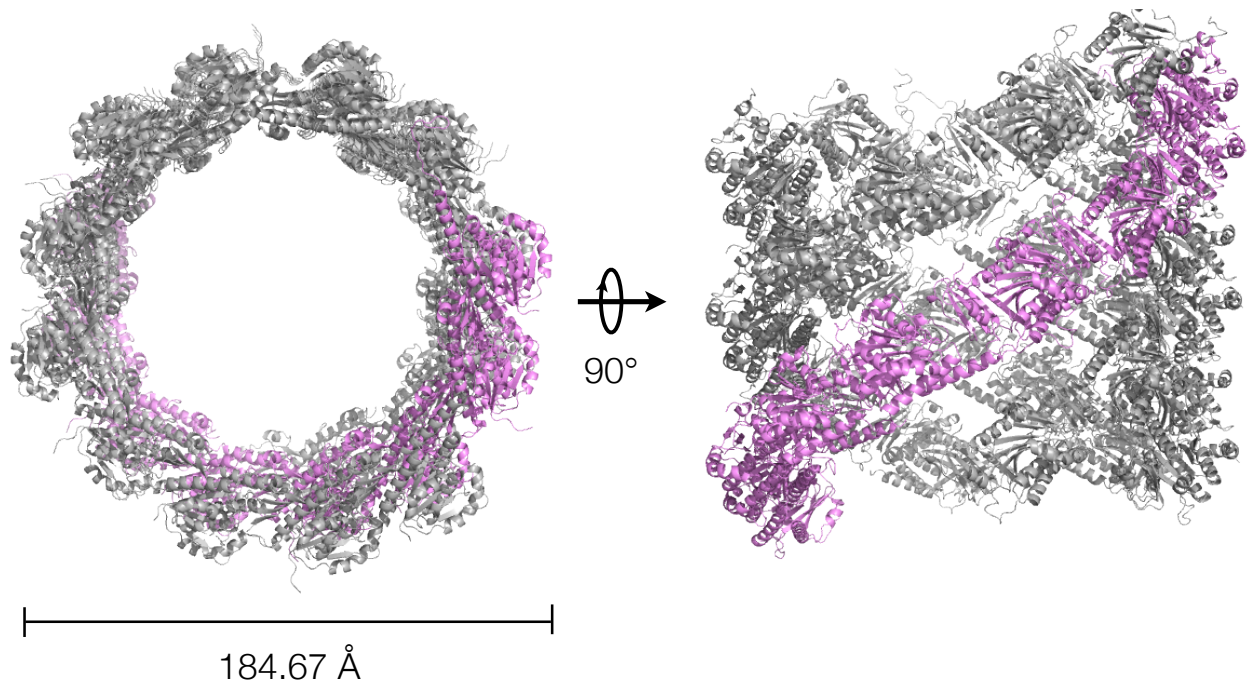


**Figure 16.** D303A/D305A-PhuZ crystallized as a tube. Top and side views of the D303A/D305A-PhuZ tube. Continuous protofilaments wrap around in a helical fashion to form an ~185 Å wide tube.



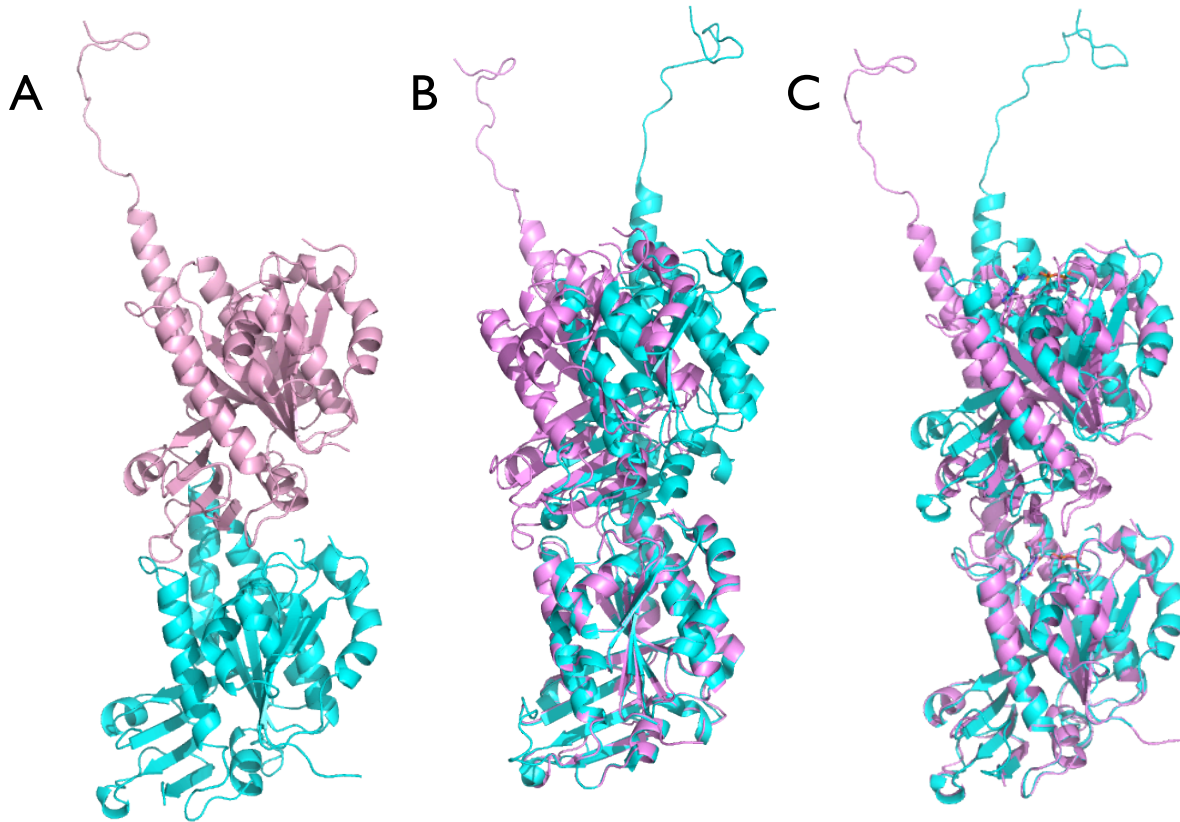


**Figure 17.** D303A/D305A-PhuZ is a dimer in the asymmetric unit. **A)** A dimer of D303A/D305A-PhuZ makes up the asymmetric unit. Only the top monomer (pink), which is at the vertex of the tube, has structure for the C-terminal tail. It is bound to the following bottom monomer. **B)** Overlay of the dimer from A (pink), with the wild-type PhuZ-GDP crystal structure dimer (cyan) showing the rotation caused to form the tube. **C)** Overlay of the dimer from A (pink), with the wild-type PhuZ-GMPCPP cryo-EM structure dimer (cyan) showing the rotation/translation caused to form the tube instead of the three-stranded filament.

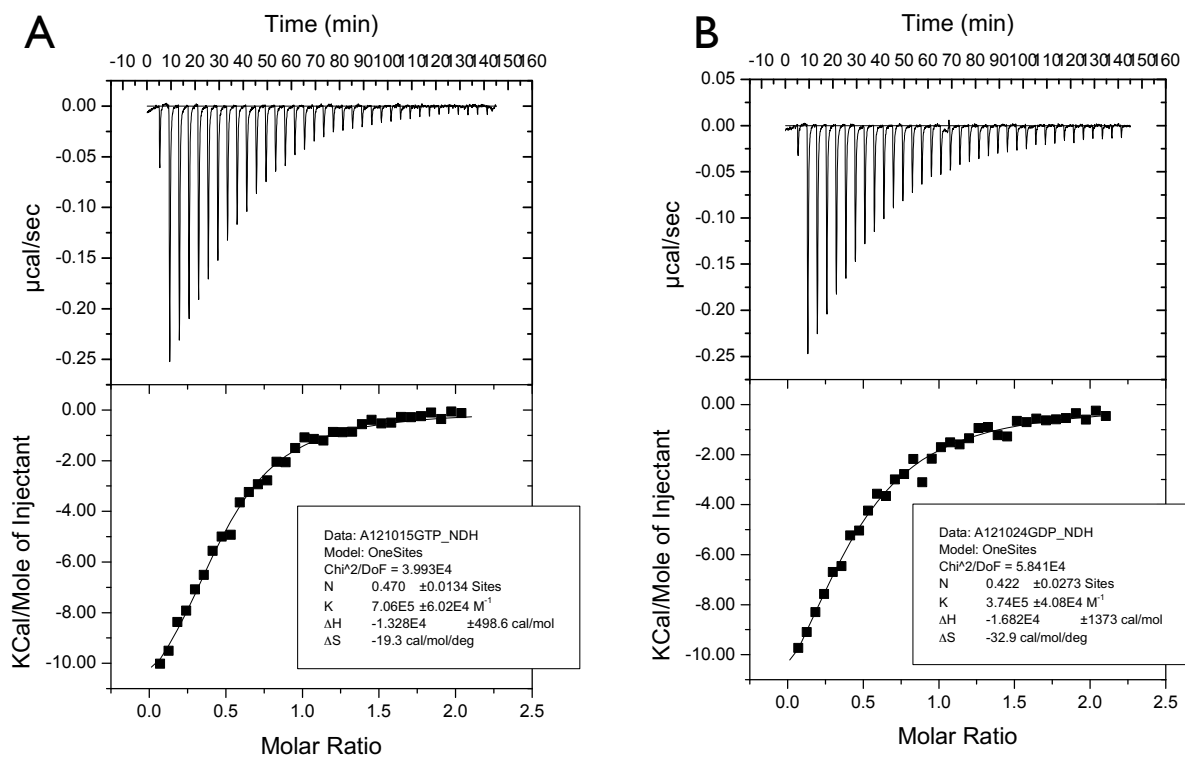


**Figure 18.** Nucleotide binding of PhuZ measured by ITC. **A)** ITC profile for  $\Delta\text{tail-D190A-PhuZ}$  binding to GTP. **B)** ITC profile for  $\Delta\text{tail-D190A-PhuZ}$  binding to GDP.

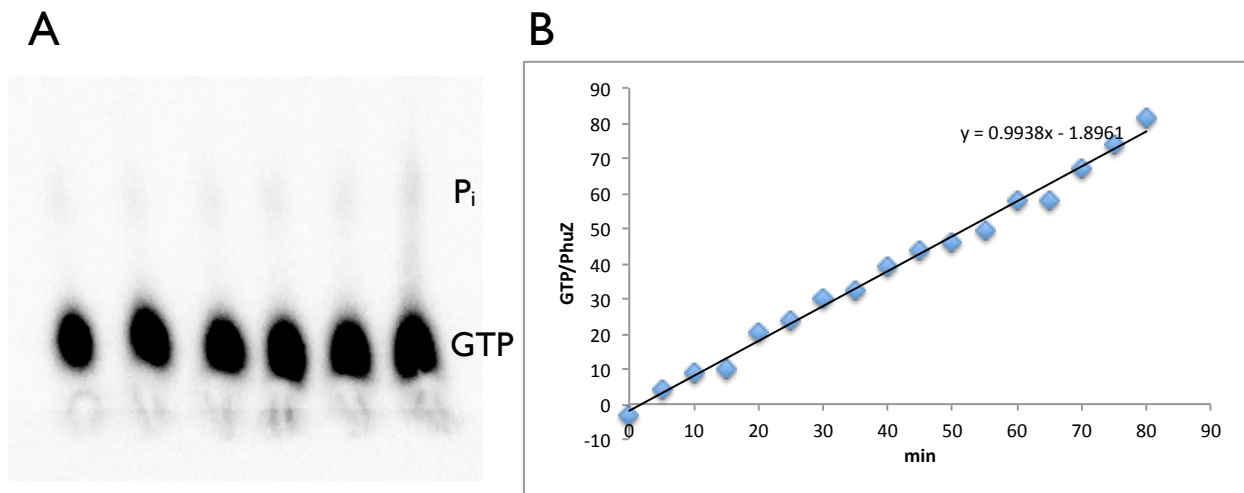


**Figure 19.** GTP hydrolysis by PhuZ. **A)** Example TLC plate showing accumulation of inorganic phosphate over time. **B)** Example data fit showing 1 GTP hydrolyzed/(min\*PhuZ).

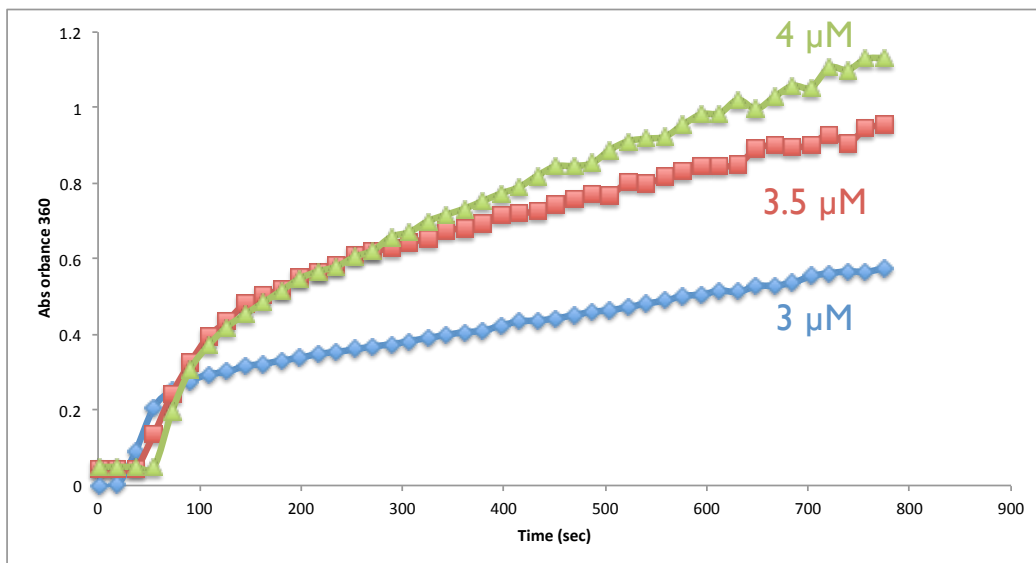


**Figure 20.** PhuZ phosphate release. Curve measuring phosphate release by the EnzChek assay at 3, 3.5, and 4  $\mu\text{M}$  in BRB80 pH 7.2. Slopes at steady-state were measured, compared to a phosphate standard, and corrected for PhuZ concentration.

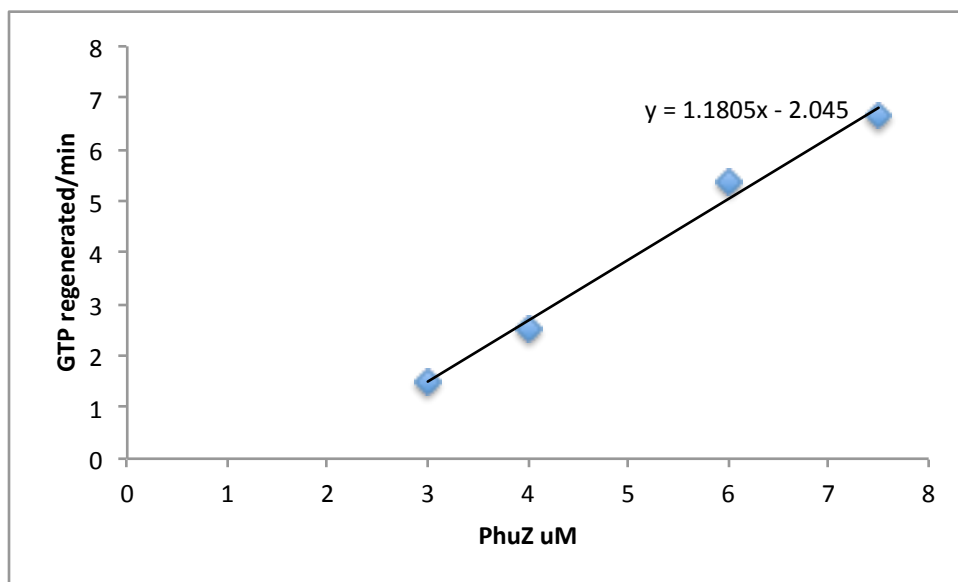


**Figure 21.** GTP turnover measured by enzyme-coupled assay. The rates collected at 4 PhuZ concentration plotted versus measured GTP regeneration rate. The slope of the line is the GTP regeneration rate per PhuZ.

## References

- Aylett, C.H., Wang, Q., Michie, K.A., Amos, L.A., and Lowe, J. (2010). Filament structure of bacterial tubulin homologue TubZ. *Proceedings of the National Academy of Sciences of the United States of America* *107*, 19766-19771.
- Chen, X., Ni, F., Tian, X., Kondrashkina, E., Wang, Q., and Ma, J. (2013). Structural basis of actin filament nucleation by tandem W domains. *Cell reports* *3*, 1910-1920.
- Chen, Y., and Erickson, H.P. (2008). In vitro assembly studies of FtsZ/tubulin-like proteins (TubZ) from Bacillus plasmids: evidence for a capping mechanism. *The Journal of biological chemistry* *283*, 8102-8109.
- Erickson, H.P., and O'Brien, E.T. (1992). Microtubule dynamic instability and GTP hydrolysis. *Annual review of biophysics and biomolecular structure* *21*, 145-166.
- Huecas, S., Schaffner-Barbero, C., Garcia, W., Yebenes, H., Palacios, J.M., Diaz, J.F., Menendez, M., and Andreu, J.M. (2007). The interactions of cell division protein FtsZ with guanine nucleotides. *The Journal of biological chemistry* *282*, 37515-37528.
- Ingerman, E., and Nunnari, J. (2005). A continuous, regenerative coupled GTPase assay for dynamin-related proteins. *Methods in enzymology* *404*, 611-619.
- Mukherjee, A., and Lutkenhaus, J. (1998). Dynamic assembly of FtsZ regulated by GTP hydrolysis. *The EMBO journal* *17*, 462-469.
- Ni, L., Xu, W., Kumaraswami, M., and Schumacher, M.A. (2010). Plasmid protein TubR uses a distinct mode of HTH-DNA binding and recruits the prokaryotic tubulin homolog TubZ to effect DNA partition. *Proceedings of the National Academy of Sciences of the United States of America* *107*, 11763-11768.

Rice, L.M., Montabana, E.A., and Agard, D.A. (2008). The lattice as allosteric effector: structural studies of alpha-beta- and gamma-tubulin clarify the role of GTP in microtubule assembly. *Proceedings of the National Academy of Sciences of the United States of America* *105*, 5378-5383.

Zeeberg, B., and Caplow, M. (1979). Determination of free and bound microtubular protein and guanine nucleotide under equilibrium conditions. *Biochemistry* *18*, 3880-3886.

**Chapter Six**  
**Future Directions**



## **Introduction**

From all of the work described above, we have gained a new appreciation for the molecular diversity of tubulins. Not only have we described new roles and polymerization mechanisms for a tubulin, but we have also opened up a brave new world of bacteriophage cell biology. As with all scientific work, the work is never done; in this chapter, I will briefly outline future directions from this work, both broad ideas and some promising details.

## **Molecular Origins of Polymerization**

It is our hope that from studying prokaryotic tubulins we will be able to gain insights into both properties conserved across all tubulins and ones defined by their uniqueness. Although studied for many years, and the exact molecular role and requirement of GTP in the polymerization of tubulins has remained elusive. Now, strong evidence exists that the energy GTP provides stabilizes a high-energy filament state (Montabana and Agard, 2014; Peng et al., 2014; Rice et al., 2008) (Chapter 4, this work). However, there is still much work to be done on attempting to gain a high-resolution picture of what role the  $\gamma$ -phosphate plays.

## Crystal Structure Bound to GTP

Although all of the attempts to gain a GTP-bound PhuZ crystal structure described in Chapter 5 failed, there are still other experiments that can be tested. None of the constructs crystallized were stripped of nucleotide (with EDTA and DOWEX resin) during purification. Therefore, it is likely that PhuZ is being purified pre-loaded with GTP as is the case for FtsZ (Lowe and Amos, 1998). It is formally possible that a small percentage of protein, even in the presence of 1 mM GMPCPP, remains bound to GDP and is responsible for nucleating and

growing protein crystals. It is also possible that the salts and pH of the crystallization conditions lead to increased hydrolysis of GMPCPP, either by PhuZ or spontaneously. Mutants to the T7 catalytic loop should be used to attempt to further reduce nucleotide hydrolysis, especially in conditions where filaments or filament-like states might be present. It would also be worthwhile trying to remove  $Mg^{2+}$  from the protein buffer, as – even though it is useful for nucleotide binding – it may also increase the rate of nucleotide hydrolysis.

Even though monomeric PhuZ has a very low nucleotide hydrolysis rate, it may also be worthwhile trying to make mutants in the nucleotide-binding pocket, which should reduce the monomer's ability to hydrolyze nucleotide. Even though the monomer has an extremely low nucleotide hydrolysis rate, it could possibly still be significant on the time scale of a crystallography experiment. Similar experiments were attempted in the lab with  $\gamma$ -tubulin (see Elizabeth Montabana's thesis). If these mutants could be successfully generated, they could be useful for slowing down nucleotide hydrolysis in the crystal drop.

More work should be done on attempting to crystalize the  $\Delta$ tail-D190A-PhuZ  $\Delta$ tailbinding-PhuZ mutant pair (discussed in Chapter 5). The initial crystallography was promising, and more optimization should be done to try to reproduce these crystals. It may be worthwhile trying to gel filter the proteins prior to setting up crystal drops, as was successful for reproducing the  $\Delta$ tail-PhuZ crystals. Although the initial crosslinking trials yielded inconclusive results, it might be worth trying to do small amounts of crosslinking and gel filtration to attempt to isolate a dimer of the two mutants. One could also engineer cysteine mutants to make a disulfide bond between the two monomers (either between the tail and the body, or at the longitudinal interface) to capture the dimer bound conformation with GTP or an analog.

## High-Resolution Cryo-EM

During the course of my PhD, the field of cryo-EM has pushed resolution to new heights thanks to technology development allowing for direct electron detection and particle motion correction (Li et al., 2013). Since the cryo-EM reconstruction solved in Chapter 3 is already of fairly high resolution, it would be highly likely that use of new technologies will allow for an even higher resolution structure (already underway in the lab). If a reconstruction can be obtained below 3.5 Å resolution, side chains and the nucleotide should be readily visible. If solved to high enough resolution, such a reconstruction could provide some of the molecular insight hoped to be gained from a GTP-state crystal structure. However, a GTP-state crystal structure will still be necessary to see if there are any nucleotide-dependent conformational changes in the monomer upon GTP binding.

High-resolution cryo-EM reconstructions could also provide further insight into the origins of strain within the PhuZ filament lattice. New work coming out from Eva Nogales' lab at UC Berkeley has been getting close to understanding these questions in microtubules (unpublished data), and this EM would be highly complementary to theirs. Solving high-resolutions EM structures in the presence of GMPCPP or GTP (using the D190A-PhuZ, hydrolysis-dead mutant) as well as filaments in a GDP state could help highlight the consequences of GTP hydrolysis only hypothesized as of now (Chapters 3 and 4). Solving the structure in the presence of GTP with D190A-PhuZ may be more useful than GMPCPP. Although GMPCPP supposed the polymerization of highly stable filaments (Chapter 4), I have found that PhuZ polymerized in the presence of GMPCPP has a longer lag phase and slower growth phase than D190A-PhuZ by right-angle light scattering.

It will be important to ensure that the GDP containing sample is homogeneously in the GDP state, or at least the particles used are. Based on results from Chapter 4, wild-type PhuZ filaments polymerized in GTP should be mostly bound to GDP in the filament interior. However, it is not yet clear how far away from filament ends one would need to pick particles to ensure that all of the monomers are indeed bound to GDP and not GTP. It will be necessary to obtain a reliable GTPase rate during polymerization and couple it with the growth rate measured from TIRF microscopy (Chapter 4) to estimate how many layers deep into the filament one should go before collecting data. Even some monomers multiple layers into the filament will still be bound to GTP. If the conformational change between the GTP-state and GDP-state of the filament is small, which is highly likely, it may be difficult to sort out GTP-containing particles during the reconstruction. It is most likely that only a few loops near the nucleotide will move post GTP hydrolysis within the filament.

Another cryo-EM structure that would potentially provide insights into the origins of metastability would be of D303A/D305A-PhuZ. This mutant (discussed in Chapter 4) lacks key residues for forming important lateral interactions between protofilaments, but is still able to polymerize at high concentrations (Chapter 5). Furthermore, the filaments that do form are unstable in GTP, but the hydrolysis-dead D303A/D305A/D190A-PhuZ forms stable filaments. Obtaining high-resolution structures of both of these constructs could really shed light on PhuZ filament metastability.

### Monomer Association

Many details of PhuZ nucleation remain to be discerned. Although PhuZ appears to assemble via a hexameric nucleus, what this looks like is unclear. The mutant pair designed to

dimerize but not grow ( $\Delta$ tail-D190A-PhuZ /  $\Delta$ tailbinding-PhuZ) could be perfect for future experiments. It would be good to truly test if this pair does indeed dimerize. SAXS or MALS in the presence of GDP and GTP can be carried out to see if dimers form. AUC can also be formed in the presence of GTP and GDP to obtain a  $K_D$  for this interaction. It is also possible that AUC will reveal a  $K_D$  for the lateral association of these dimers, which would create the hypothetical nucleus we imagine.

Insights into longitudinal interactions could also be made using mutants from Chapter 3 that block lateral interactions. AUC or MALS could be conducted to try to gain an understanding of the formation of longitudinal interactions with these mutants.

#### PhuZ as a GTPase

Although I have conducted preliminary experiments about the nature of PhuZ as a GTPase, many more experiments need to be conducted to build a full kinetic model of PhuZ polymerization. Early GTP hydrolysis experiments detailed in Chapter 5 show that PhuZ has a relatively slow GTPase rate of  $\sim 1-3$  GTP/(min\*PhuZ). Considering that PhuZ is dynamically unstable, this is a surprising result. However, this is on the same order as the ATPase rate of Alp7A (personal communication with Natalie Petek, Mullins Lab), which also appears to be dynamically unstable. None of the three kinds of experiments described in Chapter 5 have yet to provide extremely consistent results as well. It is important that all of these experiments be repeated at variable PhuZ concentrations.

Quenched flow experiments like those conducted for ParM (Garner et al., 2004) should also be conducted to determine the rate of GTP hydrolysis during filament growth, as opposed to at steady-state. I have worried for some time that bundling of PhuZ at concentrations much

above the critical concentration leads to suppression of some filament dynamics. Concentrations of PhuZ above 5  $\mu\text{M}$  appear as cables in the TIRF microscope and depolymerize slowly by right-angle light scattering (unless excess GDP is spiked in). It is possible that, if filament bundling suppresses dynamics *in vitro* much above the critical concentration, the observed GTPase rate at steady state would be artificially low compared to during filament growth. If filaments are stabilized at steady state, little new filament growth or turnover will occur, and little new GTP hydrolysis will be measured. Quenched flow experiments will not have the same problems as steady state techniques.

It will also be insightful to measure the depolymerization rate of filaments in various concentrations of GTP as well as after spiking additional GDP. Combining the knowledge of a GTPase rate with these depolymerization rates, it will be possible to model the polymerization-depolymerization of PhuZ filaments *in vitro*.

ITC or other binding experiments should be continued to obtain binding constants for GTP and GDP respectively. The initial ITC experiments yielded 0.5 binding sites, and the sample most likely needs to be optimized to get better data. It is also clear from the data (see Chapter 5) that the concentration regime of protein and ligand is suboptimal, as the curves do not have a long enough lag phase, which could be preventing proper estimation of the binding constants. The estimation of protein concentration could also be wrong, as concentration has been determined by Bradford, using BSA as a standard, which may not be the most accurate way of determining protein concentration.

## **Mechanism of Phage Centering**

Beyond biophysical questions about the GTP regulation of PhuZ filaments, the work described has left open many questions about the biology of PhuZ. We have shown that PhuZ uses dynamic instability to actively center replicating phage within the host cell, but the mechanism of this centering is almost completely unknown. It will be paramount to work out the molecular details of phage DNA centering both *in vivo* and *in vitro*. Below I describe some experiments to identify other important players in phage replication, and how these alter PhuZ filament dynamics.

#### What Binds PhuZ Filaments?

We showed in Chapter 4 that PhuZ filament minus ends are stabilized at the cell pole during infection and that the plus ends are stabilized by the phage nucleoid. The components involved in these stabilization events are unknown and phage encoded. The Pogliano lab has been conducting mass spectrometry experiments to identify when specific genes are turned on during phage infection. Using a comparative analysis of proteomics from multiple phage in the  $\Phi$ KZ family, it will be possible to determine which conserved proteins are expressed at the same time during the phage lytic cycle. These data could provide for a short list of candidate proteins that may be involved in either the pole anchoring or phage nucleoid tethering processes.

An unbiased genetic screen could be undertaken to attempt to identify players in the filament stabilization process as well. The size of the phage genome (~300 kb) has been prohibitive for traditional genetics. Recent development of CRISPR interference technology (Larson et al., 2013) should allow for effective knockdown of phage genes. A screen knocking down all genes in the phage genome and monitoring phage infection and PhuZ filaments by

microscopy could have the power to reveal proteins involved in polar anchoring and nucleoid stabilization.

Another approach to identifying PhuZ binding partners is to an immunoprecipitation of PhuZ from infected cells. Tagging PhuZ with a TAP-tag and pulling on it will hopefully enable identification of binding partners. It may also be necessary to do co-pelleting experiments to see if proteins from clarified phage infected cell lysate will co-sediment with PhuZ filaments. The stoichiometry of the binding will be able to imply if binding partners are binding to the end or along the filaments. It will be key to work out the optimal stage of phage infection for the pull-down. It will also be key to work out a way to clarify the lysate without losing some of the potential key proteins. The phage themselves are quite large, and if a component of the capsid is involved in tethering PhuZ filaments to the phage nucleoid, it may come out of the lysate during the initial clarification step.

### How Do the Binding Proteins Function?

Once PhuZ binding proteins are identified, it will open the door for a wide variety of biochemical and structural experiments. Binding partners can be added to any of the assays used in the previous chapters to gain insight into how they impact PhuZ filament polymerization and dynamics. Does the protein at the pole simply anchor PhuZ filaments, or does it nucleate them as well? Using right-angle light scattering one could test to see if addition of this protein decreases the lag phase of filament growth, demonstrating nucleation. One can also test the stability of filaments in the GDP-spiking assay, so see if having both proteins protects filaments from catastrophe. Binding proteins can also be added to the TIRF polymerization assay to see how they bind and affect individual filament dynamics.



Various binding experiments should be conducted to learn how tightly these proteins bind to PhuZ monomers and filaments. Binding experiments can be conducted with PhuZ in different nucleotide states to see if they bind better to specific forms of the monomer or filament.

To gain a molecular insight into their functions, structures of PhuZ can be solved bound to the binding proteins. Co-crystal structures of monomeric PhuZ can be attempted to get an atomic-resolution understanding of their interactions. If the proteins bind along the filament, or can be forced to bind along the filament at high enough concentrations, cryo-EM reconstructions can be done to gain more insight into the interactions and how they might regulate filament dynamics. Otherwise, filament ends decorated with binding partners can be collected and used for cryo-EM reconstructions.

Once a parts list has been assembled and insight into their function is obtained, whole cell cryo-EM tomography will be able to put all the pieces together of how PhuZ filaments work in concert with binding partners to interact with the phage nucleoid. Since *Pseudomonas* are  $\sim 1 \mu\text{M}$  thick, and the cells swell at the center during infection, it will be critical to work out conditions in which the cells are small enough,  $\sim 0.5 \mu\text{M}$  in thickness, to collect good whole cell tomography data. Once these conditions have been worked out, one could collect tomograms at various time points in phage lytic growth to get high-resolution snapshots of DNA centering by PhuZ.

## **Biology of Viruses**

The discovery of the first family of tubulin homologs encoded on bacteriophage is an exciting one, which opens up a whole new subfield of questions about the cell biology of phage and the origins of life. Bacteriophage have traditionally been considered to be non-living, and as more and more complex phage with larger and larger genomes are discovered, the line between

life and non-life will become more and more blurred. The  $\Phi$ KZ phages have genomes as large as some of the smallest bacteria (Ochman and Davalos, 2006). This raises the possibility, combined with their complexity, that phage may play a role in the development of new organisms or life.

The question of the evolution of eukaryotes is also a challenging and interesting one. We know that viruses have played many roles in the evolution of organisms through gene transfer. Could a phage have possibly been involved in bringing a bipolar, tubulin-based spindle to a cell that became the first eukaryote as we know it? These are just some of the fascinating big picture questions that can now be asked.

## References

- Garner, E.C., Campbell, C.S., and Mullins, R.D. (2004). Dynamic instability in a DNA-segregating prokaryotic actin homolog. *Science* *306*, 1021-1025.
- Larson, M.H., Gilbert, L.A., Wang, X., Lim, W.A., Weissman, J.S., and Qi, L.S. (2013). CRISPR interference (CRISPRi) for sequence-specific control of gene expression. *Nature protocols* *8*, 2180-2196.
- Li, X., Mooney, P., Zheng, S., Booth, C.R., Braunfeld, M.B., Gubbens, S., Agard, D.A., and Cheng, Y. (2013). Electron counting and beam-induced motion correction enable near-atomic-resolution single-particle cryo-EM. *Nature methods* *10*, 584-590.
- Lowe, J., and Amos, L.A. (1998). Crystal structure of the bacterial cell-division protein FtsZ. *Nature* *391*, 203-206.
- Montabana, E.A., and Agard, D.A. (2014). Bacterial tubulin TubZ-Bt transitions between a two-stranded intermediate and a four-stranded filament upon GTP hydrolysis. *Proceedings of the National Academy of Sciences of the United States of America* *111*, 3407-3412.
- Ochman, H., and Davalos, L.M. (2006). The nature and dynamics of bacterial genomes. *Science* *311*, 1730-1733.
- Peng, L.X., Hsu, M.T., Bonomi, M., Agard, D.A., and Jacobson, M.P. (2014). The free energy profile of tubulin straight-bent conformational changes, with implications for microtubule assembly and drug discovery. *PLoS computational biology* *10*, e1003464.
- Rice, L.M., Montabana, E.A., and Agard, D.A. (2008). The lattice as allosteric effector: structural studies of alphabeta- and gamma-tubulin clarify the role of GTP in microtubule assembly. *Proceedings of the National Academy of Sciences of the United States of America* *105*, 5378-5383.

## **Appendix: Select Protocols**

The following pages contain select protocols for PhuZ purification and TIRF microscopy.

## **PhuZ Purification:**

### Protein Expression:

Grow 1 L culture of BL21 cells in LB to an OD of 0.5 at 37°C.

Drop temperature to 16°C and induce cells overnight after 30 min.

Pellet and freeze cultures in the morning.

### Purification:

Make sure you have prepared the following (see buffer recipes):

- 200 ml lysis buffer
- 100 ml wash buffer
- 50 ml elution buffer
- 500 ml S200 buffer
- 1 L cleavage buffer

Add 10 mM thioglycerol to the buffers fresh

Split lysis buffer in half, with one bottle containing 2 EDTA-free protease inhibitor tabs

Make sure to completely dissolve tabs

Use buffer with protease inhibitor and dounce to homogenize the pellet

Lyse cells in Emulciflex

Spin cells for 45 min @ 35k xG

During spin, prepare Ni column

Use 6 ml of Ni-NTA slurry (3 ml bed volume)

Equilibrate with the other 100 ml of lysis buffer put aside earlier

During spin, equilibrate the S200 column as well

Use S200 buffer and run the Biggfwash program

Add supe from spin to the Ni resin

Nutate in cold room for 1-1.5 hours

Flow supe through the column

Wash column with 100 ml wash buffer

Elute protein from Ni resin with 4 bed volumes of elution buffer (3 ml per fraction)

Cleave O/N with 100 ul thrombin protease in cleavage buffer in cold room

Concentrate fractions from 12 ml to ~5 ml for injection onto S200 column

Run S200 column and collect peak fractions

Concentrate peak fractions and aliquot

## **Buffer Recipes:**

### Lysis Buffer:

- 50 mM HEPES pH 8
- 250 mM KCl
- 1 mM MgCl<sub>2</sub>
- 10% glycerol
- sterile filter
- add 10 mM thioglycerol fresh

### Wash Buffer:

- 50 mM HEPES pH 8
- 250 mM KCl
- 1 mM MgCl<sub>2</sub>
- 10% glycerol
- 25 mM imidazole
- sterile filter
- add 10 mM thioglycerol fresh

### Elution Buffer:

- 50 mM HEPES pH 8
- 250 mM KCl
- 1 mM MgCl<sub>2</sub>
- 10% glycerol
- 250 mM imidazole
- sterile filter

- add 10 mM thioglycerol fresh

S200 Buffer:

- 50 mM HEPES pH 8
- 250 mM KCl
- 1 mM MgCl<sub>2</sub>
- sterile filter
- add 10 mM thioglycerol fresh

Cleavage Buffer:

- 50 mM HEPES pH 8
- 125 mM KCl
- 1 mM MgCl<sub>2</sub>
- 1 mM CaCl<sub>2</sub>
- sterile filter
- add 10 mM thioglycerol fresh



### **D190A-PhuZ Purification:**

Express cells as above.

Follow protocol as above with the following changes:

- Use a high-salt lysis buffer with EDTA
  - 500 mM KCl instead of 250 mM
  - 2 mM EDTA
- After lysate is clarified, incubate with 5 ml DOWEX resin equilibrated with high-salt lysis buffer for 10 min.
- Spin lysate in Ti 45 rotor at 35k x rpm for 1 hour to pellet DOWEX resin.
- Bind D190A-PhuZ to EDTA-resistant Ni-resin
- Cleave His-tag overnight in 250 mM KCl cleavage buffer, not 125 mM KCl.

### **Slide Preparation for TIRF Microscopy:**

1. Take 24 x 40 mm slides (VWR) and mark which side will be PEG.
2. Place slides in coplin jar and sonicate in 2M KOH for 15min.
3. Rinse the slides 5x with ddH<sub>2</sub>O and place in clean coplin jar.
4. Add piranha solution (2 parts 30% peroxide, 3 parts sulfuric acid) to the slides and sonicate the slides in piranha solution for 30 min.
5. Rinse the slides 5x with ddH<sub>2</sub>O.
6. Spin dry the coverslips using a spin coater. Store dry slides on Kimwipes before the next step.
7. Arrange the slides in a weighing jar. Take GOPTS out with hamilton syringe into glass. Put one drop of GOPTS onto each slide using Hamilton Syringe. Form a sandwich by putting another slide face-to-face onto the GOPTS. Close the weighing jars.
8. Transfer the closed jars to the oven and incubate for 1h at 75°C
9. Transfer the jars onto the 80°C hot plate, open the jars and transfer the closed slide sandwiches in a beaker containing dry isopropanol (HPLC grade). Separate the slides in isopropanol, wash in acetone 1x and store the slides in coplin jar with isopropanol.
10. Spin dry the coverslips using the dry(!) spin coater. Store dry slides on Kimwipes before the next step.
11. Prepare a saturated PEG-SEV (Laysan) mix in dry acetone. Use 150mg of PEG (1% biotin-PEG) in 500ul acetone. Vortex at max speed for 45 sec and hard spin at 14krcf for 3min.
12. Arrange the slides in a weighing jar. Put 25ul of the saturated PEG-acetone solution onto the GOPTS slides. Close the weighing jars.
13. Transfer the closed jars to the 75°C oven.
14. Incubate for 4h in the oven at 75°C

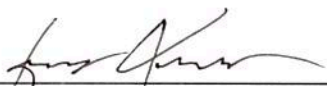
15. Take the DAPEG slides out of the oven and put them onto a hot (80°C) plate. Manually separate the sandwiches. Be quick, since the PEG solidifies rapidly at RT.
16. Dip-wash the slides in 2 subsequent MilliQ baths and store them in a fresh milliQ.
17. Sonicate for 3min, wash again in MilliQ and store in MilliQ in a fresh container.
18. Spin-dry the clean GOPTS-DAPEG slides. Store slides between lens cleaning paper at 4°C for several month. Can also be stored for ~1 month in the dark at RT.

**Publishing Agreement**

*It is the policy of the University to encourage the distribution of all theses, dissertations, and manuscripts. Copies of all UCSF theses, dissertations, and manuscripts will be routed to the library via the Graduate Division. The library will make all theses, dissertations, and manuscripts accessible to the public and will preserve these to the best of their abilities, in perpetuity.*

**Please sign the following statement:**

*I hereby grant permission to the Graduate Division of the University of California, San Francisco to release copies of my thesis, dissertation, or manuscript to the Campus Library to provide access and preservation, in whole or in part, in perpetuity.*

  
\_\_\_\_\_  
Author Signature

4/25/14  
\_\_\_\_\_  
Date